# Physiology and plasticity of myelinated long-range projections in the adult brain

Alberto Lazari

# Contents

# Acknowledgements

I'd like to dedicate this thesis to all the healthcare workers, including some clinicians from WIN, who are currently working to keep us safe during the fight against COVID-19. Grazie di cuore.

The work presented in this thesis would not have been possible without the help of a huge number of people, to whom I am extremely grateful.

I have been lucky to have an unusually large team of mentors during my DPhil: Heidi, Charlie, Matthew, Piergiorgio, Lennart and David.

My special thank you goes out to Heidi. You have been an incredible role model. Before I joined the Plasticity lab, I believed the commonly held assumption that people can either be genius scientists or kind humans, but not both. You are the living proof that this is untrue - the best scientists are also the kindest. I am not sure how to put my gratitude into words, so I will just say that in tough situations I often find myself thinking: "What would Heidi do?", and so I hope you won't mind me knocking on your door for advice in the future.

Charlie, thank you for welcoming me with open arms into your lab after the Tinbergen building shut down, and adopting me into PiNG without asking much in return. As an associate member of PiNG, I have directly experienced how a young PI can make a difference by creating an inclusive, fun, innovative and cutting-edge environment for their lab members. It's an experience I have treasured, and will continue to treasure.

Matthew, thank you for being such an open, kind and creative collabora-

tor and mentor. You've set an example of kindness and leadership that will stay with me past my PhD time.

Piergiorgio, your mentorship and collaboration has been one of the most fun experiences of my PhD, which I hope will continue past this thesis and past our time in Oxford.

Lennart, thank you for supporting me throughout the mammoth TMS project and for sharing your TMS secrets with me. You have taught me how to have fun with brain stimulation, and have been a fantastic example of supportive mentoring.

David, thank you for co-supervising me and being a role model of scientific and moral integrity.

To my wonderful students, who truly made the DPhil a special time for me. Olof, who helped me make sense of TMS data early on in my PhD, and managed to make even the most tedious TMS sessions fun. Bronwyn, who did some of the early analyses of Chapter 5 and made me realise I cannot live without biltong. Sebastian, who spent a small amount of time in the lab but left a big mark on the electrophysiology project. David, who helped in the last leg of the TMS project and did a fantastic job recruiting participants. It has been a privilege working with all of you.

To my fellow doctoral musketeers, Zeena and Thomas, for listening to my rants on a daily basis and for being overall awesome companions.

To the Plasticity group for creating an inclusive, fun, stimulating workplace that has always been a pleasure to be a part of. Thank you to Tom, Marilien, Tulika, and all the other people who helped collect the TMS data.

Thank you Malte and Cassandra for the boozy chats about myelin. Special mention goes to Caro and Ioana for being amazing dancing as well as scientific companions.

To all the people who supported the multidisciplinary projects in the thesis. Michiel and Matthew, thank you for your constant patience with my computing problems - this thesis would not contain as many analyses as it does without your help. Daniel, thank you for establishing the MPMs and helping with data collection issues. A special thank you to Juliet, Nicky and Nico for exceptional (and exceptionally fun) radiography at OHBA. Big thanks to Seb for always managing to fix the things that no one else knows how to fix.

To all the volunteers that lent their time and their data for abstract, basic research. Without their help, this thesis would be empty.

My biggest gratitude goes to my family, my Mom and to my chosen family - Alex B, Alex V, Ruairi, Helen, Giulia, Frantola, Alberto, Niki, Laia and the Serratosa Capdevillas - for always being there for me despite the distance. Thank you Chan, Pascal, Maria, Nicole, Ross, Lisa and Maddy for all your support in Oxford.

My gratitude also goes to the Wellcome Trust, which kindly funded both me and my experiments over the past few years.

# Related Publications

Chapter 1 contains material partially overlapping with:

Lazari, A., Koudelka, S., Sampaio-Baptista, C. (2018). Experience-related reductions of myelin and axon diameter in adulthood. Journal of neurophysiology, 120(4), 1772-1775.

Chapter 3 contains material overlapping with:

Lazari, A., Salvan, P., Cottaar, M., Papp, D., van der Werf, O. J., Johnstone, A., ... Johansen-Berg, H. (2020). Heterogeneous relationships between white matter and behaviour. bioRxiv.

In addition, I contributed to the following published work during my PhD, which was not included as it was beyond the scope of this thesis:

Kaller, M. S., Lazari, A., Blanco-Duque, C., Sampaio-Baptista, C., Johansen-Berg, H. (2017). Myelin plasticity and behaviour—connecting the dots. Current opinion in neurobiology, 47, 86-92.

Sampaio-Baptista, C., De Weijer, A., Van Der Toorn, A., Otte, W. M., Winkler, A. M., Lazari, A., ... Johansen-Berg, H. (2019). Skill acquisition increases myelination and strengthens functional connectivity in the sensorimotor circuit of the adult rat. BioRxiv, 661546.

Lazari, A., Giuffre, A., Nandi, T. (2020). White matter damage and altered connectivity between primary motor cortices in chronic obstructive pulmonary disease. The Journal of Physiology.

Salvan, P., Lazari, A., Vidaurre, D., Mandino, F., Johansen-Berg, H., Grandjean, J. (2020). Causal evidence of network communication in whole-brain dynamics through a multiplexed neural code. BioRxiv.

Lazari, A., Lipp, I. (2021). Can MRI measure myelin? Systematic review, qualitative assessment, and meta-analysis of studies validating microstructural imaging with myelin histology. NeuroImage, 117744.

# Chapter 1: What are the rules governing plasticity of myelinated long-range projections?

*Parts of the text from this thesis chapter appear in the following article: Lazari, A., Koudelka, S., Sampaio-Baptista, C. (2018). Experience-related reductions of myelin and axon diameter in adulthood. Journal of neurophysiology.*

## 1.1 What are myelinated long-range projections?

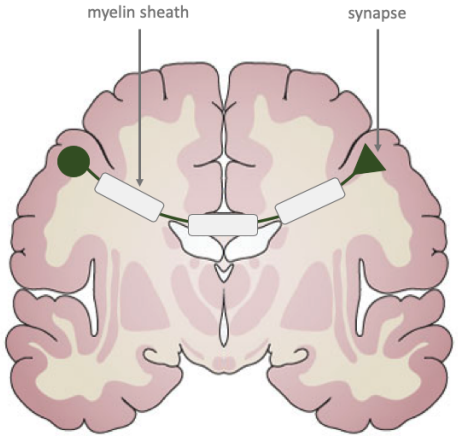


Figure 1.1: Simplified diagram of a myelinated axon. Multiple axons, grouped into a bundle, make up a projection. Adapted from (Di Pino et al., 2014)

Myelinated long-range projections are a key building block of the brain. Each projection is in turn made up of smaller building blocks, known as axons, which get grouped together in bundles. An axon is a cell component that

protrudes from the soma of a neuron in a given cortical area, travels for some distance, and then synapses into the dendrites of another neuron, which can be in a different cortical area (Figure 1.1). These long axons become heavily myelinated once they leave the cortex, giving rise to chunks of white matter (so called because of the presence of fatty myelin macromolecules giving it a light appearance) below the cortical sheet. Axonal projections are key to healthy brain function, as they allow distant brain areas to communicate with each other. So how do they work, and why do they need to be myelinated?

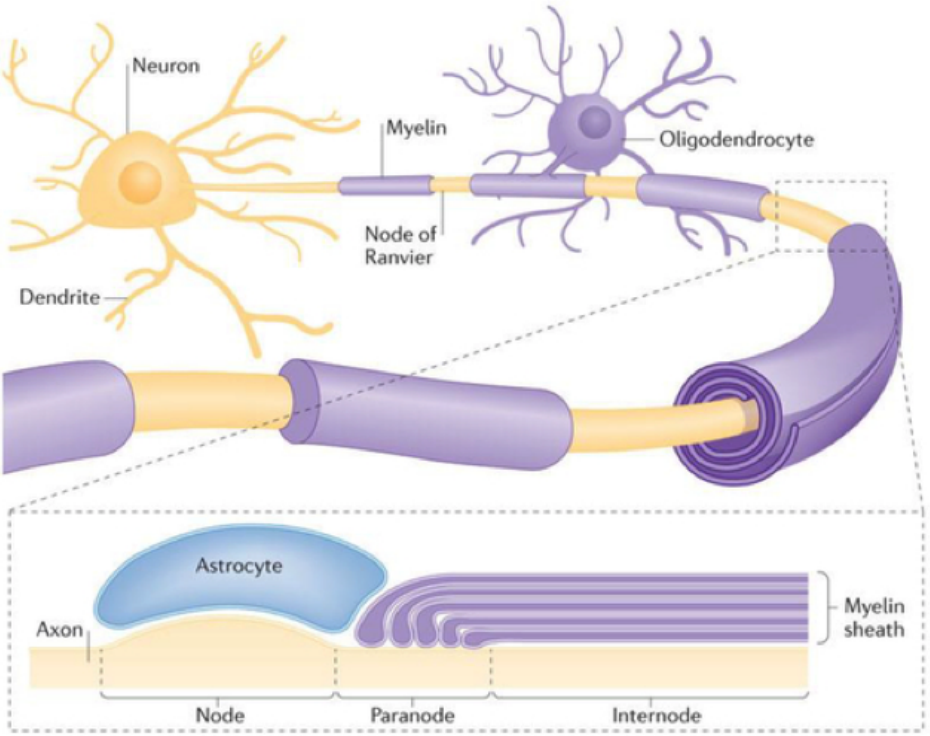


Figure 1.2: Morphology of myelinated long-range projections. Reproduced from (Fields, 2015).

The textbook notion of myelination is that it allows to increase the conduction velocity of axons by insulating them, a little bit like rubber insulation of electrical wires that are standard in modern homes. Insulation is certainly a key reason why the long-range projections in our brain need to be myelinated - to achieve similar conduction speeds without insulation would require unreasonably big axons and would be energetically inefficient (Snaidero and Simons, 2014). However, the past decade has seen an increased appreciation for the complexity of myelin's function. It is increasingly clear that nodes of Ranvier and internode sizes are finely tuned for the purposes they subserve (Ford et al., 2015) (Arancibia-Carcamo et al., 2017). It is also becoming an influential theory that oligodendrocytes provide trophic support to axons (Fünfschilling et al., 2012, Lee et al., 2012), which may happen in an adaptive, activity-dependent way (Saab et al., 2016).

We also understand more about the morphology of the myelinated axon than we did a decade ago. The traditional notion of myelin morphology posited that most neurons in the brain would be expected to be myelinated, and that the degree by which they are myelinated is dependent on the axon diameter, following a so-called "g-ratio" so defined:

$$g - ratio = \frac{diameter_{\text{inner axonal diameter}}}{diameter_{\text{outer myelin sheath diameter}}} \tag{1}$$

which has been estimated to be optimal for the central nervous system around values of 0.6 (Rushton, 1951). However, we are increasingly appreciating that myelination is not so straighforward. Firstly, we now know

that different neurons have different patterns of myelination (Tomassy et al., 2014). This sometimes leaves large portions of the axon completely unmyelinated (Tomassy et al., 2014), and there are hints of myelination patterns being dependent on the cell type being myelinated (Tomassy et al., 2016), with some neurons such as parvalbumin interneurons being preferentially myelinated (Micheva et al., 2016) (Stedehouder et al., 2017), potentially due to their intrinsic morphological properties (Stedehouder, 2019, eLife, in press). Moreover, oligodendrocytes and their precursors (Oligodendrocyte Precursor Cells, or OPCs) are themselves being increasingly found to be diverse in gene expression (Marques et al., 2016) and function (Spitzer et al., 2019), with recent studies even highlighting spatial diversity in the white matter tract they are synaptically connected to (Mount et al., 2019).

In addition to all these recent findings, perhaps the most striking development regarding our understanding of myelination is that we now know that myelination remains an active process, responsive to neuronal activity and behavioural stimulation during adulthood. The plasticity of myelinated long-range projections, and more specifically the plasticity of the synapse and of the myelin within them, are the focus of this thesis. But first, what is brain plasticity, and what do we know about it?

## 1.2 A tale of two plasticity mechanisms: synapses and myelin

### 1.2.1 Plasticity and the rules governing it

The term "plasticity" was first used in reference to the nervous system in 1890 by William James (Berlucchi and Buchtel, 2009), to define physiological processes taking place in the brain according to mechanisms other than physical ones (e.g. thermal and mechanical). Although it was always thought the brain had some degree of plasticity, allowing it to respond to experience, the real extent of such changes has been a recurring debate in neuroscience. What components of the brain change with experience? What guiding rules do these changes follow? How fast do plastic changes occur? What behavioural functions do they subserve?

### 1.2.2 Synaptic Plasticity

Synapses and their function have been at the centre of controversies since the beginning of neuroscience. For decades, between the late 19h and early 20th century, their very existence was a crucial debate in neuroscience, which resolved with the rise of the "neuron doctrine", i.e. the notion that neurons are cellular entities which connect through synapses, rather than a shared, mesh-like cell body. In fact, this debate did not find its final conclusion until the 1940s, when light microscopic studies of abnormally large synaptic junctions allowed to confirm that there was in fact, a gap between neurons (Guillery, 2004).

In light of these discoveries, it is no coincidence that the first postulation of a plasticity mechanism involving connections between synapses also took place in the 1940s. Donald Hebb, in 1949, famously proposed that "neurons that fire together, wire together", and that plasticity in the wiring between different neurons could be a key site for associative plasticity underpinning associative learning (Hebb and Hebb, 1949).

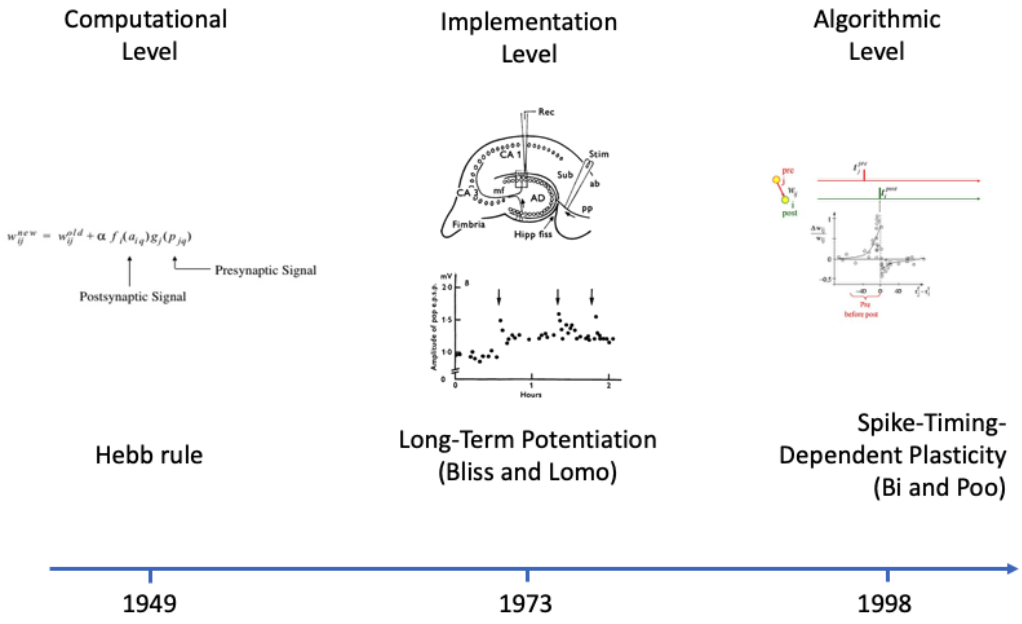


Figure 1.3: A very brief history of synaptic plasticity. Images reproduced from (Bi and Poo, 1998, Bliss and Lømo, 1973, Hebb and Hebb, 1949).

However, the principle put forward by Hebb was at its core a computational hypothesis of plasticity mechanisms, rather than a theory of how plastic changes are actually implemented in the brain. In particular, Hebb thought the idea of neurons wiring together as a function of coincident ac-

tivation was an simple and elegant way of explaining associative memory (Lansner, 2009). However, for nearly three successive decades, Hebb's theory remained what it was at the time: a theoretical contribution, steeped in mathematics, but difficult to prove or disprove empirically.

As showed in Figure 1.3, it was not until the 1970s, once extracellular recordings became more technically manageable, that Bliss and Lomo managed to provide key evidence of synaptic plasticity in the hippocampus (Bliss and Lømo, 1973). Following that discovery, a whole field of investigation emerged, focussing on disentangling the rules of synaptic plasticity through experiments and theoretical modelling. This branch of neuroscience research is undoubtedly still ongoing, but one influential model of synaptic plasticity was agreed in the 1990s, i.e. the Spike-Timing Dependent Plasticity (STDP) mechanism (Bi and Poo, 1998).

Nowadays, synaptic plasticity is considered to be a major mechanism of plasticity in the brain and a potential building block of learning, although the precise behavioural consequences of impaired synaptic plasticity are controversial (Bannerman et al., 1995, Moser et al., 1998, Sakimura et al., 1995, Saucier and Cain, 1995, Tsien et al., 1996). Although it is no longer considered to be acting on its own, no other plasticity mechanism has been shown to take place in the absence of synaptic plasticity.

A recent breakthrough in the study of associative plasticity in the brain has been the development of Non-Invasive Brain Stimulation (NIBS) techniques capable of inducing associative plasticity during the 2000s and 2010s. Most seminal studies on synaptic plasticity took place in ex vivo brain slices

from rodents, making it difficult to interpret to what extent the same rules apply to humans in an in vivo context. By contrast, NIBS techniques can be applied in live humans. Paired Associative Stimulation (PAS), for instance, allows to induce local plasticity in primary motor cortex (M1) by coordinating Transcranial Magnetic Stimulation (TMS) of M1 with peripheral stimulation of median nerve fibers that project to M1 (Stefan et al., 2000). This approach has been replicated not only with different timing intervals (Wolters et al., 2003) and in other areas of the cortex (Wolters et al., 2005), but its general principles have also been applied to cortico-cortical projections by concurrent, coordinated stimulation of two cortical sites through paired associative TMS (paTMS) (Buch et al., 2011). This recent approach has since been applied to a variety of different cortical areas: M1 and M1 (Rizzo et al., 2009), Supplementary Motor Area (SMA) and M1 (Arai et al., 2011), Posterior Parietal Cortex and M1 (Chao et al., 2015, Koch et al., 2013, Veniero et al., 2013), visual area V5 and primary visual cortex (V1) (Chiappini et al., 2018, Romei et al., 2016), and ventral Premotor Cortex (PMv) and M1 (Buch et al., 2011, Fiori et al., 2018, Johnen et al., 2015). Although it is impossible to test directly whether PAS or paTMS induce synaptic plasticity, the Hebbian nature and spike-timing dependency of the plasticity effects they generate is a potential indicator that synaptic plasticity mechanisms may be involved (Buch et al., 2011, Müller-Dahlhaus et al., 2010). This makes NIBS a promising approach to apply our knowledge of a key brain plasticity mechanism in humans.

### 1.2.3 Open question 1: Synaptic plasticity: how does it work in long-range projections in humans?

Although much is known about the details of how long-range projection synapses change in rodents, many questions are still open about how they change in humans. Do associative principles apply to different areas, whereby if two areas fire together, the synapses connecting them get potentiated? And what effect does this have on behaviour, physiology and wider brain networks?

### 1.2.4 Myelin Plasticity

The history of myelin plasticity is very different from that of synpatic plasticity. First, myelin plasticity was discovered much more recently. Until a little over a decade ago, myelination was considered to be completely static during adulthood. Even more strikingly, a key historical difference between these two plasticity mechanisms is that unlike synaptic plasticity, myelin plasticity had not been postulated to exist before it was discovered. And in fact, its computational and algorithmic properties are still unclear, as summarised in Figure 1.4.

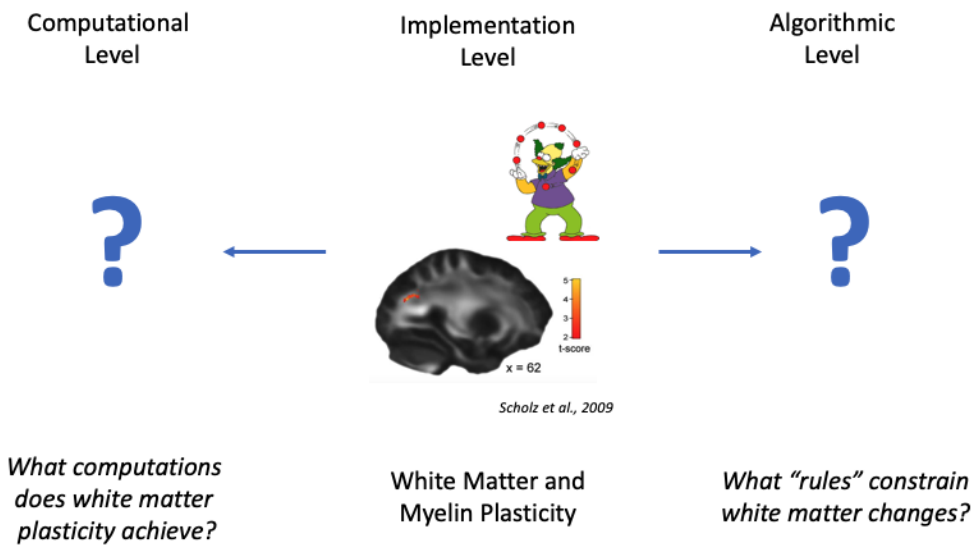


Figure 1.4: A very brief history of myelin plasticity. Images reproduced from (Scholz et al., 2009).

Although adaptive myelination had been known to happen in vitro (Demerens et al., 1996, Stevens et al., 1998), it was not until recently that multiple streams of evidence accrued to demonstrate that white matter can also be modified in vivo and during adulthood. More specifically, it is now clear that adult neuronal activity on its own can lead to production of new myelin, whether it is induced by electrical stimulation (Li et al., 2010), optogenetics (Gibson et al., 2014), or chemogenetics (Mitew et al., 2018). We also know that experience and learning can induce myelin changes (Hughes et al., 2018, Sampaio-Baptista et al., 2013) similar to white matter changes observed in humans following similar experiences (Scholz et al., 2009) and (Sampaio-Baptista et al., 2019, biorxiv). Finally, it is increasingly clear that produc-

tion of new myelin happens throughout adult life (Grydeland et al., 2018, Hill et al., 2018, Yeung et al., 2014).

Despite these advances, we still know relatively little about myelin plasticity, and the parallel with synaptic plasticity is a useful framework to expose our lack of knowledge about the rules governing myelin plasticity (Fields, 2015). For example, we know that synaptic plasticity is bidirectional (i.e. synapses can undergo potentiation and de-potentiation), but we do not know if myelin can also undergo decrements as well as increments in its morphological features. Most studies of myelin plasticity so far have focussed mainly on increases in myelination following learning (Sampaio-Baptista et al., 2013) and following increases in neuronal activity (Gibson et al., 2014, Li et al., 2010, Mensch et al., 2015). Reports of decreases in myelination have been sparse, and always entangled with developing systems (Etxeberria et al., 2016), which are known to be particularly sensitive to reduced stimulation, or with stressful conditions such as social deprivation or defeat (Lehmann et al., 2017, Liu et al., 2012, Makinodan et al., 2012), where the underlying changes in neuronal activity are complex, or with specific or pathological patterns of neuronal activity (Stevens et al., 1998, Tagoe et al., 2014). Only recently, a paper by (Sinclair et al., 2017) has clearly demonstrated experience-dependent and behaviourally-relevant decreases in myelination in adulthood.

How, when, and why myelin changes occur, is still to be fully understood. Nevertheless, the emerging concept of adaptive myelin plasticity is appealing: it could not only provide an underappreciated mechanism by which timing

in neural circuits can be dynamically regulated throughout life, but it could also provide a mechanism of brain plasticity that is spatially and temporally more extended than currently known brain plasticity mechanisms, such as synaptic plasticity.

To conclude, the histories of synaptic and myelin plasticity shape the current debates and questions around them. The study of synaptic plasticity has always been steeped in theoretical studies, but over the years more and more questions have emerged about how exactly this mechanism is implemented in the brain, and what its physiological consequences are. The study of myelin plasticity started from unexpected empirical observations of changes in myelin, and is thus now moving towards mechanistic and causal studies aiming to understand the rules regulating it.

### 1.2.5 Open question 2: Myelin plasticity: is there an STDP-like mechanism for long-range projections?

Unlike for synaptic plasticity, the algorithmic and computational properties of myelin plasticity are unclear. A first step to better understand the computational properties of myelin plasticity is to investigate what rules define when it happens. In particular, although we know STDP mechanisms apply to synaptic plasticity, we don't know whether myelin plasticity has a similar spike-timing-dependent nature.

## 1.3 The plasticity family grows: new plasticity mechanisms

Synaptic and myelin plasticity are in themselves incredibly complex - and yet they may not be the whole story of how the brain changes with experience. It is now clear that that a number of other cellular compartments undergo plastic changes in adulthood, including astrocytes (Zhou et al., 2019), microglia (Shemer et al., 2015) and the axon initial segment (Grubb et al., 2011). Moreover, additional patterns of coordinated cellular change will likely be discovered by looking at gene expression of whole gene networks simultaneously (Sampaio-Baptista et al., 2019b).

Axon diameter is also an understudied potential locus of plastic changes. Until recently, most myelin plasticity studies have focused on the plastic potential of myelin sheath properties rather than that of the axon diameter. There are a few exceptions - notably, a recent paper by (Chéreau et al., 2017). This study applied stimulated emission depletion microscopy to resolve axonal morphology in hippocampal slices and reported a long-term increase in axon diameter following high-frequency neuronal firing. However, whether the same mechanism would apply *in vivo* and to behavioral paradigms known to induce myelin plasticity is unknown. For instance, it has not been explored whether axon diameter changes during learning as myelin does. Because fractional anisotropy, a commonly used marker of white matter microstructure in humans, increases with both increases in myelination and decreases in axonal diameter, axonal plasticity could also be compatible with multiple

results showing learning-related and experience-related changes in diffusion metrics in humans (Sampaio-Baptista and Johansen-Berg, 2017)) including alterations in the corticospinal tract following two weeks of sensorimotor deprivation (Langer et al., 2012).

It has even been suggested that Nodes of Ranvier may undergo plastic change. Like myelin thickness and axon diameter, a recent study by Arancibia-Cárcamo et al. (2017) suggested that Nodes of Ranvier (NoR) might also regulate features of an axon's neurophysiology. The article by (Arancibia-Carcamo et al., 2017) highlighted that the length of NoR is highly heterogeneous, but less variable within the same axon than between different axons, suggesting that NoR length may be regulated in a axon-specific manner. Moreover, the study used simulations to show that changes in NoR length may allow adjustment of axon conduction velocity with a smaller change in membrane area, and thus in a more energy-efficient manner, compared with myelin sheath changes. Given previous evidence that node diameter increases progressively in distal axon segments in the trapezoid body (Ford et al., 2015), the contribution of nodal features is especially likely to be relevant.

Taken together, this expanding range of plasticity mechanisms is key to our understanding of how adult brain plasticity could operate on a cellular level and sets the stage for further investigations into the circuit-level and behavioral relevance of such plastic changes.

## 1.4 The usefulness of motor learning paradigms to study basic rules of plasticity

In the face of what seems like an ever-expanding library of adult brain plasticity mechanisms, it becomes increasingly informative to integrate the study of biological plasticity mechanisms with the study of behaviour in rodents. In this respect, motor learning is particularly appealing as a behavioural test bed of plasticity, for several reasons: first, motor behaviour is relatively easily quantified; second, we can build upon a large literature on the physiology of the motor system across species; third, its basic principles might be generalisable across brain systems and may be reasonably well conserved across species. A further reason is that by studying motor learning, we can use well-established behavioural paradigms. Several motor tasks are available to study motor learning in mice, each with its associated pros and cons. In particular, the skilled reaching and the complex wheel paradigms have been influential in the past decade.

In the Skilled Reaching Task, the rodent is placed in a custom box where it learns to extend its paw through a slit, to grasp a pellet (in the case of a rat, or a millet seed in the case of a mouse) and then to bring it inside the cage, to its mouth. The paradigm and the sequence of movements are described in detail in Figure 1.5. This paradigm has been thoroughly characterised (Farr and Whishaw, 2002, Metz and Whishaw, 2000, Whishaw and Tomie, 1989) and has been used in several plasticity studies to date (Kleim et al., 2002, 2004, 2007, Rioult-Pedotti et al., 1998, 2015, Tennant et al., 2012). It is

particularly appealing as a model to study plasticity as it involves a specific body part, making it easy to compare the contralateral M1 area undergoing plasticity with other brain areas.

The Complex Wheel paradigm involves placing a wheel with missing rungs in the rodent's home cage. Once exposed to the complex wheel over days, a rodent learns not only a pattern of movements that allows them to run faster on the wheel, but also a general strategy that they are capable of applying to wheels with different patterns of irregularly-spaced rungs (McKenzie et al., 2014). Similar to skilled reaching, this paradigm also builds upon a large literature characterising it (Mandillo et al., 2014, Schalomon and Wahlsten, 2002) , and it is typically used as an assay to phenotype different strains of mice (Liebetanz and Merkler, 2006). A limitation of complex wheel studies is related to control conditions. A simple wheel (i.e. a wheel with no rungs missing) is often used as a control, but as animals may not always use the same patterns of movement with the same wheel type, it is a less accurate control compared to unskilled reaching, making the complex wheel a less specific test of motor learning compared to skilled reaching. Nonetheless, recent years have seen the successful adoption of the complex wheel as a less specific, but more scalable plasticity-inducing paradigm in a number of experiments (McKenzie et al., 2014, Xiao et al., 2016) .

Both Skilled Reaching and Complex Wheel have been used to study motor learning-related plasticity, but each comes with its pros and cons. The Complex Wheel has a more simplistic readout in its binary wheel movements and it can only capture whether the mouse performed the full sequence of

movements correctly. Skilled reaching is a more fine-grained assay and allows to measure each step individually, as well as having a precise control condition to characterize effects related to motor learning but not physical exercise. However, assessment of skilled reaching behaviour is laborious, takes place off-line (Chen et al., 2014), and it is often difficult to assess the final steps of reaching (e.g. whether the mouse has successfully eaten the millet seed, or dropped it, once the paw is inside the cage). Moreover, reaching takes places outside of the home cage, at regular times of day (Chen et al., 2014) so it is relatively un-naturalistic, whereas complex wheel running hijacks a spontaneous behaviour – in fact most animals like running on wheels when exposed to wheels in the wild (Meijer and Robbers, 2014). Finally, it is harder to teach mice a trial structure for reaching compared to rats (Chen et al., 2014, Kleim et al., 2002), which often results in multiple attempts per trial, making it difficult to assess accuracy. In practice, this makes the complex wheel paradigm more flexible and allows it to be deployed over larger sample sizes.

## 1.5 Summary of chapters by question

The thesis attempts to answer these two open questions, as follows:

1) Chapter 2 introduces the methods used in the thesis;

2) Chapter 3 and 4 build the methodology needed to tackle the questions;

3) Chapter 5 aims to answer the two open questions directly, with the methods developed throughout the thesis.

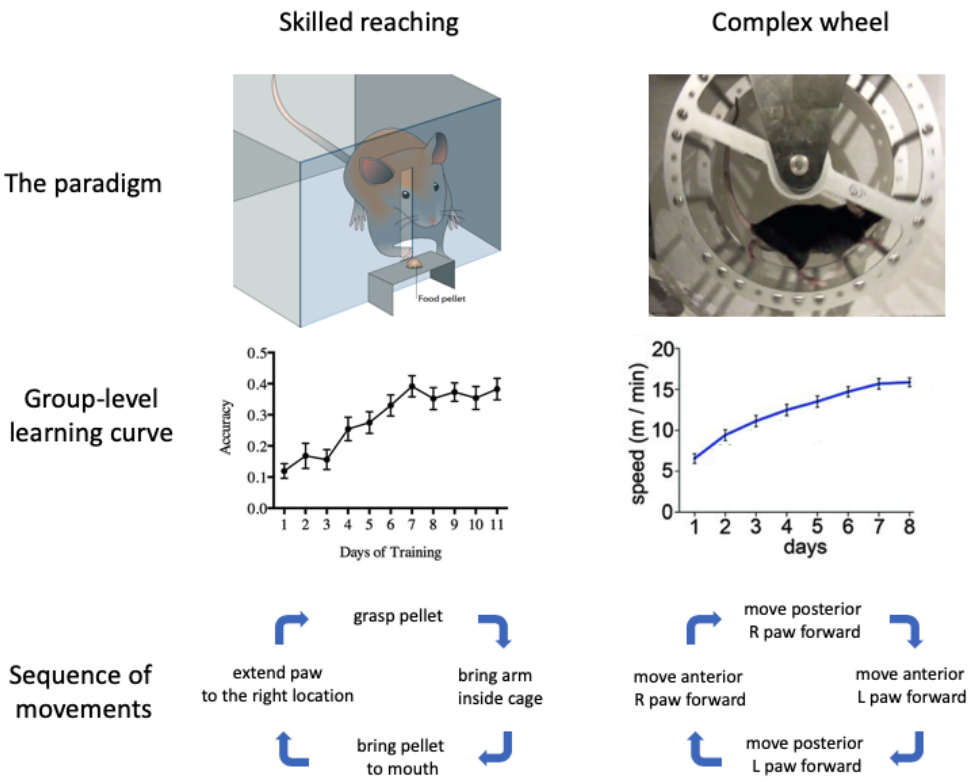


Figure 1.5: Motor learning: comparing running wheel and skilled reaching. Figures adapted from Fields 2015 and (McKenzie et al., 2014) and (Sampaio-Baptista et al., 2013).

# Chapter 2: Methods for investigating myelinated long-range projections

## 2.1 Tradeoffs in measuring myelinated long-range projections

What techniques can we use to study myelinated long-range projections? Compared to 30 years ago, we have an incredibly expanded arsenal of techniques at our disposal (Lerch et al., 2017), and we truly stand on the shoulders of giants in terms of technological developments to study the brain, especially when it comes to studying its long-range connections.

However, tradeoffs still abound in the measurement of myelinated long-range projections. As exemplified in Figure 2.1 and Figure 2.2, the principal limitation that concerns any technique is scale. One can use MRI, for instance, to probe connectivity between areas across the whole brain, but MRI cannot resolve individual nerve fibers, or even bundles of fibers. On the other hand, tracing can be used to map out the projections of specific cell types from any given area of the cortex, but it can be done only for one area at a time. To complicate things, non-invasive techniques have typically coarser resolution, generating a further tradeoff between investigating fine-grained details invasively in rodents and measuring coarser details but in naturalistic set-ups in humans.

This thesis uses a wide range of methods, but the majority of the work

has made use of coarser, non-invasive techniques (the techniques used are highlighted in green in Figures 2.1 and 2.2). Therefore, this introduction to the thesis Methods will focus on them.

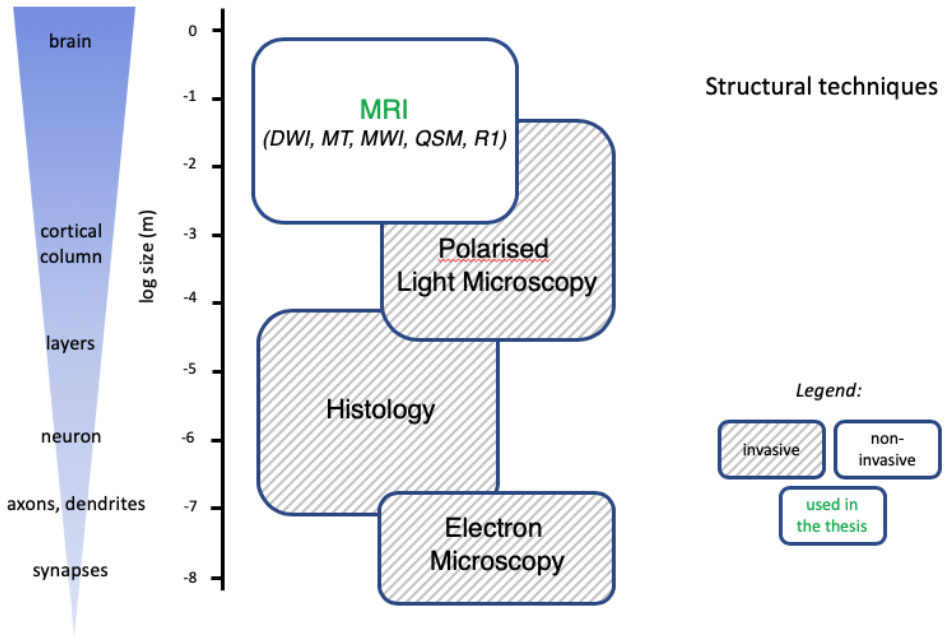


Figure 2.1: **Structural techniques to study myelinated long-range projections.** Multiple techniques are available to study the structure of long-range projections, but non-invasive investigations are only possible at lower resolution.

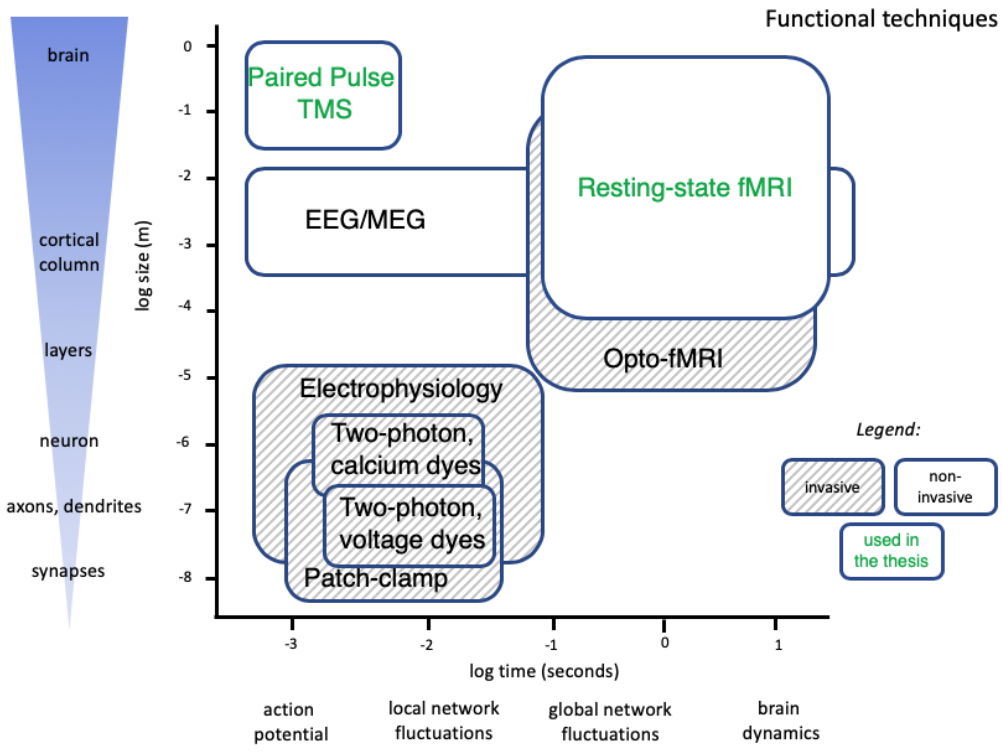


Figure 2.2: **Functional techniques to study myelinated long-range projections.** Multiple techniques are available to study functional and physiological aspects of long-range projections, but there is a trade-off between spatial resolution, temporal resolution, and invasiveness of the technique.

## 2.2 The rise of MRI

Magnetic Resonance is one of the most versatile and fast-developing technologies of the past 50 years, and the story of its development is arguably paradigmatic of the success and failures of multidisciplinary science. The field of research initially started with the discovery of spin and magnetic moment properties of atoms by Pauli in the 1920s, which was then harnessed to

develop Nuclear Magnetic Resonance (NMR) by Purcell and Bloch in 1945. After these seminal discoveries, however, the field stalled. Although NMR became widely employed in chemistry, no biological applications were further developed for two decades (Huettel, Song and McCarthy, 2004). Once it was realised that NMR could be used in biology, progress was rapid: Damadian developed NMR to get signal from biological tissues in 1971 (Damadian, 1971), and within a decade of that Lauterbur and Mansfield lead key hardware advances (the introduction of gradients (Lauterbur, 1973) and echo-planar imaging (Huettel et al., 2004, Mansfield, 1977, Stehling et al., 1991) respectively).

Once the technical limitations to developing images from MR were surpassed, it quickly became widespread in medicine for structural imaging in the 1980s (Huettel, Song and McCarthy, 2004). With this advancement, came also the realisation that MRI was a flexible enough tool to have wider potential applications. In particular, the late 80s/early 90s saw the advent of functional imaging(Bandettini et al., 1992, Belliveau et al., 1991, Kwong et al., 1992, Ogawa et al., 1990), while diffusion-weighted imaging (Basser et al., 1994, Moseley et al., 1990a) and other microstructural imaging techniques (Wolff and Balaban, 1989) were created around the same time, but only became more available and popular in the 00s and 10s respectively. Crucially, many of these techniques allow us to extract meaningful biophysical information about white matter and myelinated long-range projections, and the following paragraphs will aim to explain how, and to what extent, they are able to do so.

## 2.3 Resting-state fMRI

Resting-state fMRI takes advantage of the Blood Oxygen Level-Dependent (BOLD) effect. It does so by using a contrast sensitive to iron-sensitive dephasing (R2*-weighted) of the proton signal (Matthews and Jezzard, 2004), and measuring the change between oxygenated and de-oxygenated hemoglobin, which have different magnetic properties (Pauling and Coryell, 1936). When an area becomes active, its vasculature becomes richer in oxygenated hemoglobin. Less signal is lost due to paramagnetic de-oxygenated hemoglobin's induced dephasing, and more overall signal is detectable (Matthews and Jezzard, 2004). Like most traditional MRI techniques, fMRI is a qualitative technique, and hence it does not allow *quantification* of vascular parameters. Rather, it can track vascular signals over time and trace temporal patterns within them (Bandettini et al., 1992, Belliveau et al., 1991, Kwong et al., 1992, Ogawa et al., 1990).

fMRI can be used to track local fluctuations in blood flow during a task, but most of the signal, even during explicit task performance, is explained by intrinsic global fluctuations (Gratton et al., 2018). In fact, the topography of these resting-state fluctuations can even predict functional task-based activations (Tavor et al., 2016). A class of methods to quantify these fluctuations, which go under the umbrella of functional connectivity, take advantage of this fact to learn something about the brain.

### 2.3.1 What are we measuring with resting-state fMRI?

The term "connectivity" is often used when studying both structural and functional imaging. In many ways, connectivity between two areas is the conceptual flip-side of a long-range projection: a strong long-range projection between two areas means that there should be a strong connectivity between the two areas being connected.

In practice, "true" connectivity is not so easily measured. An intrinsic limitation of fMRI is that it does not allow to capture the whole landscape of brain activity, but rather it only captures broad population activity like LFPs (Logothetis et al., 2001), with gamma-range LFPs best explaining variation in BOLD signal (Magri et al., 2012) Crucially, an influential study has shown that, in the visual circuit, synaptic activity without associated spiking can also induce BOLD-like neurometabolic coupling (Viswanathan and Freeman, 2007). This suggests that it is in principle possible to measure the strength of synaptic connections between two areas by tracking their coordinated fluctuations. Studies comparing neuronal activity and neurovascular coupling across different brain areas have found this to be true, to an extent. Arterioles show ultraslow vasomotor fluctuations, which are entrained to an envelope of gamma activity (Mateo et al., 2017). While these coordinated vasomotor oscillations are diminished in absence of major tracts connecting them, its is also true that they are still partially present in complete absence of their underlying long-range projections (Mateo et al., 2017).

In conclusion, functional connectivity remains an indirect measure and

although they are highly correlated, there is no 1:1 relationship between rs-fMRI based functional connectivity and underlying axonal connectivity (Grandjean et al., 2017). Crucially, it has been shown that inducing Hebbian plasticity between two cortical areas increases their connectivity (Johnen et al., 2015), suggesting that rs-fMRI has the sensitivity to detect subtle changes in synaptic strength. When it comes to functional connectivity, this thesis takes a pragmatic approach: it deploys functional connectivity as an imperfect yet practical tool that is sensitive to synaptic strength as well as different biological factors, and interprets the results as a consequence of this.

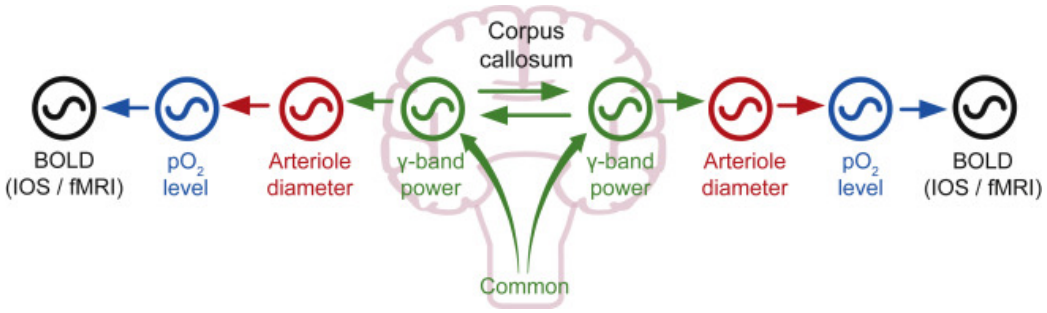


Figure 2.3: Schematic of a putative mechanism linking long-range projections, neurovascular coupling, and functional connectivity as measured by BOLD fMRI (Mateo et al., 2017)

## 2.4 Microstructural imaging

Microstructural imaging is an umbrella term used to refer to a heterogenous group of MR contrasts used to study White Matter (WM). In recent years, an increasing number of MR techniques have been successfully applied to study WM microstructure. As WM is dominated by myelinating oligoden-

drocytes, many of these techniques have focussed on detecting direct signals from myelin, which makes up the sheaths that envelop axons, or from iron, which is enriched in the cell body of oligodendrocytes. To adopt a similar framework to the one presented by (Heath et al., 2018), microstructural imaging techniques/modalities can be clustered into five broad categories:

1. Methods using water diffusion-based weighting (**Diffusion-Weighted Imaging, or DWI**).

   These methods take advantage of a phenomenon discovered in the early 1990s, whereby micron-scale diffusion in the brain, which is restricted by similar-scale biological structures, can be measured by applying diffusion gradients of different intensities and directions to a tissue, thus achieving biologically meaningful contrasts of the direction in which water diffuses (Basser et al., 1994, Chenevert et al., 1990, Cleveland et al., 1976, Doran et al., 1990, Le et al., 1993, Moseley et al., 1990a,b).

   Since then, enormous data acquisition advances, such as multiband imaging (Feinberg et al., 2010, Moeller et al., 2010, Setsompop et al., 2012), have taken place, making day-to-day collection of DWI data easier. This has resulted in an even larger increase in methods available to model and analyse such data. Given how indirect diffusion data is, these methods need to balance model assumptions with biological interpretability (Beaulieu, 2002, Jbabdi et al., 2012): some now well-established methods like tensor-based models (e.g. Diffusion Tensor Imaging (Behrens et al., 2003)) make few assumptions about the data,

but remain difficult to interpret (even in more complex iterations, such as Constrained Spherical Deconvolution based models and Apparent Fiber Density, or AFD (Tournier et al., 2007)). At the other end of the spectrum, multi-compartmental models like NODDI (Zhang et al., 2012) aim to model different compartments giving origin to the observed data, thus creating more interpretable results (e.g. about intra axonal vs extra axonal water diffusion), but in doing so they also make more assumptions about the data, which might not hold true across experimental contexts.

2. Methods taking advantage of the **Magnetisation Transfer (MT)** effect.

   Protons bound to macromolecules exhibit short T2 decay times, making their signal difficult to detect with standard protocols (Heath et al., 2018). This same family of protons, however, is also more sensitive to other MR frequencies, making it measurable using off-resonance pulses to produce a Magnetisation Transfer contrast (Wolff and Balaban, 1989), so called due to the transfer of energy from macromolecule-bound water protons to free water protons following the off-resonance pulse (Heath et al., 2018). This effect can be quantified by acquisition of two scans, one acquired with an off-resonance pulse and one without, and through calculation of a ratio between the two scans (Fralix et al., 1991). Multiple scans with a range of off-resonance pulse parameters can also be acquired, thus allowing detailed modelling of the MT effect

to calculate the relative size and fraction of macromolecule-bound to free water proton pool (Heath et al., 2018, Sled and Pike, 2001, Tofts et al., 2005, Yarnykh, 2002).

3. Methods mapping the magnetic **susceptibility** of the tissue

   This set of methods include T2* mapping, Susceptibility Weighted Imaging (SWI) and Quantitative Susceptibility Mapping (QSM) (De Crespigny et al., 1993, Haacke et al., 2009, Weiskopf et al., 2013). Although MRI protocols aim for homogenous phase alignments of protons, in practice the local composition of tissues often alters the phase alignment of protons. Though using different techniques, all these methods aim to quantify the local dephasing of the tissue in a given voxel. As shown in Figure 2.4, myelin is diamagnetic (reduces the dephasing of a tissue) while iron, which is present at higher concentrations in oligodendrocytes, is paramagnetic (increases the dephasing of a tissue) (Li et al., 2011, Schweser et al., 2012). This makes dephasing measurement methods unspecific, but versatile tools to study myelinated long-range projections.

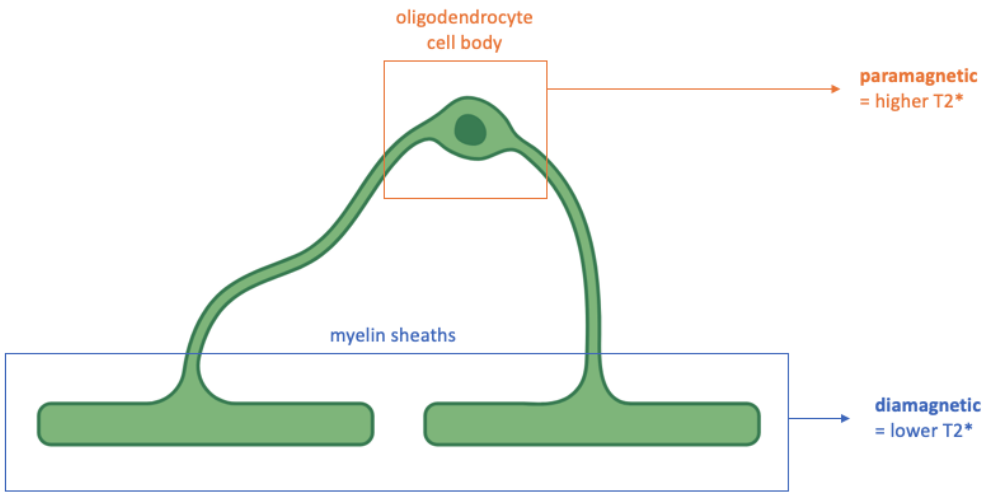


Figure 2.4: Opposing effects of different oligodendrocyte cell compartments on T2* values.

4. **T2-relaxation** based methods (often termed "relaxometry")

   These methods take advantage of the unique T2 relaxation time exhibited by the water in between the different layers of the myelin wrap (Mackay et al., 1994) (**Myelin Water Imaging, or MWI**) and have been shown to be effective in producing signals that relate to tissue myelination (Laule et al., 2007, Wood et al., 2016). However, these empirical results are in contrast with theoretical and simulation studies which highlight their limitations. The Multi-echo T2 model, for example, does not take into account exchange between compartments, which is likely to influence its estimates (Harkins et al., 2012, Levesque and Pike, 2009). Another influential alternative relaxometry model, multicomponent driven equilibrium single pulse observation of T(1)/T(2)

(mcDESPOT, (Deoni et al., 2008)), seems to be providing unstable estimates (Lankford and Does, 2013). As the literature on MWI is unclear (Heath et al., 2018), it was not adopted in the making of this thesis.

5. Methods using a diverse range of contrasts which produce sensible **cortical myelin maps**

   The methods include T1w/T2w imaging and R1 mapping, whose spatial distributions across the cortex have been found to match histology-based myelin atlases by (Glasser and Van Essen, 2011) and (Lutti et al., 2014) respectively. A validation study has shown that cortical GM and gyral WM R1 values are influenced by myelin (and to a smaller extent, by iron (Stueber et al., 2014)). While it is to be expected that contrasts which detect small regional differences in cortical myelin would be able to quantify myelin in the white matter, the usefulness of both contrasts to study White Matter fiber bundles is still to be explicitly tested.

### 2.4.1 What are we measuring with microstructural imaging?

All these techniques have been used to detect some key feature of myelinated long-range projections. However, since they arise from physical rather than biological signals (e.g. in the case of MT: macromolecules, rather than myelin *per se*), none of them are entirely specific to any given aspect of WM. This makes it crucial to test their sensitivity to a given aspect of WM in studies where both MR-based signals and biology-based signals are collected, i.e.

so-called "validation studies".

Magnetisation Transfer has been shown to relate strongly to myelination in a number of validation studies (Deloire-Grassin et al., 2000, Dousset et al., 1995, 1992), with some highlighting in particular the specificity of fraction of macromolecule-bound to free water proton pool measures (Heath et al., 2018, Ou et al., 2009, Samsonov et al., 2012). Diffusion-based Fractional Anisotropy (FA), on the other hand, has been shown to be sensitive to myelin (Aung et al., 2013, van Eijsden et al., 2011), but also to a number of other aspects of the cellular make-up (Zatorre et al., 2012) such as axon caliber, axon packing (Takahashi et al., 2002), fiber orientation (Wedeen et al., 2005), vasculature, neuronal and astrocytic cell swelling (Bai et al., 2016) just to name a few. Metrics from NODDI have also been shown to relate to myelin content (Grussu et al., 2017) and fiber orientation (Schilling et al., 2018), but as with many other diffusion models, NODDI has not received the same level of attention in validation studies as FA yet.

As with diffusion, R1 and R2* are not only sensitive to myelin, but also to other features of the tissue - in this case, iron content. R1 has been shown to detect spatial distributions of myelin in grey matter (Glasser et al., 2014). As explained above, it is sensitive to myelin in cortical GM and gyral WM (Stueber et al., 2014), but the degree to which it can pick up signals from WM myelin is still unexplored. In terms of their sensitivity to iron, reports of relationships between R1 and iron are sparse (Stüber et al., 2014), while R2* mapping has been validated as an iron marker in several validation studies (Sun et al., 2015). As expected from the physical

basis of R2*, dephasing-based signals correlate with iron and myelin(Heath et al., 2018, Langkammer et al., 2012, Stüber et al., 2014), they increase with myelin reductions and iron increases (Callaghan et al., 2014, Liu et al., 2011, Lodygensky et al., 2012), and they decrease with myelin increases and iron reductions (Li et al., 2014). That said, the picture is complicated by the fact that blood vessels, and specific areas of the brain, such as the basal ganglia, are also rich in iron, which constrains potential interpretations of effects arising from QSM/SWI/T2* images. It is also worth noting that both R1 and R2* have been reported to be more sensitive to myelin than iron (Argyridis et al., 2014, Stüber et al., 2014), but the relative sensitivity of R2* and R1 across different neuroanatomical locations and across experimental contexts remains an open empirical question.

As this thesis relied heavily on validation studies to aid interpretation of microstructural results, it is worth pointing out one of their key limitations. Although validation studies often aim to compare MR signals with 'ground truth' histological information, it is worth considering that all methods, including histology, have some inherent level of bias. For example, tissue processing techniques for electron microscopy may shrink tissues compared to MRI (Horowitz et al., 2015), and the relationship between the concentration of, say, myelin, and the histological signal associated with it may be different than its relationship with MR signal. In this context, it is clear that the more validation studies performed with independent histological techniques, the more reliable our knowledge of the biological bases of MR signals.

Used in combination, this treasure trove of MR techniques can help to

understand whether a given multimodal effect is likely to arise from e.g. myelination, oligodendrocytes, or fiber orientation, and thus moving towards a better biological interpretability of microstructural signals. This begs the question: how can we best combine this wealth of microstructural information? Methods to pool data from multiple microstructural modalities fall broadly into three categories (similarly to what has been described by (Cercignani and Bouyagoub, 2018)):

1. **Joint inference methods** perform independent statistical tests across all modalities, and pool p-values or effect sizes post-hoc through a predefined equation (e.g. Fisher, Stouffer, Tippett) (Winkler et al., 2014). The thesis has made heavy use of these methods, as they have the advantage of not making assumptions about the mathematical relationship between the different microstructural signals. However, they also have the disadvantage of potentially being less sensitive than methods using modality-weighting, or shared variance across modalities.

2. **Model-based approaches** aim to find an optimal combination of multimodal signals, often exemplified by a linear model, that can best match "ground truth" myelin signals as described with histology (Melbourne et al., 2014, Stikov et al., 2015, Stueber et al., 2014).

3. **Data-based approaches** aim to find shared variance across different modalities. This type of approach is less common in the literature, and most often relies on Independent Component Analysis (ICA) (Mangeat et al., 2015), or some variant of ICA which involves prior weighting of

different modalities (Groves et al., 2011, 2012). The strength of these approaches is that they can uncover common information present across different modalities, and in the case of a suite of myelin-sensitive modalities, this common information may be related to myelin (Mangeat et al., 2015). Finding common information across modalities can however be a double-edged sword: as well as uncovering common biological origins of the signals, ICA can also pick up noise that is common across modalities (Cercignani and Bouyagoub, 2018). For real-life applications, this is particularly likely to happen, as motion-driven degradation of signal is strongly subject-dependent and is likely to be related across modalities.

### 2.4.2 Thesis work related to microstructural imaging: quantitative MRI

As part of the work in the next chapters, the thesis author collaborated with physicists in Oxford to set up new modalities of microstructural imaging and validate that the new sequences were working as expected.

The key sequence used in every chapter of the thesis is called Multi-Parameter Mapping (MPM), which was developed as a way to efficiently estimate multiple quantitative parameters (R1, R2* and MT) through a single sequence (Helms et al., 2008, 2009, Weiskopf et al., 2011).

An important feature of MPM is that it allows quantitative mapping, i.e. contrasts where voxel values are meaningful and can be reproduced across different days and different scanners (Weiskopf et al., 2013), which is not the

case for any type of weighted images.

To confirm our MPM sequence was of the standard needed to measure myelinated long-range projections, we verified that similar qMRI values were found in the brain of the thesis's author across different days (Figure 2.5). Moreover, a pilot dataset on 18 subjects was collected, showing comparable subject-level and group-level Coefficient of Variance (CoV, Figure 2.5) between our dataset and the values reported by (Weiskopf et al., 2013).

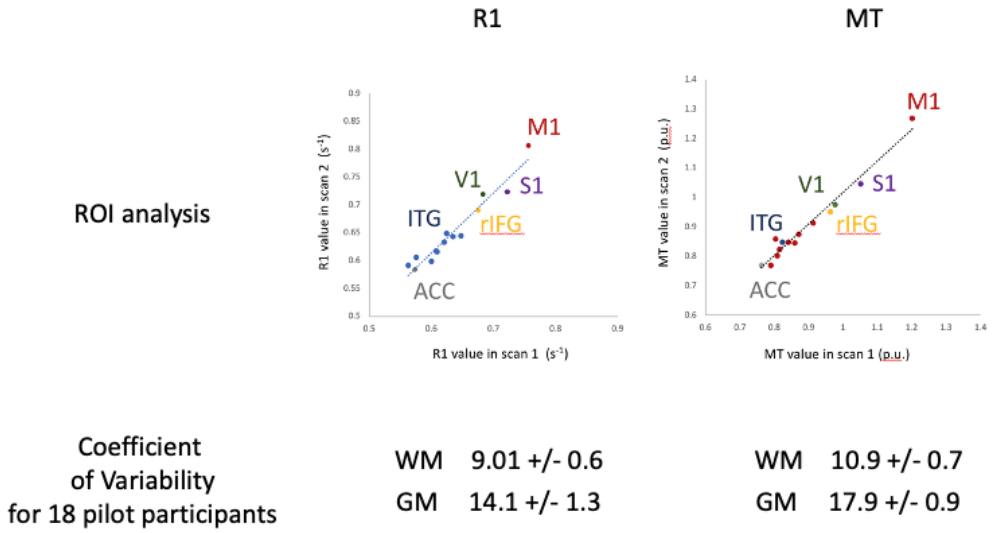


Figure 2.5: **Quality Control of the Multi-Parameter Mapping (MPM) sequence.** Top: We find that R1 and MT values from MPM have high test-retest reliability within the same scanner. Bottom: Coefficient of Variability (CoV) of White Matter (WM) and Grey Matter (GM) values from 18 participants are in line with previous reports on the MPM sequence.

## 2.5 Paired-pulse TMS (PP-TMS)

In the same decade as the MRI machines described above were starting to produce the first images of biological tissues, another application of magnetism in biology came to fruition: Transcranial Magnetic Stimulation (TMS). In the 1980s, it became increasingly clear that the human brain could be stimulated without needing to resort to invasive techniques. Merton and Morton made initial attempts to use electricity to induce neuronal activity non-invasively in the human brain and were succesful in eliciting the first so-called Motor-Evoked Potential (MEP) (Merton and Morton, 1980). However, the use of electricity also caused pain due to its interaction with the skin, and it was not until 1985 that a team based in Sheffield managed to achieve painless MEPs by means of a magnetic stimulator, the precursor of the TMS coils we now use in the lab (Barker et al., 1985, Hallett, 2007).

How does TMS stimulate the brain? The physics that allows TMS to work has been described at length elsewhere (Hallett, 2007). In terms of the neurobiology of TMS effects, it is widely believed that single TMS pulses induce an overall activation of neurons (Hallett, 2007) but most of what is known about TMS effects is from pragmatic approaches to measuring its indirect effects with EMG (Muellbacher et al., 2000), EEG (Ilmoniemi et al., 1997) and behavioural paradigms (Takeuchi et al., 2005, Tunik et al., 2005). More recently, mechanistic studies have shed light on the issue, and shown that TMS induces a transient increase in overall firing rate of neurons (Mueller et al., 2014), which is strikingly spatially restricted to an area of 2mm di-

ameter (Romero et al., 2019). However, these studies remain rare due to the considerable technical demands of having to combine TMS with invasive electrophysiology in animal models with similar cortical folding as humans.

Although question marks about the cellular-level effects of TMS remain, it is possible to use TMS for a wide variety of purposes while still being agnostic to its mechanisms. In the 1990s, researchers quickly understood the broad potential that non-invasive induction of brain activity could have for the study of the brain. For instance, a pair of TMS pulses can be delivered to the cortex, in order to measure the effect that the first one (Conditioning Pulse or CP) has on the second one (Test Pulse or TP). This effect depends on both their intensities and on the interval between them.

For example, a subthreshold CP (a CP that does not reach the intensity threshold to evoke an MEP) over primary motor cortex has an excitatory effect if delivered at 10-15 ms interval (called Intra-Cortical Facilitation, or ICF), but has an inhibitory effect if delivered at 1-5ms interval (called Short Interval Intra-Cortical Inhibition, or SICI) (Ziemann et al., 1996). To take a different example, inhibition can also be observed if the CP is suprathreshold and at a long enough interval to the TP (Long Intra-Cortical Inhibition, or LICI). These effects are extremely useful because it is clear that they reflect physiological processes of the motor cortex that can be studied across subjects (Stagg et al., 2011) and in different task conditions (Reis et al., 2008). However, their drawback is that their exact cellular underpinnings are unknown, and have only been explored through pharmacological studies (e.g. testing the effect of GABAA and GABAB antagonists on SICI and LICI

(Di Lazzaro et al., 2000, Werhahn et al., 1999)).

An important consideration for this thesis is that paired pulse approaches can be applied not just to a single location, but also to two separate ones, in order to better understand how activity in one area would affect activity in another one. This approach goes by a variety of names, but it is most often referred to as dual-coil paired pulse TMS, or simply ppTMS. ppTMS was initially established to study how the two primary motor cortices interacted (Ferbert et al., 1992) and was extended to interactions between premotor and motor areas in seminal work by (Civardi et al., 2001).

The early 2000s saw an explosion of work using ppTMS to characterise the physiology of areas connecting to M1. For example, a host of early studies found that PMv exerts inhibitory or excitatory effects over M1 during different types of gripping movements (Davare et al., 2008) and during action reprogramming compared to action selection (Buch et al., 2010). Moreover, the direction of the modulation also depends on the intensity of the conditioning stimulus (Bäumer et al., 2009). Similarly, PMd is facilitatory over M1 during specific stages of action selection(O'Shea et al., 2007), while it is inhibitory at rest (Koch et al., 2006). Taken together, these approaches can help build a picture of the motor system and its projections (Davare et al., 2010) in more detail than is possible, for instance, with resting-state fMRI, which does not allow to disentangle transient and directional interactions between areas.

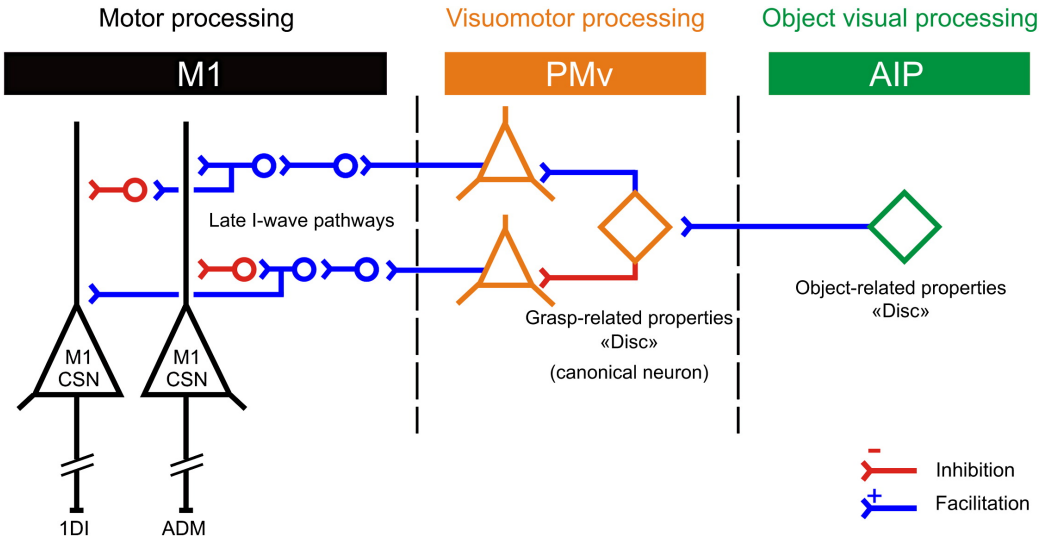


Figure 2.6: A TMS-derived model of motor network physiology. Image reproduced from (Davare et al., 2010)

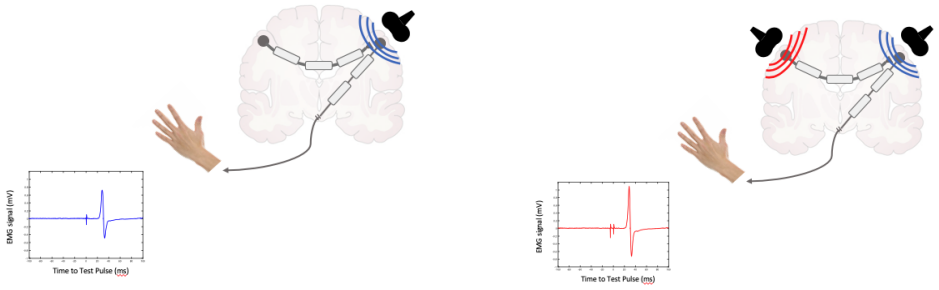

(a) Single Pulse condition (b) Paired Pulse condition

Figure 2.7: Schematic of how Paired Pulse TMS works. In a Single Pulse condition (SP, left) a test pulse (red) over left motor cortex elicits a Motor-Evoked Potential in the right hand; in a Paired Pulse condition (PP, right) the test pulse (red) is preceded by a conditioning pulse (blue) over right ventral premotor cortex. The ratio of hand Motor-Evoked Potential amplitude between the Single Pulse and Paired Pulse conditions (PP/SP ratio) can be used as a measure of cortico-cortical interaction.

### 2.5.1 What are we measuring with PP-TMS?

This thesis makes use of paired pulse TMS as a way to extract information about long-range projections that would be unavailable through other methods. As shown in Figure 2.2, paired pulse TMS stands out compared to other techniques in its capacity to detect long-range interactions on a broad spatial, but short temporal, scale.

This spatio-temporal resolution is both a blessing and a curse for those wishing to use the technique. On one hand, it allows to pick up brief cortico-cortical interactions that may be invisible to fMRI. On the other, this means that the same two areas may interact at specific, brief spans of time during a task, but may not interact in the same way if probed at a different timing during the same task (Mars et al., 2009). Moreover, the spatial breadth of the electric field generated by the TMS coil makes it difficult to target specific areas and to achieve fine control over the neuroanatomical area being targeted (Fox et al., 2012).

Another strength of ppTMS is its task and state dependency, which captures a more naturalistic aspect of how long-range projections work in real life. As highlighted before, this allows to identify brief interactions between cortical areas that may only happen during a specific task, as shown for PMd-M1 facilitatory interactions during specific stages of action selection(O'Shea et al., 2007).

However, the state-dependent nature of ppTMS also makes it less amenable to "validation" type approaches that are employed for MRI, as histology can

only be carried out *ex vivo*. One possibility to overcome this shortcoming is by using another non-invasive technique such as MRI, and draw correlations between ppTMS measures and MR-derived measures. This approach has generated a broad literature which confirms expected physiological links, for example between SICI/ICF and neuromodulatory metabolites (Dyke et al., 2017, Stagg et al., 2011), and between ppTMS with Diffusion-Weighted Imaging (Boorman et al., 2007, Groppa et al., 2012, Mars et al., 2009, Neubert et al., 2010). However, especially for approaches involving ppTMS with Diffusion-Weighted Imaging, all results reported in the literature are based on small sample sizes and exploratory approaches, while confirmation of these findings is still lacking (for a full discussion of exploratory and confirmatory analysis, see next sub-chapter).

In addition, ppTMS comes with a series of limitations that are not present for MRI (Fox et al., 2012). Not only is the approach limited to areas on the cortical surface, and to subjects that have a clear effect from the Test Pulse (e.g. the MEP or the phosphene, which are absent in a certain percentage of the population). It is not measuring connectivity in its physiological, natural state, given that TMS is associated with many effects that are difficult to mask (e.g. auditory stimulation from the click, skin sensation on the scalp), and most importantly, the cortical stimulation is an exogenous, non-naturalistic stimulus which may or may not produce results that are generalisable to naturalistic conditions (Fox et al., 2012).

## 2.6 The need for reproducible and open science

*'Replicating results is not glamorous, and falls far short of "understanding". But replicating your results is its own special kind of rush. The ability to replicate your phenomenon empowers you to embark on the grander quest of trying to understand it. Replication reveals your own control over the little speck of the universe that you are trying to understand. You are making it come and go at will. You are playing peek-a-boo with nature'* Nancy Kanwisher (Kanwisher, 2017)

The early 2010s have been a decade of particularly fast-paced transformation for all areas of science, and particularly for neuroscience. The fourth industrial revolution is still under way and has impacted all the facets of the scientific process, from data collection to data analysis to publishing of scientific results. Moreover, the years following 2012 have been particularly influenced by the reproducibility crisis, i.e. the growing worry and appreciation of the shortcomings in producing reproducible scientific results from much of modern scientific standard practices. These worries actually started being voiced already in the early 00s (Ioannidis, 2005) and a few years later the reproducibility crisis started being fully especially felt in cancer biology (Begley and Ellis, 2012) and psychology (Carpenter, 2012).

Although the causes and extent of the reproducibility crisis in neuroscience are still debated, it has had the undoubted effect of sparking a prolonged debate on improving research practices in the field. This thesis will not detail all the putative causes and promising solutions to the reproducibility

crisis, but among other, publication bias, (whether volitional or, more often, unknowing) p-hacking, underpowered studies, lack of data sharing, mixing of exploratory and confirmatory analyses - all these practices contribute to a skewed view of the phenomenon being studied. How to minimise these practices and maximise reproducibility is an equally controversial topic, but a few have gained traction: pre-registration, and data/code sharing, and increased sample sizes/power analysis.

The case for pre-registration has been debated at length (Nosek et al., 2018) and is robust. In a striking illustration of how profound the effects of pre-registration are on the reported results, a paper by (Kaplan and Irvin, 2015) has provided evidence that the introduction of a policy making clinical trial pre-registration compulsory increased the likelihood of null effects being reported, suggesting that without pre-registration, some of these null results might have not been reported, or even been reported as positive.

However, a key objection to pre-registration is that it is not practical for the workflow of most neuroscience projects: in many cases, especially when behaviour and physiology are the subject of the inquiry, there are too many free parameters to allow for a clear pre-registration of all fine details of the analysis before any preliminary exploration of the data (Poldrack, 2019). A relatively easy way to work around this problem, which is gaining ground in many neuroscience labs, is to run internal replication studies for each project. Internal replication involves collecting/using one *exploratory* dataset where all analysis details are piloted and finalised, and a second *confirmatory* dataset where the now finalised pipeline can be applied to the data to check

the robustness of potential findings. This approach might seem counter-intuitive - pooling together the two datasets would increase the statistical power of the overall analysis after all. However, this two-stage approach has the key advantage of preventing p-hacking and circular analyses, which have been described at length elsewhere (Kriegeskorte et al., 2009, Munafò et al., 2017) and present a key limitation of many studies in the literature.

Evidence about how data and code sharing impacts reproducibility is more scarce (Gøtzsche and Ioannidis, 2012, Munafò et al., 2017), but open data and open code practices have other intuitive and demonstrated benefits: they allow for the data's lifetime to be extended, and carefully crafted re-analysis of the data have the double benefit of both maximising the usefulness of the dataset and of functioning as a reproduction and quality check on the initial analysis (Munafò et al., 2017). Interestingly, a case study of data sharing in neuroimaging has even found that a data sharing initiative increased the amount of multi-disciplinary work carried out on the dataset's topic (Milham et al., 2018). Nonetheless, data sharing is still hindered by many practical hurdles (e.g. where to share data and how to ensure full anonymisation and compliance with ethics in the data sharing process), which at least partially explain the existing culture in human neuroscience and psychology, where datasets are typically sizeable and sensitive in nature, and data and code sharing are not consistently practised (Wicherts et al., 2006).

Finally, the limited statistical power in many studies has been a concerning topic that gained a lot of attention, especially in the field of neuroimaging.

Not only are underpowered studies less sensitive to true effects that might actually be present in the data; but they are also more likely to produce false positive results or disproportionately big effects, as explained in depth in an influential paper from 2013 (Button et al., 2013). This report sent shock waves through the neuroscience community, as low statistical power is a key factor in determining reproducibility of results, and many standard practices in the neuroscience community unintentionally lead to a reduced statistical power. One perhaps less well-appreciated example of this is the practice of 'increasing sample size until significance is reached' (as used in a recent paper which sparked controversy, (Weber et al., 2018)), which leads to repeated tests of the same hypothesis within the same sample, thus inflating the Type I error rate.

Therefore, as is probably obvious to any statistician, the only real way to test the right sample size for each study is to conduct a power analysis *before* the study is conducted. This approach seems appealing especially in line of further analyses of the original Button et al. (2013) paper (Nord et al., 2017), which suggest that statistical power ranges widely between subfields of neuroscience and thus that sample sizes should be dependent on the details of each study. However, this is often tricky to do for neuroimaging studies. For example, the studies in this thesis relied on new sequences, such as multi-shell diffusion imaging and multi-parameter mapping, which had not been extensively used for longitudinal studies in the past, making it difficult to conduct a power analysis and to predict what a realistic effect size might be. Basing the sample size on previous literature can be problematic (Poldrack

et al., 2017), but much of the work in this thesis have based their sample size on (De Santis et al., 2014), which are around n=10 for T1, between n=10 and n=50 for T2, and between n=20 and n=40 for FA.

In conclusion, some of these recommended measures were adopted in this thesis to ensure the reproducibility of the findings, as follows:

| | Data and code sharing | Blinding and Randomisation | Pre-registration | Internal Replication | Power Analyses |
|---|---|---|---|---|---|
| **Chapter 3** | Yes | N/A | Yes | No | No |
| **Chapter 4** | Yes | N/A | No | No | No |
| **Chapter 5** | Yes | Yes | No | Yes | No |

# Chapter 3: Heterogeneity in white matter's relationships with behaviour

## 3.1 Abstract

An established neuroimaging literature has reported extensive relationships between White Matter (WM) and behaviour. Although different features of the WM microstructure could underlie this, studies traditionally focus on an individual modality, often diffusion-weighted imaging (DWI), making it difficult to disentangle what biological aspects of white matter may drive WM-behavior relationships.

Here, we first assess the robustness of the relationship between DWI and behaviour. We build upon DWI-behaviour relationships reported in previous literature and test a pre-registered set of WM-behaviour correlations. Surprisingly, we find support for relationships between DWI and behaviour in only one of the three pre-registered tests, suggesting few DWI-behaviour relationships from the literature are easily generalisable.

As a second step, we then test the pre-registered WM-behaviour correlations across multiple modalities with different biological sensitivity profiles (DWI, Magnetisation Transfer, R1 and R2*), and look for common multimodal microstructural signatures that correlate with behaviour. While in some cases individual modalities correlate with behaviour, we find no evidence for consistent multimodal signatures. Rather, effect sizes of each modality differ considerably for each specific tract-behaviour relationship.

These results highlight a broad heterogeneity in white matter's relationship with behaviour, which may explained by variability in the biological effects shaping WM-behaviour relationships. This study demonstrates the

added value of multimodal imaging approaches, as different neuroimaging modalities might be best suited to detect different WM-behavior relationships. It also highlights practical limits to the possibility of developing a one-size-fits-all approach to study white matter-behaviour relationships, due to their inherent diversity.

## 3.2 Introduction

Human brains are strikingly variable, reaching up to two-fold variability in whole brain size in developing samples (Giedd et al., 2015, Reardon et al., 2018). Such variability represents not only a challenge to the study of the brain, making it harder to compare different individuals (Robinson et al., 2018), but also a potential opportunity, as different brain features could covary - and in fact have been reported to covary - with differences in behavioural performance across people (Boekel et al., 2015). This, it has been argued, could provide useful evidence about the relevance of different brain structures to the function of the brain. Since little is known about what aspects of brain biology most contribute to shaping human behaviour, drawing such brain-behaviour correlations is of great interest to neuroscientists, and has given rise to a substantial literature (Kanai and Rees, 2011).

Brain-behaviour correlations focussing on White Matter (WM) have gained particular attention in recent years (Johansen-Berg, 2010, Roberts et al., 2013). Once thought to be a static, uninformative relay of information between cortical areas of grey matter, the past decade has shown that WM, and in particularly the myelinated structures that dominate it, have more varied functions than previously thought, from trophic support of axons (Fünfschilling et al., 2012, Nave, 2010) to active regulation of physiological and behavioural processes (Kaller et al., 2017, Lazari et al., 2018, Steadman et al., 2019). These basic biology findings have opened the door to the possibility of studying WM as a way to better understand brain physiology and

behaviour, and also to the chance of targeting WM for therapeutic gain in brain-related disorders.

Conceptual advances hailing from basic biology have gone hand in hand with technological advances in brain MRI. The development of increasingly more sophisticated and robust sequences to perform diffusion-weighted imaging has allowed to uncover a large number of putative correlative links between WM diffusion metrics, most often Fractional Anisotropy (FA), and a wide range of behaviours (Boekel et al., 2015).

The presence of FA-behaviour relationships has been particularly clear for the corpus callosum and for the cingulum. The corpus callosum allows the nodes of the motor network in each hemisphere to communicate with one another, and both positive and negative relationships have been widely reported been callosal FA and various types of bimanual performance ((Johansen-Berg et al., 2007, Muetzel et al., 2008, Sullivan et al., 2001) and (Gooijers and Swinnen, 2014) for a comprehensive review of callosal-bimanual behaviour relationships). The cingulum, on the other hand, has been often implicated in cognitive control (Bathelt et al., 2019), and cingulum FA has been found to strongly correlate with performance on neuropsychological tasks (Metzler-Baddeley et al., 2012).

FA-behaviour relationships have also been thoroughly explored in behavioural paradigms that require inter-hemispheric transfer of information, as they would logically be expected to rely on long-range connectivity between inter-hemispheric areas. As mentioned above, bimanual motor performance has been the subject of much literature, and so has bilateral sensory

processing. In the visual domain, topographic organisation and visuospatial capacity have both been shown to relate to callosal microstructure (Saenz and Fine, 2010, Todorow et al., 2014). In the auditory domain, relationships have been established between perceptual acuity and WM microstructure, although mostly in pathology (Husain et al., 2011, Lin et al., 2008, Wang et al., 2019). While there have been no previous studies on WM relationships with somatosensory acuity, it would be logical to expect a similar relationship between somatosensory perceptual acuity and microstructure of WM in relevant tracts.

Although these studies provided seminal evidence for a link between WM and behaviour, two open questions persist regarding WM-behaviour relationships.

First, many previous studies, especially early studies using DWI, have focussed on exploratory analyses of relatively small datasets (Boekel et al., 2015). This means issues like publication bias (Turner et al., 2008) and under-powered analyses (Button et al., 2013) in the published literature may have inadvertently inflated the true effect size of DWI-behaviour relationships. Therefore, confirmatory, well-powered evidence on DWI-behaviour relationships is needed (Munafò et al., 2017, Nosek et al., 2018).

Second, DWI-behaviour relationships are also difficult to interpret. Diffusion signals are sensitive to a particularly broad range of tissue properties: myelination levels, fiber orientation, axon diameter, astrocyte and vascular morphology, just to name a few (Sampaio-Baptista and Johansen-Berg, 2017). Therefore, a given FA-behaviour correlation could arise from a size-

able diversity of microstructural patterns (Zatorre et al., 2012).

In recent years, an increasing number of MR techniques have been successfully applied to the study of white matter microstructure (Figure 3.1). As WM is dominated by myelinating oligodendrocytes, many of these techniques have focussed on detecting direct signals from myelin or from iron, which is enriched in the cell body of oligodendrocytes. Magnetisation Transfer, for example, allows to quantify the signal from macromolecule-bound water, and has been shown to relate strongly to myelination in a number of validation studies (Deloire-Grassin et al., 2000, Dousset et al., 1995, 1992). R2* mapping, on the other hand, allows to quantify local field distortion caused by iron, and has been confirmed as an iron marker by several validation studies (Sun et al., 2015). Many other markers are also available - R1 for instance has gained attention recently as a quantitative metric for myelin mapping, and although its effectiveness as a WM myelin marker has not been directly tested, it has been shown to detect spatial distributions of myelin in grey matter (Glasser et al., 2014).

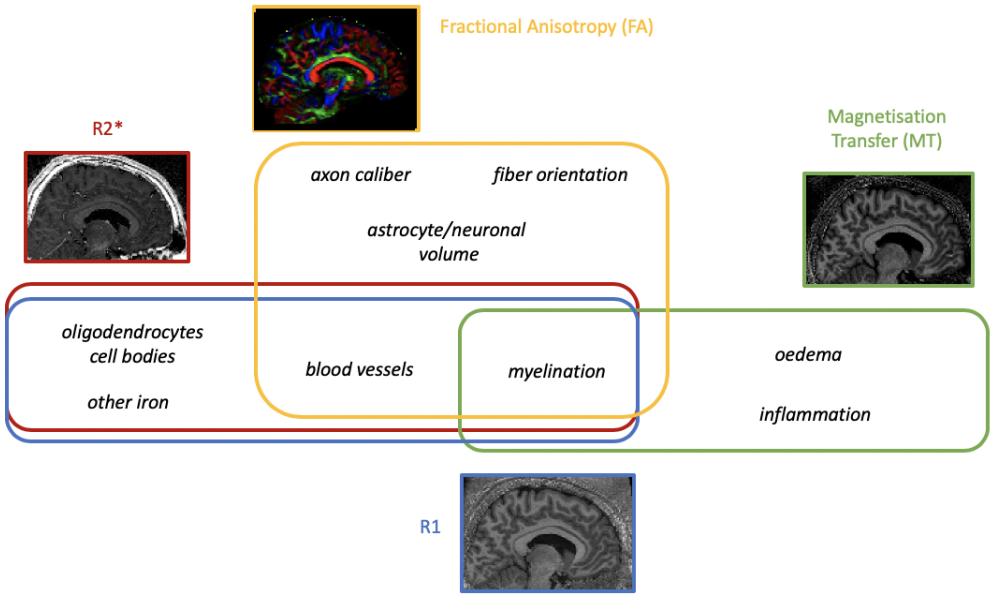


Figure 3.1: Each MR modalities is sensitive, but not specific, to different features of the biological tissue.

Used in combination, this treasure trove of MR techniques can help to move towards a better biological interpretability of microstructural signals. Multimodal data can be optimally combined to best match "ground truth" myelin signals as described with histology (Cercignani and Bouyagoub, 2018), and an "a priori" linear combination of modalities can be defined to enhance the biological specificity of inferences from multimodal data (Melbourne et al., 2014, Stikov et al., 2015, Stueber et al., 2014).

Applying these approaches to study WM microstructural techniques could be extremely helpful to clarify the mechanisms behind WM-behaviour relationship. It could allow to disentangle whether reported FA-behaviour correlations are driven by myelination, oligodendrocytes, or fiber orientation. In

turn, if all WM-behaviour relationships share a common biological mechanism, then establishing multimodal patterns related to behaviour could help build an a priori model of how to combine information from different modalities, with powerful implications for future studies looking at WM-behaviour relationships and biomarker development. As WM-behaviour studies to date have mostly consisted of unimodal approaches (Boekel et al., 2015), it is still unclear to what extent multimodal microstructural imaging can add explanatory value to WM-behaviour relationships.

To tackle these open questions around WM-behaviour relationships, we set out to:

1) Perform systematic, pre-registered testing of DWI-behaviour relationships.

2) Perform systematic, pre-registered testing of microstructural imaging across myelin-sensitive modalities to test WM-behaviour relationships.

3) Identify multimodal microstructural signatures which may provide insights into the underlying biology of WM-behaviour.

## 3.3 Methods

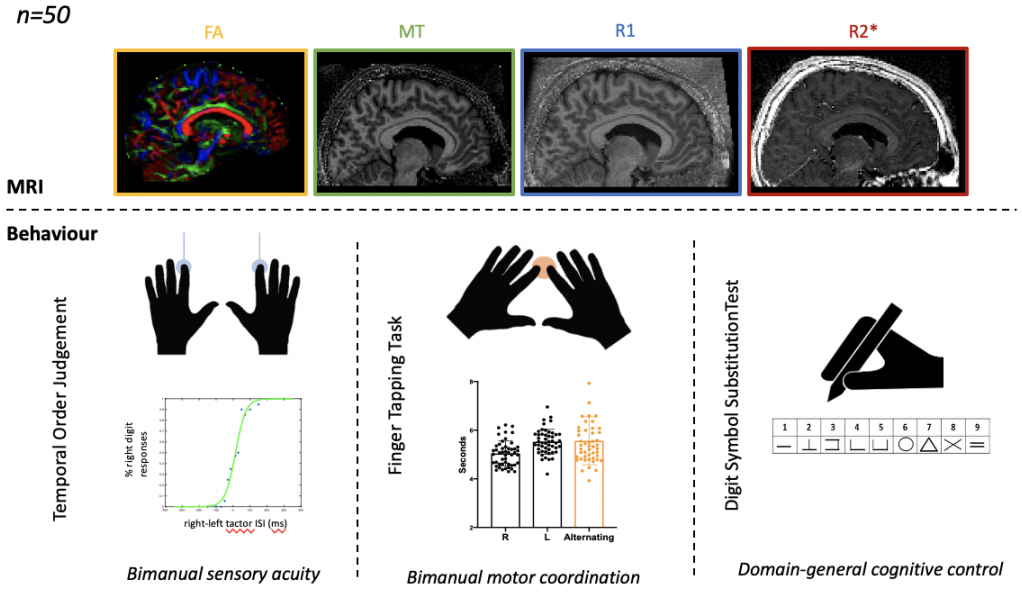


Figure 3.2: Summary of MRI and behavioural data acquisitions.

### 3.3.1 Participants

Figure 3.2 summarises the study design. 50 healthy participants (25 female; aged 18-38 years, mean 26.2 years, median 26 years) underwent a single session of behavioural testing and MRI on the same day. All participants were self-reported right-handed and their handedness was further assessed through the Edinburgh Handedness Inventory (Oldfield, 1971) (score range 60-100, mean 87.2, median 90). All participants were screened for MRI safety, received monetary compensation for their participation, and gave their informed consent to participate in this study. All study procedures were

reviewed and approved by the local ethics committee at the University of Oxford, and followed the Declaration of Helsinki.

### 3.3.2 Preregistration

Details of the task data collection and analysis plans were pre-registered on the Open Science Framework website (full pre-registration available here: https://osf.io/ar7zs/).

We report here some relevant text from the pre-registration: "Overall aim: testing whether previously reported correlations between behavioural measures and fractional anisotropy (FA) measures in long-range projections obtained using diffusion-weighted magnetic resonance imaging (dw-MRI) are related to indices of myelin content obtained using novel quantitative magnetic resonance imaging (qMRI) protocols. To this end, we aim to replicate a sample of previous studies, and extend these FA/behaviour analyses to myelin qMRI/behaviour analyses".

Specific brain/behaviour predictions were made for each task and these are given in the brain/behaviour anlaysis section below.

### 3.3.3 Behavioural tasks

A set of behavioural tasks was selected to build on prior studies that had reported relationships between behaviour and WM microstructure. Testing for a relationship between callosal FA and bimanual motor performance aimed to directly replicate a wide-ranging literature on the topic (reviewed by (Gooijers and Swinnen, 2014) ). Testing for a relationship between cingulum

FA and performance on neuropsychological tasks aimed to extend a previous finding in older adults by (Metzler-Baddeley et al., 2012) to a younger population. Testing for a relationships between FA in somatosensory tracts and somatosensory perceptual acuity aimed to extend previous findings in the visual and auditory domain, to the sensory system.

### 3.3.4 Alternating Finger Tapping (AFT) task

The finger tapping task aimed to test the participants' bimanual coordination. The task was based on (Muetzel et al., 2008) and (Pelletier et al., 1993) and ran as follows. Three blocks were repeated four times (the first one for training purposes): during the first block, participants were asked to tap their right index finger on a buttonbox (Current Designs, Inc., Philadelphia, PA) 30 times, as fast as they could (right monomanual condition); during the second block, participants were asked to tap their left index finger (left monomanual condition); during the third block, participants were asked to alternate between right and left index finger button presses (bimanual condition). For each block, after the 30 button presses were finished, the total elapsed time was fed back on the computer screen. The experimenter inspected the participant movement by eye to ensure they were correctly switching between fingers and that they were moving the finger rather than the hand. Participant posture and hand position was carefully kept constant throughout all blocks. 1 participant did not carry out the AFT due to a hardware problem.

### 3.3.5 Analysis of the Alternating Finger Tapping (AFT) task

Alternating Finger Condition (AFC) duration was extracted, i.e. average total time needed for 30 taps on the alternating finger condition (Muetzel et al., 2008). 3 participants were identified as outliers ( >3 SD away from the mean) and thus excluded from further analyses. Total time needed for 30 taps on the monomanual conditions was used as a covariate in group-level analyses, (Pelletier et al., 1993), together with age and gender.

### 3.3.6 Digit Symbol Substitution Test (DSST)

A paper-based Digit Symbol Substitution Test (DSST) was run as per https://healthabc.nia.nih.gov/sites/default/files/dsst_0.pdf. After training on substituting 10 digits for symbols, participants were asked to sequentially fill in the remaining 90 symbol-digit boxes in 90 seconds. The score was calculated as the total number of symbols filled in correctly by the end of the task. 2 participants were identified as outliers ( >3 SD away from the mean) and thus excluded from further analyses.

### 3.3.7 Temporal Order Judgement (TOJ) task

The Temporal Order Judgement (TOJ) task aimed to test participants' capacity to discriminate between two closely timed tactile stimuli delivered to the fingertips. The task was based on (Kolasinski et al., 2016) and ran as follows. A PC computer running a PsychoPy script delivered, via a USB 6501 card (National Instruments) and an amplifier (Tactamp, Dancer De-

sign), two asynchronous pulses to two vibrotactile stimulators (also known as tactors, Dancer Design) positioned within holes in a foam pad. The participant was asked to keep their hands relaxed on the foam pad, with their index fingers gently lying on the tactors. A piece of cardboard was used to block visual input from the tactors; similarly, headphones playing low levels of pink noise were used to block the auditory input from the tactors. Participants performed a two alternative forced choice (2AFC) task and were asked to press on one of two foot pedals, depending on the side of the pulse that they thought had come first. Participants were asked to respond within 2 seconds. If they did not respond within this time then no response was recorded and a new trial was started. They were also instructed that if it was hard to judge which pulse came first, they should just make their best guess. Intervals between pulses ranged from 0 to 300 ms. The task featured a practice session with 10 trials and a full session with 280 trials, for a total duration of roughly 12 minutes.

### 3.3.8 Analaysis of the Temporal Order Judgement (TOJ) task

After trials with no response were discarded, the number of right pedal responses were plotted as a function of inter-stimulation interval and a logistic regression was fitted to the data. At this stage, 6 participants were excluded as the logistic regression failed to fit the data correctly. The slope of the curve and the Just Noticeable Difference (JND) were used as key metrics of performance on the task (Kolasinski et al., 2016, Shore et al., 2005).

### 3.3.9 MRI data collection

Magnetic Resonance Imaging (MRI) data were collected with a 3.0-T Prisma Magnetom Siemens scanner, software VE11B (Siemens Medical Systems, Erlangen, Germany). Participants were asked to keep their head still and to wear earplugs during scanning in order to reduce the impact of MRI-related noise.The sequences were collected as follows: T1-weighted image (T1w), resting-stated fMRI (rs-fMRI), Multi-Parameter Mapping (MPM) and Diffusion-Weighted Imaging (DWI). MRI scan pre-processing, analysis and statistical comparisons were performed using FMRIB Software Library (FSL, v6.0), except for the MPM quantitative map estimation step which was carried out using the hMRI toolbox implemented in Matlab-based SPM, as described in (Tabelow et al., 2019).

The T1w sequence had a TR of 1900 ms, TE of 3.96 ms, a 1mm isotropic resolution and a large Field of View (FOV, 256mm) to allow for the nose to be included in the image and thus facilitate neuronavigation later on in the paradigm. The sequence used GRAPPA with an acceleration factor of 2.

The diffusion-weighted Echo-planar imaging (EPI)sequence had TR=3070 ms, TE=85.00 ms, FOV=256mm, voxel size=1.5mm isotropic, multiband factor of 4. Diffusion scans were collected for two b-values (500 and 2000 $s/mm^2$), over 281 directions. An additional 23 volumes were acquired at b=0, 15 in AP phase-encoding direction and 8 in the PA phase-encoding direction.

The MPM sequence (as per (Weiskopf et al., 2013)) included three multi-

echo 3D FLASH (fast low-angle shot) scans with varying acquisition parameters, one radio frequency (RF, or B1+) transmit field map and one static magnetic (B0) field map scan, for a total acquisition time of roughly 22 minutes. To correct for inter-scan motion, the position-specific receive coil sensitivity field was calculated and corrected for, as per (Papp et al., 2016). The three types of FLASH scans were designed to be predominantly T1-, PD-, or MT-weighted by changing the flip angle and the presence of a prepulse: 8 echoes were predominantly Proton Density-weighted (TR = 25ms; flip angle = 6 degrees; TE = 2.3-18.4ms), 8 echoes were predominantly T1-weighted (TR = 25ms; flip angle = 21 degrees; TE = 2.3-18.4ms) and 6 echoes were predominantly Magnetisation Transfer-weighted (MTw, TR = 25ms; flip angle = 21 degrees; TE = 2.3-13.8ms). For MTw scans, excitation was preceded by off-resonance Gaussian MT pulse of 4 ms duration, nominal flip angle, 2 kHz frequency offset from water resonance. All FLASH scans had 1 mm isotropic resolution and field of view (FOV) of 256x224x176 mm. The B1 map was acquired through an echo-planar (EPI)-based sequence featuring spin and stimulated echoes (SE and STE) with varying flip angles, FOV of 192x192x256 mm and TR of 500 ms. The TE for SE was 37.06 ms, while the TE for STE was 68.28 ms. The B0 map was acquired to correct the B1 map for distortions and off-resonance effects. The B0 map sequence had a TR of 1020.0 ms, first TE of 10 ms, second TE of 12.46 ms, field of view (FOV) of 192x192x256 mm and read-out bandwidth of 260 Hz/pixel.

### 3.3.10 MRI preprocessing

An automated custom pipeline based on existing FSL tools was developed for our diffusion sequence. The topup tool was run on average images of AP b0 volumes and PA b0 volumes. After applytopup was used to correct for the resulting susceptibility-induced off-resonance field, eddy was run (with flags optimised for multiband diffusion data) to correct for eddy currents and subject movement. To generate Fractional Anistropy (FA) maps, a diffusion tensor model was fit to each voxel through DTIFIT, with flags optimised for multi-shell data processing, such as the –kurt option.

MTsat, R1 and R2* quantitative maps were estimated through the hMRI toolbox (Tabelow et al., 2019). In order to register MPM volumes to FA volumes, we used the following steps. Boundary-Based Registration was used to calculate a DWI-to-T1w registration using AP b0 images (with high tissue boundary contrast). A customised pipeline was used to ACPC align the MPM maps and register them to T1w space. At this stage, 1 participant was excluded as the MPM scan was heavily corrupted due to movement artefacts; 1 participant was excluded due to lower quality signal in the MPM scan, which resulted in poor registrations with other modalities. Once registration matrices for MPM-T1w and DWI-T1w were calculated, they were inverted, concatenated and applied as needed to bring MPM volumes into DWI space with minimal interpolation. Registrations were assessed manually and one participant was excluded due to poor registration across all analyses.

### 3.3.11 Multimodal voxelwise analysis

To bring all volumes into a common space, native FA volumes were skeletonised with Tract-Based Spatial Statistics (TBSS), and the skeletonisation transforms were subsequently applied to MPM-to-DWI registered volumes. Group-level analyses were then conducted in skeleton space for all data.

All behavioural performance measures were normalised (through z-scoring or rank-based normalisation if z-scoring failed to produce a normal distribution) and correlations between MRI metrics and behaviour were assessed for each behavioural measure separately. Relevant text from the preregistered analysis plan is as follows:

Callosum and bimanual coordination: "We aim to replicate a reported relationship between callosal FA and AFC duration in the finger tapping task (Sullivan et al. 2001; Muetzel et al., 2008). We further aim to test for a relationship between myelin metrics in the corpus callosum and AFC duration"

Sensorimotor tracts and TOJ: "Performance on the temporal order judgement task is not associated with integrity of a single specific white matter tract, but rather with a set of tracts involving multiple sensorimotor areas. Accordingly, we plan to run exploratory analyses[...], testing for associations between JND/slope values and FA/qMRI."

Cingulum and neuropsychological tests: "We aim to replicate a reported relationship between two neuropsychological task measures ([...]number of substituted digits in the Digit Substitution test) and cingulum FA (Metzler-

Baddeley et al., 2012) in a sample of participants of on average a younger age range than previously reported, and to extend the protocol to investigate qMRI myelin/behaviour relationships."

Covariates of age, sex, and performance on control tasks (unimanual finger tapping speed for the bimanual finger tapping assay, and visuomotor speed for DSST) were included. For each behavioural assay, voxelwise analyses were restricted to voxels within a different predefined anatomical mask which was chosen from standard atlases included in FSL based on the a priori hypotheses: a callosal mask for bimanual coordination, a cingulum mask for the neuropsychological tasks and a mask of sensorimotor tracts for TOJ. The masks were derived from the JHU ICBM-DTI-81 Atlas, the JHU White-Matter Tractography Atlas and the Human Sensorimotor Tracts Atlas, respectively. Within these masks, multimodal analyses were conducted with voxelwise maps of FA, MT, R1 and R2*. Joint voxelwise inference across these MRI modalities, testing for correlations between MRI modalities and behavioural measures, was performed using Non-Parametric Combinations (NPC) as implemented in the Permutation Analysis of Linear Models (PALM) (Winkler et al., 2014, 2016) and correcting for multiple testing across modalities. Resulting z-score maps were thresholded using a cluster-forming threshold of 1.7 (equivalent to $p<0.05$, based on the degrees of freedom) and a corrected significance threshold of 0.05.

To systematically test for the presence of unimodal effects across all modalities, Tippett test was carried out as follows (with $p_k$ being each modality's p-value):

$$min(p_k) \tag{2}$$

To uncover common concordant trends across modalities, voxelwise joint inferences was performed, implementing a voxelwise Fisher test with the following equation (as described in (Winkler et al., 2016)):

$$-2\sum_{K=1}^{K} ln(p_k) \tag{3}$$

with $p_k$ being each modality's p-value and K being the total number of modalities being combined.

### 3.3.12 Estimation of effect sizes

As it is problematic to report voxelwise $r_2$ values (which cannot be corrected for multiple comparisons), or to report ROI-based effect sizes (which average many anatomically heterogeneous voxels within the regions of interest), we decided instead to report peak absolute t-statistics as a measure of effect size. This analysis was carried out to provide a clear visualisation of peak effect size for each pair of MR modality and behaviour. However, these values only highlight the voxel that correlates the most with behaviour and thus cannot be used as a substitute for unimodal statistical inference.

## 3.4 Results

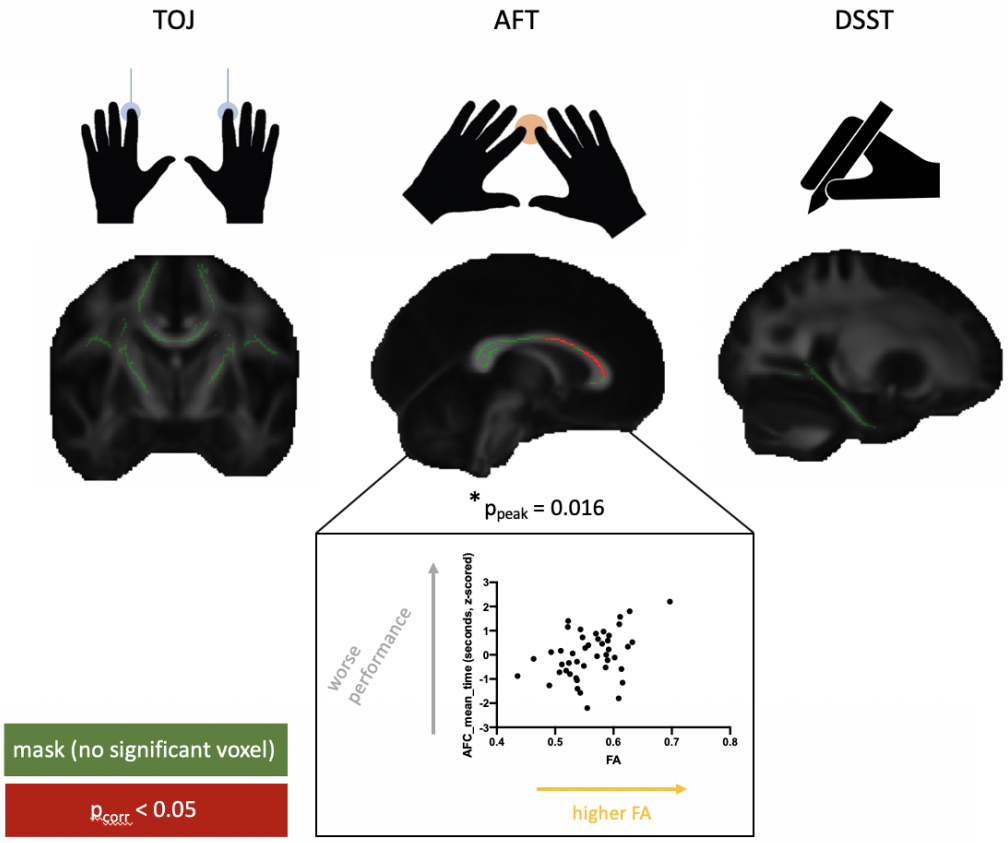


Figure 3.3: Unimodal relationships between FA and behaviour were tested across anatomical masks (shown in green) that were selected for each task. Results highlight that the Alternating Finger Tapping task (AFT), but not Temporal Order Judgement task (TOJ) and Digit Symbol Substitution Test (DSST) has a significant relationship with FA (red cluster shows voxels with corrected p-values below 0.05). Within that cluster, mean FA is extracted for each subject and plotted against performance in the scatterplot, that is for visual assessment of the correlation, rather than for statistical inference.

Unimodal analyses aimed to test for correlations between behavioural measures and DWI-derived FA (Figure 3.3). For both TOJ and DSST no relationships were found between behaviour and FA within tracts of interest (TOJ:

peak $p_{corr}$=0.08; AFT: peak $p_{corr}$=0.49). For AFT, a significant correlation was found between callosal FA and AFT performance (peak $p_{corr}$=0.016).

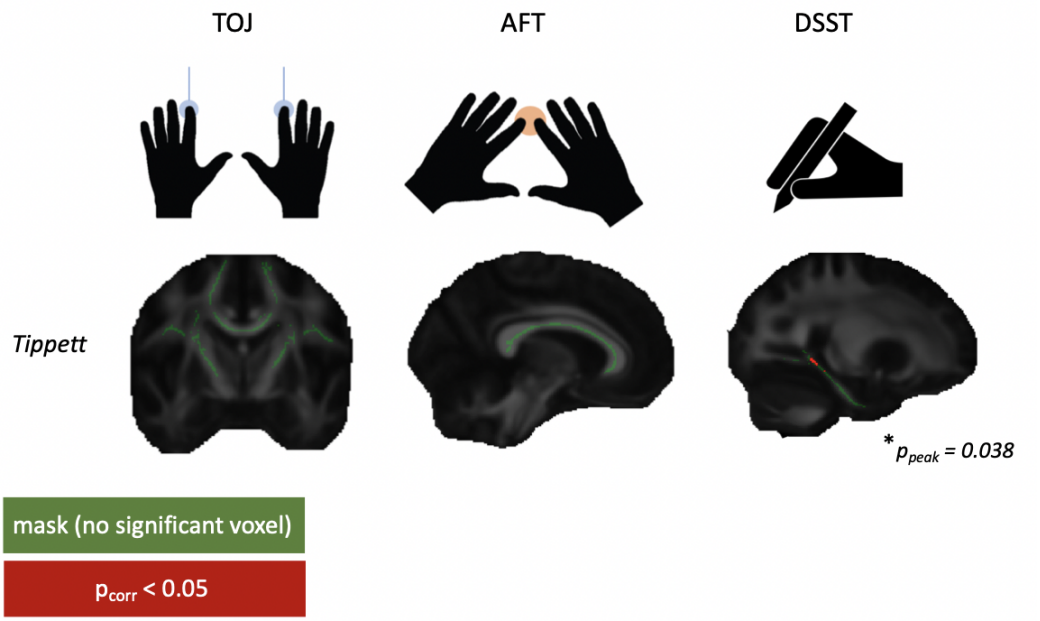


Figure 3.4: Multimodal relationships between WM and behaviour across MRI metrics (FA, MT, R1 and R2*) show that the Digit Symbol Substitution Test (DSST) has a significant relationship with cingulum WM. Only voxels with corrected p-values below 0.05 are reported.

Tippett multimodal analysis aimed to test for correlations between behavioural measures and each individual MRI metric (FA, MT, R1 and R2*, Figure 3.4). For both TOJ and AFT no relationships were found between behaviour and multimodal MRI metrics within tracts of interest (TOJ: peak pcorr=0.339; or callosum: peak pcorr=0.09). For DSST, a significant correlation was found between parahippocampal cingulum and DSST (peak $p_{corr}$=0.038), driven entirely by R1 (only modality with any voxel of $p_{corr}$

<0.05).

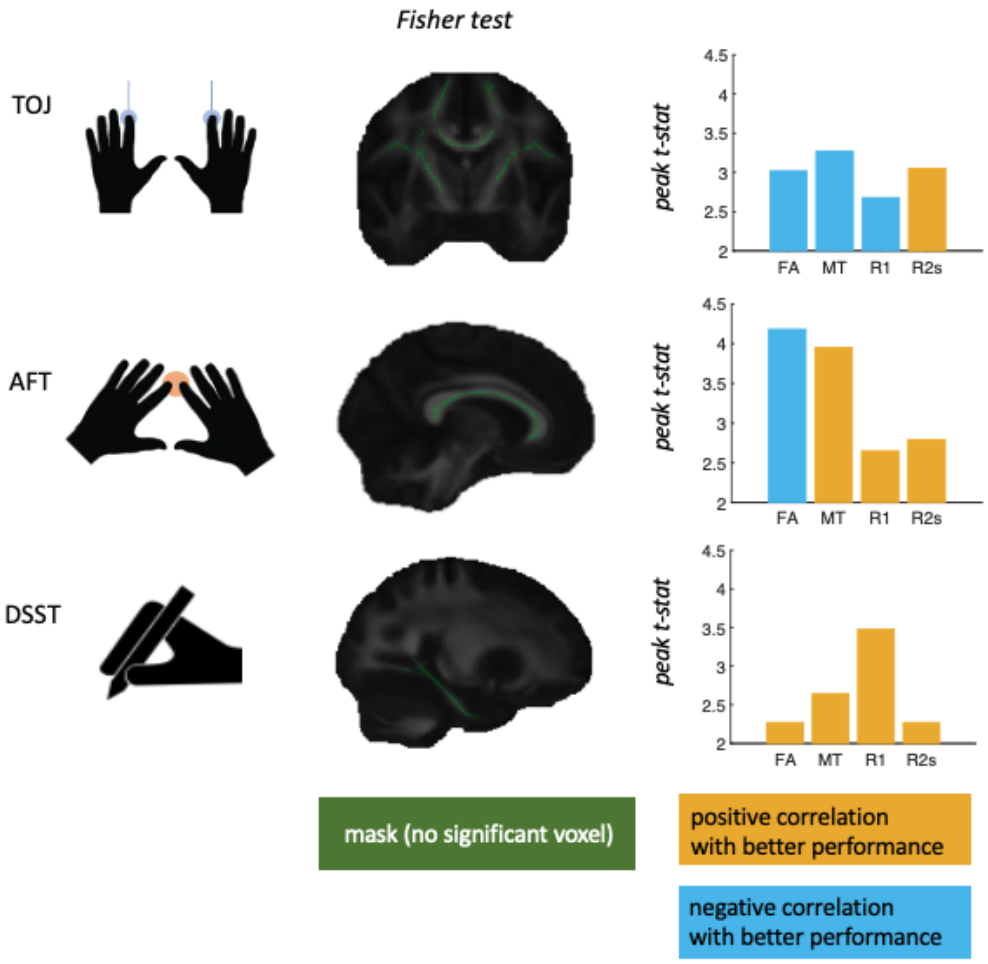


Figure 3.5: Lack of multimodal microstructural signatures relating WM to behavior for Temporal Order Judgement tak (TOJ), Alternating Finger Tapping task (AFT) and Digit Symbol Substitution Test (DSST). A Fisher test was used to test for multimodal microstructural signatures relating WM to behavior but no significant effects were found (middle column). Effect sizes are reported for each modality-behaviour correlation, as measured by peak absolute t-statistic (right column).

Fisher analysis aimed to test for multimodal microstructural signatures between behavioural measures and multiple MRI metrics (FA, MT, R1 and

R2*, Figure 3.5). For all tasks, no relationships were found between behaviour and multimodal MRI metrics within tracts of interest (TOJ: peak $p_{corr}$=0.532; AFT: peak $p_{corr}$=0.184; DSST: peak $p_{corr}$=0.2).

To further understand why no common microstructural signature was found, despite the significant correlations between FA and AFT and between R1 and DSST, we interrogated the effect sizes of each of the modality-behaviour correlations. We find that within each WM-behaviour correlation, each modality is associated with a different *size* and *directionality* of statistical effect. Strikingly, modalities are associated with differential *size* and *directionality* of statistical effect also across WM-behaviour correlations, and the modality that correlates most with behaviour differs for each behaviour: it is MT for TOJ, FA for AFT and R1 for DSST.

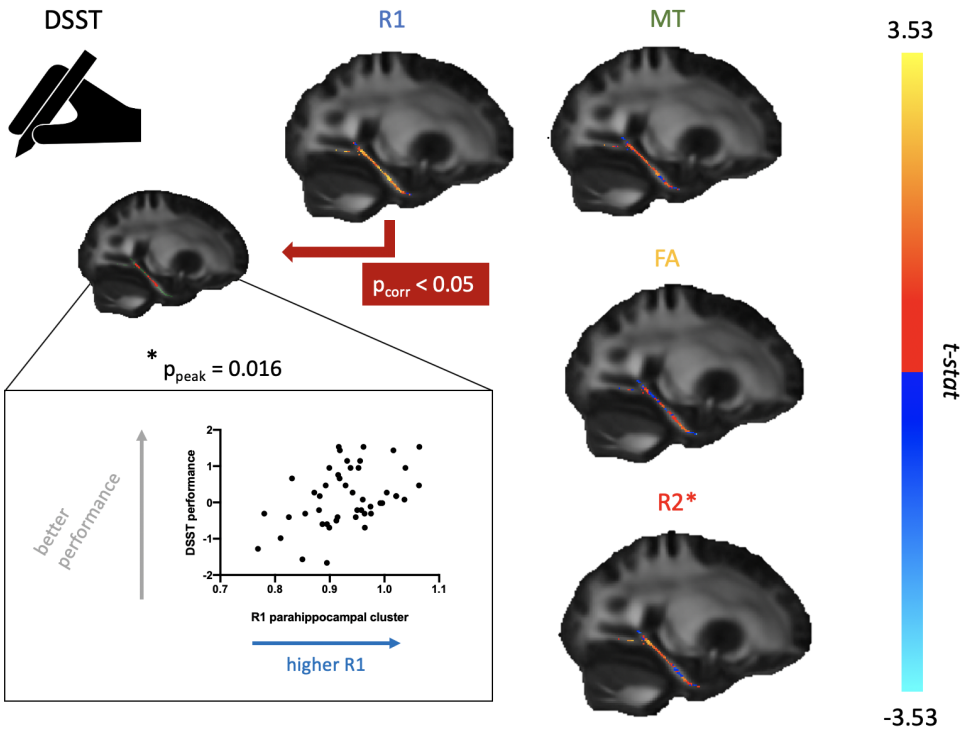


Figure 3.6: Correlation between DSST performance and cingulum microstructure, reported as univariate results. For each modality, unthresholded t-statistics are visualized according the colour bar (right). For R1 only, a cluster of voxels survived the threshold of p <0.05. Average R1 values within that cluster are shown against performance score in the scatterplot, which is presented for visualisation and is not used for statistical inference.

For completeness, we also report analyses of this dataset using "traditional" univariate approaches, considering each modality separately. We find that if each modality-behaviour correlation was run as a separate analysis, each behaviour would show significant correlation with one modality, without correcting for multiple comparisons across modalities (Figures 3.6, 3.7, 3.8).

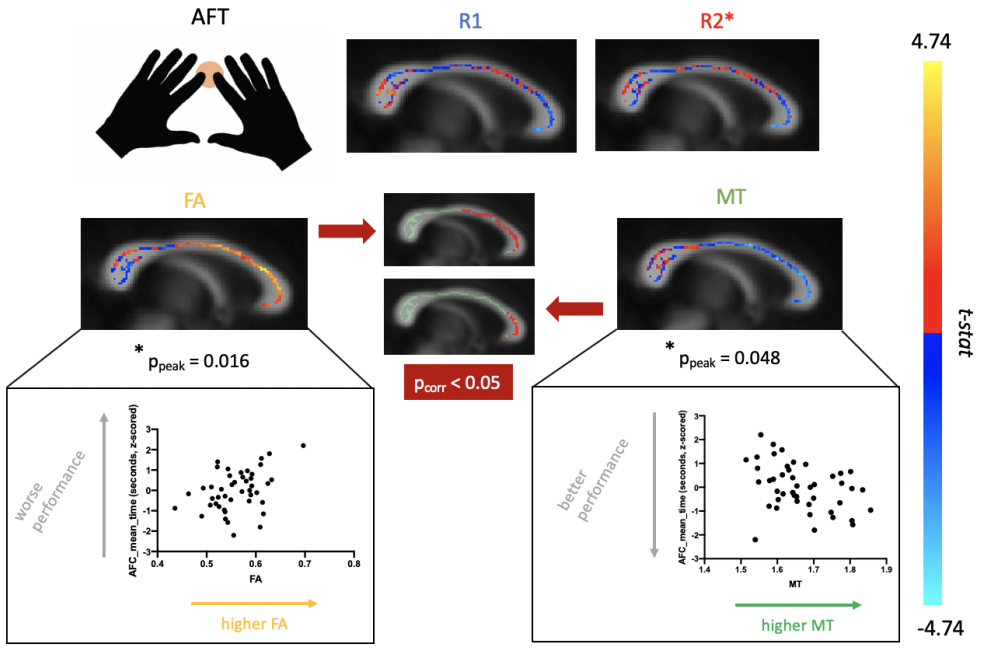


Figure 3.7: Correlation between AFT and callosal microstructure, reported as univariate results. For each modality, unthresholded t-statistics are visualized according the colour bar (right). For FA and MT, clusters of voxels survived the threshold of $p<0.05$. Average FA/MT values within that cluster are shown against performance score in the scatterplots, which are presented for visualisation and are not used for statistical inference.

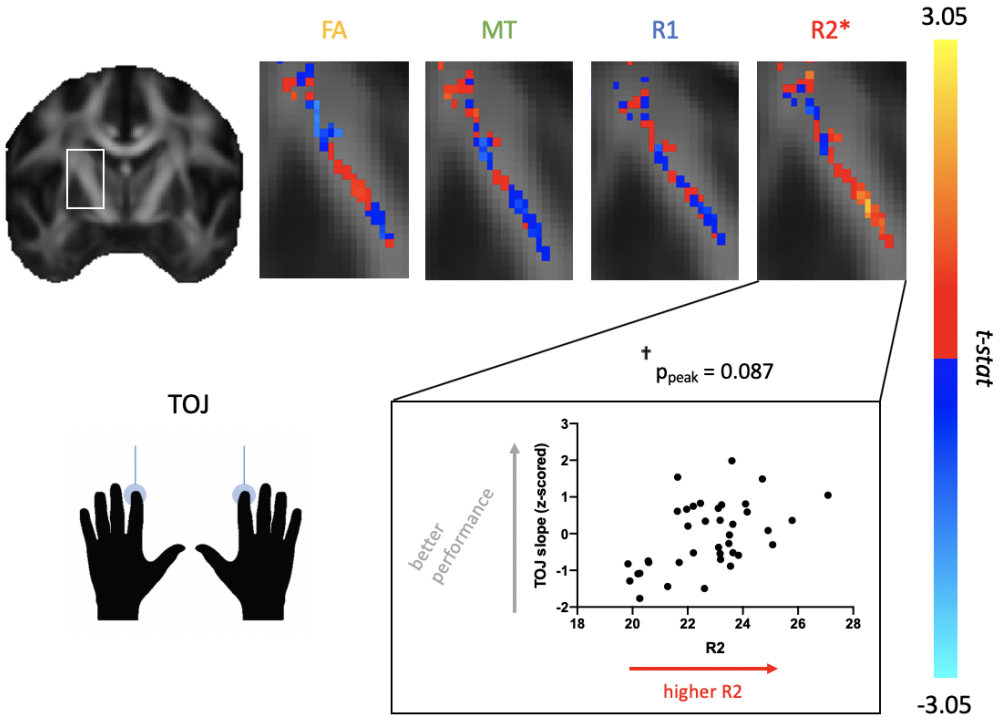


Figure 3.8: Correlation between TOJ performance and CST microstructure, reported as univariate results. For each modality, unthresholded t-statistics are visualized according to the colour bar (right). For R2* only, a cluster of voxels reached p=0.087. Average R2* values within that cluster are shown against performance score in the scatterplot, which is presented for visualisation and is not used for statistical inference.

## 3.5 Discussion

Our first aim was to probe the robustness of the relationship between DWI and behaviour. We find a unimodal correlation between the corpus callosum and bimanual coordination, in accordance with previous literature (Bathelt et al., 2019, Gooijers and Swinnen, 2014, Johansen-Berg et al., 2007, Metzler-Baddeley et al., 2012, Muetzel et al., 2008, Sullivan et al., 2001), but a robust relationship between DWI and behaviour is identified in only one out of three analyses. This can be due to several reasons. One possible explanation is that effect sizes reported in previous studies might have been overinflated due to publication bias (Turner et al., 2008) and under-powered analyses (Button et al., 2013). However, it is worth noticing that only the FA-AFT experiment, which successfully identified a DWI-behaviour relationship, was a direct replication of the previous literature, whereas the other correlations were inspired by previous findings, but did not aim to precisely replicate experimental conditions and analysis steps. This suggests that relationships between FA and behaviour that have been established in the literature may be robust and replicable, but it needs to be better understood in which circumstances they can be extrapolated to different populations, for example to different age groups.

A second aim of the study was to probe whether multimodal MR can provide additional information on WM-behaviour relationships. We find that this is the case in at least one of the WM-behaviour relationships we tested: R1 correlates with DSST performance, which allows to identify a

WM-behaviour relationship that would have been out of reach by using FA on its own. This confirms that there is value in multimodal imaging, as some modalities can detect relationships that are inaccessible to other ones.

A third aim was to test whether there are common multimodal microstructural patterns in WM-behaviour relationships, which may provide insights into the underlying biology. We fail to find robust evidence for multimodal effects and cross-modality signatures. Rather, we find that effect sizes and directionality of effect in the relationship between each modality and each behaviour are highly heterogeneous. This means that MR modalities in each tract not only show heterogeneity in how they relate to the same behaviour, but also depending on which tract-behaviour correlation is being analysed.

A key insight from the study is therefore that the relationship between WM and behaviour is highly varied. Given that each modality has a specific pattern of sensitivity to the underlying biology, the results suggest that different aspects of WM biology may be driving different WM-behaviour correlations. There are two prominent sources of biological heterogeneity in white matter, which are likely relevant to the results in this study.

One driver of heterogeneity may be at the level of myelination itself. As all the sequences we used are sensitive to myelin, we expected that if myelination was responsible for WM-behaviour relationships, a common multimodal pattern across all relationships could be identified. While the results run contrary to our hypothesis that amount of myelination in a tract would relate to behaviour, they do align with recent advances in cellular biology. In recent

years histological studies have increasingly highlighted the heterogeneity of features in the myelinated axon, which can vary independently of each other (Almeida and Lyons, 2017). For instance, we know that Nodes of Ranvier, myelin sheath thickness, myelin sheath length, and number of myelin sheaths, can all independently affect an axon's physiological properties, which one would expect to in turn shape behaviour (Kaller et al., 2017). As all these parameters influence the overall amount of myelin in a given voxel, it is possible that different aspects of the myelinated axon may be driving different WM-behaviour relationships that were observed in this study, which would explain the lack of common microstructural patterns across tests compatible with a simple effect of total myelin content in the areas of interest.

A second important driver of heterogeneity is non-myelin features of WM. As exemplified in Figure 3.1, while all sequences we used are sensitive to myelin, some are also sensitive to fiber orientation (FA), and some are sensitive to iron and vasculature (R1 and R2*). Therefore, one possible interpretation of the data is that the relationship between AFT performance and the corpus callosum is highly influenced by fiber orientation, whereas the relationship between the DSST performance and the cingulum is shaped by vasculature. Previous studies have highlighted that both fiber orientation (Chang et al., 2017, Wedeen et al., 2005) and vasculature (Licht et al., 2011, Rhyu et al., 2010, Thomas et al., 2016) are important for brain function, and our data thus draws further attention to the fact that these factors may be influential in WM-behaviour relationships.

When combining these two factors together, it is unsurprising that there is

no single aspect of WM which drives behaviour. Rather, our findings confirm that heterogeneity at the cellular level is reflected in neuroimaging markers, leading WM-behaviour relationships to be driven by a variety of mechanisms, rather than a unitary effect. Importantly, this emphasizes that there is no single modality or single combination of modalities which is optimal to study WM-behaviour relationships. In this respect, our study poses practical limits to the possibility of developing a one-size-fits-all approach to study white matter-behaviour relationships, due to their inherent diversity.

While this heterogeneity means it is not straightforward to predict which MR modality is best suited for each study of WM, it also suggests that multimodal studies of WM should tailor their MR sequence protocols and analyses pipelines to privilege markers and statistical approaches that can test and compare biologically-driven models. For example, with an appropriate acquisition sequence and a joint multimodal statistical framework, one might be able to test whether a given WM-behaviour correlation is driven by myelination, vasculature (Thomas et al., 2016), or connectivity (Sui et al., 2014).

Moreover, the direction of observed effects is also informative. In this study, the correlation between R1 and DSST performance follows the same direction as previous literature (Metzler-Baddeley et al., 2012), with higher R1 correlating with better performance, indicating that there might be a robust correlation between cingulum microstructure and cognitive control, and that different markers may be most sensitive to this correlation in different contexts. By contrary, AFT performance correlated negatively with FA - as

expected by previous studies (Gooijers and Swinnen, 2014, Sisti et al., 2012) - but positively with MT. These two opposing correlations could be explained by larger callosal axons leading to better AFT performance, as that would lead to negative correlations with FA (larger axons have less restricted diffusion) and positive correlations with MT (larger axons have more myelin because of the constant g-ratio). Such approaches, taking into account multiple modalities and the directionality of their correlations with behaviour, are most likely to generate further insights into WM-behaviour relationships in the future.

One key limitation of the study is that the results cannot disentangle to what extent neuroanatomical heterogeneity in WM contributes to the observed diversity of WM-behaviour relationships. One could argue, for example, that our results demonstrate that FA is more important for WM-behaviour relationships involving the corpus callosum, whereas R1 is more important in studies about cingulum and MT/R2* are more important in investigations of the corticospinal tract. Because each of the behaviours we selected relates to a different WM tract, this makes it impossible to disentangle whether different kinds of behaviours are most strongly driven by different microstructural patterns, or whether there is neuroanatomical heterogeneity in the importance of different microstructural features of each tract. Although both are likely to matter, further studies relating individual tracts to multiple behaviours will be needed to answer this question.

The results also hold useful lessons for statistical aspects of future multimodal studies of WM. WM-behaviour correlations often have small effect

sizes, and in our results we find that these effects are sometime not detected when multiple hypotheses are tested concurrently. Back-of-the-envelope calculations can easily show that testing for effects across modalities increases the false discovery rate proportionally to the number of modalities tested, and thus needs to be adequately corrected for in order to reach appropriate interpretations. However, while multiple comparison correction has long been the gold standard statistical advice, multimodal brain imaging studies often do not report whether, and if so, how, correction for multiple comparisons was carried out (Bezukladova et al., 2020, Winston et al., 2020). Surprisingly, even gold standard guidelines in the field like COBIDAS do not report best practices for statistical reporting in multimodal imaging (Nichols et al., 2017), and many packages that support multi-modality statistical testing do not allow to perform joint statistics, thus leaving room for needless analytic flexibility. Our results suggest there is a need for increased transparency in reporting of multimodal statistics, which statistical guidelines on multimodal imaging might facilitate in the future. In this respect, our results also add weight to previous calls to pre-register what modalities are being used in a given analysis (Picciotto, 2018), and to report all tested modalities in publications.

This aspect of statistics in multimodal studies also needs to be further taken into account when assessing the power of a given analysis. Compared to unimodal studies, multimodal studies require multiple statistical tests across modalities. Therefore, for the same effect size, a multimodal study may need more subjects to achieve the same power, and it is important to take this

into account in power analyses. We thus recommend using larger sample sizes for multimodal compared to unimodal studies. We also advise that in scenarios where multimodal data is available but only powered for unimodal tests, resorting to dimensionality reduction techniques (Groves et al., 2011, Sui et al., 2014) may help to preserve statistical power.

In conclusion, these results highlight a broad heterogeneity in white matter's relationship with behaviour. They also underscore the added value of multimodal imaging approaches, as different neuroimaging modalities might be best suited to detect different WM-behavior relationships. However, this added value needs to be weighted carefully against the need for more power and/or dimensionality reduction approaches in multimodal studies. Finally, the results effectively limit the possibility of developing a one-size-fits-all approach to study white matter, and suggest that different aspects of WM biology may be driving different WM-behaviour correlations.

# Chapter 4: A macroscopic link between tract myelination and tract physiology during behaviour

## 4.1 Abstract

Myelination of long-range projections is increasingly being implicated in function and dysfunction of the human brain. Although it has been argued that the amount of myelination in a tract influences its physiological properties, there is a dearth of empirical evidence on how myelination in a circuit shapes its physiology and the resulting behaviour in humans.

Here, we hypothesise that physiological interactions between two brain areas may be shaped by the amount of myelin in the tract connecting them. As a test bed for this hypothesis, we use a well-defined motor circuit (ventral Premotor Cortex projections to Primary Motor Cortex). We combine millisecond-level TMS-derived measures of cortico-cortical interactions during action reprogramming with multimodal myelin markers (MT, R1, R2* and FA), in a large cohort of healthy subjects.

We find that metrics of physiological premotor-to-motor connectivity correlate broadly with multiple myelin markers, suggesting interindividual differences in myelination may play a role in motor network physiology. Moreover, myelination metrics do not directly relate to action switching behaviour or to local M1 dynamics during action reprogramming, but rather they relate to physiological connectivity, which links indirectly to action switching by influencing local M1 dynamics.

These findings suggest that myelination may influence millisecond-level cortico-cortical interactions during tasks. They also unveil a link between physiology of the motor network and the myelination of tracts connecting its

components, and provide a mechanism mediating the relationship between brain myelination and human behaviour.

## 4.2 Introduction

Myelination of axonal projections is increasingly being appreciated as key regulator of brain function. This is widely thought to be because the properties of an axon's myelination influence its physiological properties. Conduction velocity, for instance, increases with myelin thickness, as demonstrated by empirical studies (Waxman, 1980) and *in silico* simulations (Goldman and Albus, 1968, Moore et al., 1978, Smith and Koles, 1970). Multiple studies have also found that changes in myelin thickness alter conduction velocity, whether they are driven by pathology (Schauf and Davis, 1974, Verhoeven et al., 2003) or by experience (Etxeberria et al., 2016). Other sources have also stressed a broader importance for myelination in information processing (Moore et al., 2019), for example in enabling high-frequency conduction (Saab et al., 2016) and in regulating the timing of action potentials in a circuit-dependent manner (Lang and Rosenbluth, 2003, Pajevic et al., 2014, Salami et al., 2003).

However, all current evidence linking myelination of a circuit to its neurophysiological properties has been derived from animal studies, often focusing on *in vitro* results. Little is known about how levels of myelination may influence properties of circuits in humans and how this may play out during behaviour. In terms of grounding myelination and physiology into behaviour, individual axons are likely not to be as behaviourally relevant as bundles of axons in macroscopic white matter tracts, but precisely how myelination levels in a tract influence its physiology is also not well understood.

Here, we combine recent advances in Magnetic Resonance Imaging (MRI) and Non-Invasive Brain Stimulation (NIBS) within a large dataset in order to improve our understanding of the link between myelination and physiology of neural circuits.

MRI studies have traditionally aimed to probe properties of white matter through Diffusion-Weighted Imaging (DWI) (Basser et al., 1994, Chenevert et al., 1990, Cleveland et al., 1976, Doran et al., 1990, Le et al., 1993, Moseley et al., 1990a,b). DWI, however, provides remarkably unspecific metrics: although it can detect myelin sheath-driven restricted diffusion, it is also sensitive to fiber orientation and other cellular compartments (Zatorre et al., 2012). Recently, several advances have improved our ability to study myelination through MRI. Surging interest in quantifying myelin non-invasively has led to the development of MR sequences sensitive to myelin through a variety of different biophysical mechanisms: macromolecular tissue content in the myelin lipid bilayer can now be quantified by Magnetisation Transfer (Heath et al., 2018, Sled and Pike, 2001, Tofts et al., 2005, Yarnykh, 2002), local concentrations of diamagnetic myelin and paramagnetic iron-rich oligodendrocytes can can be measured through susceptibility-weighted contrasts (Haacke et al., 2009, Weiskopf et al., 2013), and quantification of relaxation rate allows to map anatomical variability in myelin content (Lutti et al., 2014). In conjunction with this accruing of MR technologies to quantify myelination, advances in statistics, such as the development of joint inference permutation testing (Winkler et al., 2014, 2016) also allow to optimally pool multimodal data together to extract reliable information from

such wide-ranging MR signals.

Although functional MRI (fMRI) has been widely deployed to study cortico-cortical interactions, fMRI cannot detect directional, causal influence of an area's neuronal activity on the activity of another area. fMRI's low temporal resolution also precludes studying millisecond-level cortico-cortical interactions which are known to take place during a task (Buch et al., 2010, Neubert et al., 2010). Paired Pulse Transcranial Magnetic Stimulation (ppTMS), by contrast, can be delivered with millisecond precision to allow insights into directional interactions between two brain areas. This high temporal resolution allows ppTMS to pick up subtle variation in rapid cortico-cortical interactions which likely reflects a tract's physiological properties (which are often on millisecond scales), but is averaged out and not detectable in fMRI studies. We therefore hypothesized that myelin variability would have fine-grained effects on rapid cortico-cortical interactions, which would be made noticeable by the use of ppTMS.

Premotor to motor projections in the motor network are well-characterised both in tracing studies (Boussaoud et al., 2005, Jenny, 1979) and in physiological studies showing complex, state-dependent patterns of modulation of M1 by forward projections from ventral premotor cortex (PMv) (Bäumer et al., 2009, Buch et al., 2010, Davare et al., 2008). These projections allow for inhibition of incorrect motor programmes (Forstmann et al., 2008, Mars et al., 2007) and are thus engaged during low-level motor tasks such as action reprogramming (Neubert et al., 2010), making them accessible to study during behaviour and providing a clear read-out of participant behaviour to

relate to their function (Isoda and Hikosaka, 2007). Taken together, these features of premotor-to-motor projections make them an ideal test bed for hypotheses about how myelin shapes circuit function and behaviour in humans.

## 4.3 Methods

### 4.3.1 Participants

64 healthy participants (36 female; mean age 24.69 years) underwent a single session of MRI and, on a different day less than a week apart, a time-of-day-matched TMS session which included task-based Paired Pulse TMS. All participants were self-assessed right-handed and their handedness was further confirmed through the Edinburgh Handedness Inventory (Oldfield, 1971), (mean EHI score: 88.65). All participants were screened for TMS and MRI safety, received monetary compensation for their participation, and gave their informed consent to participate in this study. All study procedures were reviewed and approved by the local ethics committee at the University of Oxford (Central University Research Ethics Committee (CUREC)), and followed the Declaration of Helsinki.

### 4.3.2 Magnetic Resonance Imaging (MRI)

Magnetic Resonance Imaging (MRI) data were collected with a 3.0-T Prisma Magnetom Siemens scanner, software VE11B (Siemens Medical Systems, Erlangen, Germany). T1-weighted imaging (T1w), Multi-Parameter Mapping (MPM) and Diffusion-Weighted Imaging (DWI) sequences were collected.

The T1w sequence had a TR of 1900 ms, TE of 3.96 ms, a 1mm isotropic resolution and a large Field of View (FOV, 256mm) to allow for the nose to be included in the image and thus facilitate neuronavigation later on in the paradigm. The sequence used GRAPPA with an acceleration factor of 2.

The diffusion-weighted Echo-planar imaging (EPI) sequence had TR=3070 ms, TE=85.00 ms, FOV=256mm, voxel size=1.5mm isotropic, multiband factor of 4. Diffusion scans were collected for two b-values (500 and 2000 $s/mm^2$), over 281 directions. An additional 23 volumes were acquired at b=0, 15 in anterior-posterior (AP) phase-encoding direction and 8 in the posterior-anterior (PA) phase-encoding direction.

The MPM sequence (as per Weiskopf et al., 2013) included three multi-echo 3D FLASH (fast low-angle shot) scans with varying acquisition parameters, one radio frequency (RF, or B1+) transmit field map and one static magnetic (B0) field map scan, for a total acquisition time of roughly 22 minutes. To correct for inter-scan motion, the position-specific receive coil sensitivity field was calculated and corrected for, as per Papp et al., 2016. The three types of FLASH scans were designed to be predominantly T1-, PD-, or MT-weighted by changing the flip angle and the presence of a pre-pulse: 8 echoes were predominantly Proton Density-weighted (TR = 25ms; flip angle = 6 degrees; TE = 2.3-18.4ms), 8 echoes were predominantly T1-weighted (TR = 25ms; flip angle = 21 degrees; TE = 2.3-18.4ms) and 6 echoes were predominantly Magnetisation Transfer-weighted (MTw, TR = 25ms; flip angle = 21 degrees; TE = 2.3-13.8ms). For MTw scans, excitation was preceded by off-resonance Gaussian MT pulse of 4 ms duration, nominal flip angle, 2 kHz frequency offset from water resonance. All FLASH scans had 1 mm isotropic resolution and field of view (FOV) of 256x224x176 mm. The B1 map was acquired through an echo-planar (EPI)-based sequence featuring spin and stimulated echoes (SE and STE) with varying flip angles,

FOV of 192x192x256 mm and TR of 500 ms. The TE for SE was 37.06 ms, while the TE for STE was 68.28 ms. The B0 map was acquired to correct the B1 map for distortions and off-resonance effects. The B0 map sequence had a TR of 1020.0 ms, first TE of 10 ms, second TE of 12.46 ms, field of view (FOV) of 192x192x256 mm and read-out bandwidth of 260 Hz/pixel.

MRI scan pre-processing, analysis and statistical comparisons were performed using FMRIB Software Library (FSL, v6.0), except for the MPM quantitative map estimation step which was carried out using the hMRI toolbox implemented in Matlab-based SPM, as described in (Tabelow et al., 2019). All T1w images were preprocessed through a standard FreeSurfer pipeline (Fischl et al., 2004) to correct for bias field and achieve ACPC alignment (for use in Neuronavigation).

An automated custom pipeline based on existing FSL tools was also developed for our diffusion sequence. The topup tool was run on average images of AP b0 volumes and PA b0 volumes. After applytopup was used to correct for the resulting susceptibility-induced off-resonance field, eddy was run (with flags optimised for multiband diffusion data) to correct for eddy currents and subject movement. To generate Fractional Anistropy (FA) maps, a diffusion tensor model was fit to each voxel through DTIFIT, with flags optimised for multi-shell data processing, such as the –kurt option.

MTsat, R1 and R2* quantitative maps were estimated through the hMRI toolbox (Tabelow et al., 2019). In order to register MPM volumes to FA volumes, we used the following steps. Boundary-Based Registration was used to calculate a DWI-to-T1w registration using AP b0 images (with high

tissue boundary contrast). A customised pipeline was used to ACPC align the MPM maps and register them to T1w space. At this stage, 1 participant was excluded as the MPM scan was heavily corrupted due to movement artefacts; 1 participant was excluded due to lower quality signal in the MPM scan, which resulted in poor registrations with other modalities. Once registration matrices for MPM-T1w and DWI-T1w were calculated, they were inverted, concatenated and applied as needed to bring MPM volumes into DWI space with minimal interpolation.

### 4.3.3 Neuroimaging statistics

To bring all volumes into a common space, native FA volumes were skeletonised with Tract-Based Spatial Statistics (TBSS), and the skeletonisation transforms were subsequently applied to MPM-to-DWI registered volumes. Group-level analyses were then conducted in skeleton space for all data. To uncover common trends across modalities, voxelwise joint inference was performed through Permutation Analysis of Linear Models (Winkler et al., 2014), which implements a voxelwise Fisher test with the following equation (as described in (Winkler et al., 2016)):

$$-2\sum_{K=1}^{K} ln(p_k) \tag{4}$$

### 4.3.4 Transcranial Magnetic Stimulation (TMS) set-up and Neuronavigation

Two DuoMAG MP-Dual Paired Pulse TMS monophasic stimulators (DeyMed DuoMag, Rogue Resolutions Ltd.) were used to deliver pulses to two figure-eight coils, one 70mm-diameter coil over primary motor cortex (M1) and one 50mm-diameter coil over right inferior frontal gyrus (rIFG).

The 70mm/M1 coil was held by the main experimenter throughout the experiment. This coil was kept tangential to the skull and at roughly a 45° angle to the scalp's midline, resulting in a Posterior Anterior (PA) current direction, perpendicular to the central sulcus. The 50mm/rIFG coil was positioned in place through a clamp sustained by a Manfrotto Variable Friction Arm (Wex Photo Video, Calumet Photographic Limited) which was clamped to the same table as the chinrest. The position of the coil was determined through the participant's T1w image, and the coordinates were x = 58, y = 15, z = 30 in MNI (Montreal Neurological Institute) space, based on (Neubert et al., 2010). The angle of the rIFG coil was 0° relative to midline.

Participants sat on a chair and were asked to position their head on a chin rest in order to minimize head movement. Before the start of any TMS stimulation, participants were asked to keep feet relaxed and flat on the ground. The participants were free to move their body between task blocks, but they were asked to move the hand with the electrodes as little as possible both during the task and between task blocks. All participants wore earplugs to reduce the effects of TMS-related clicking noise.

Neuronavigation was achieved through a Polaris camera and the Brainsight (Rogue Resolutions, Inc.) software. The participant was tracked via a headband with reflective spheres attached to it; the coils were tracked with coil trackers that were re-calibrated at the beginning of each testing day. In addition, extensive hard-ware checks were performed before each session, including that the coils worked on a peripheral muscle, that cable connections were correctly in place, and importantly, a PicoScope6 (Pico Technology) was used to check the timing of the two pulses to ensure they were correct and identical between task and rest blocks at sub-millisecond precision.

Online neuronavigation was used in all subjects to ensure the coil was targeting the cortical area of choice throughout the task. Moreover, a sample of the coil location was collected for each participant during the session, and analysed offline. An automated Brainsight tool was used to find the closest brain voxel to the sampled stimulation site. The coordinates for this voxel were then transformed in standard space to allow overlaying of stimulation sites from different participants. At this stage, a total of 47 stimulation locations were included, as 2 participants' stimulation locations failed to save due to software fault, 3 participants were not sampled due to time limits, and 4 participant's stimulation locations could not be automatically determined with Brainsight. As previous literature suggests a diameter of 4 cm would capture the overall area where 30% of the peak magnetic field may still be effective (Siebner et al., 2009), spheres of 4 cm diameter were created around the sample stimulation location, and overlaid upon each other, as shown in Figure 4.1. All stimulation sites were within 1 cm of target location, as

described in previous publications (Buch et al., 2011, Johnen et al., 2015).

### 4.3.5 Electromyography (EMG)

Electromyography (EMG) was recorded from the participant's right hand in a tendon-belly montage, aiming to record from the First Dorsal Interosseus muscle. After scrubbing the three electrode sites with alcohol wipes, 25-mm electrodes (Kendall Neonatal ECG Electrodes Puppydog) were applied. A ground electrode was placed on the hand's carpus and the exact location of the electrodes was carefully replicated across days for the same participant. In order, the EMG signal output was processed through a D440 amplifier (Digitimer), a Humbug Noise Eliminator, 50Hz (Digitimer) to notch-filter the data, and a CED micro1401 Mk.II A/D converter (Cambridge Electronic Design) to digitise the signal and relay it to a PC running Spike2 (Cambridge Electronic Design). Sampling rate was 5000 Hz, and bandpass filters were set between 10 and 1000 Hz.

### 4.3.6 Motor hotspot and parameter determination

The M1 coil intensity was increased and slowly moved around over the left side of the scalp until a motor hotspot could be identified. Several criteria were applied to confirm the correct coil location had been reached: reliability of the MEPs, smoothness of the MEP shape, selectivity of finger movement during MEPs, and degradation of MEP response as the coil moved away from the identified spot. The location of the motor hotspot was recorded through neuronavigation during the first session.

After determining the location of the motor hotspot, three parameters were determined for each participant: the intensities for 1mV, resting motor threshold (rMT) and active motor threshold (aMT). 1mV was determined as the intensity giving reliable and stable 1mV MEPs at rest over around 10 pulses; stability of the MEPs, rather than a precise mean value of 1mV across 10 pulses, was used as the key parameter in determining 1mV intensity. rMT was determined as the intensity at which 5 out of 10 pulses give MEP responses greater than 0.05 mV.

After 1mV and rMT determination, a brief, standardised protocol was used to determine aMT as per (Stagg et al., 2011). A separate screen was moved towards the participant so that they could observe their own FDI EMG trace in real time from the chinrest. After the participants verbally confirmed they could see the screen, they were asked to squeeze the thumb against the index finger as hard as they could twice to determine their maximum contraction. A sliding line on the screen was then set to 20% of maximum muscle contraction, and participants were asked to try and keep their contraction levels around that line. If this level of contraction caused fatigue or was too close to the noise level, then maximum contraction was calculated once again. This FDI-contraction set-up allowed measurement of the aMT, which we defined in this experiment as the intensity at which 5 out of 10 TMS pulses produced an MEP that was time-locked to the TMS pulse, and was followed by a cortical silent period (time-locking and presence of cortical silence period were chosen as criteria because MEP size is influenced by background muscle contraction during aMT). Presence of time-locked MEPs,

rather than presence of cortical silent period, was used as the key parameter in determining aMT.

### 4.3.7 paired pulse TMS (ppTMS)

Paired pulse TMS was carried out by stimulating the motor hotspot at 1mV in half the trials, and carrying out the same stimulation, preceded by a conditioning rIFG pulse 6ms earlier, at 110% of rMT. The pulses were always delivered 175ms after cue onset, and were randomly assigned in an equal fashion to stay vs switch trials and to right-hand vs left-hand trials.

### 4.3.8 Motor Evoked Potential (MEP) analysis

EMG analysis focused on TMS-induced Motor-Evoked Potential (MEPs), and more specifically on the peak-to-peak amplitude of MEPs. MEP recording, preprocessing and analysis procedures were identical for all experiments. MEPs were identified based on recorded TMS timings, pre-processed in MATLAB (Version R2018b, Mathworks, MA, USA) and visualised for quality control purposes. Absent or unusually small MEPs ( <0.2 mV) or unusually high MEPs ( >9 mV) were excluded from further analyses. Trials with incorrect, premature ( <150 ms) and slow ( >800 ms) responses were also excluded from further analyses. Trials with significant Trials with significant 'precontraction' (i.e. muscle contraction above 0.4 mV in the 100 ms before the MEP and the test pulse) were also excluded. Once all exclusion criteria were applied, Grubb's outlier detection was carried out on the data. 6 participants had less than a third of MEPs per condition which could be included,

and were thus excluded from further analyses. After preprocessing, MEP ratios (ppTMS/spTMS) were obtained from the median MEP for switch and stay trails separately (see below).

### 4.3.9 Action Reprogramming Task

The Action Reprogramming task was implemented based on a task originally developed by (Isoda and Hikosaka, 2007) for monkeys and then adapted for use in human TMS studies by (Neubert et al., 2010). The task aimed to probe action execution and action reprogramming. Cues consisted of a central square (either red or green) with two 'flanker' squares (one red and one green). Participants were instructed to press the button on the side where the flanker colour matched the colour of the central square. The flankers kept switching sides at random, whereas the central square was the same colour for 3-7 trials at the time. This way, participants simply had to execute a movement when the central cue colour stayed the same ('stay trials'), but they had to inhibit the movement and carry out a different one in the trials where the central cue colour had switched ('switch trials'). Each participant underwent a session of 112 switch trials and corresponding stay trials (for a total of 678 trials). Each session included 3 automatic breaks in between to ensure participants had a chance to rest if they wished to do so. Participants were told to be as fast and accurate as they could. They received detailed task instructions in paper format at the beginning of each session; in addition, the instructions were reiterated in a computer-based fashion at the beginning of the task (full code available here: https://github.com/lazaral/paTMS_task).

Before the task, they undertook roughly 100 trials to make sure first that they understood the rules of the task, then that they had habituated to the task, and finally that they could tolerate TMS pulses while performing the task. Participants were pressing the two buttons with index fingers from their two hands, and were instructed to keep their hands relaxed between trials until the cue appeared; they were occasionally reminded to keep their hands relaxed if the experimenter observed noticeable muscle contractions between trials.

### 4.3.10 Mediation Analysis

Mediation analyses were run in PROCESS (to derive 95% Confidence Intervals (Hayes, 2013)) and in BRAVO (to derive p-values (Wager et al., 2008), which cannot be derived in PROCESS for our model). In both toolboxes, we used a significant indirect (X-M) pathway as the key requirement to test mediation, and applied bootstrapping with 10000 repetitions(Hayes, 2013, Zhao et al., 2010).

## 4.4 Results

### 4.4.1 Multimodal myelin markers, cortico-cortical interactions, and action reprogramming

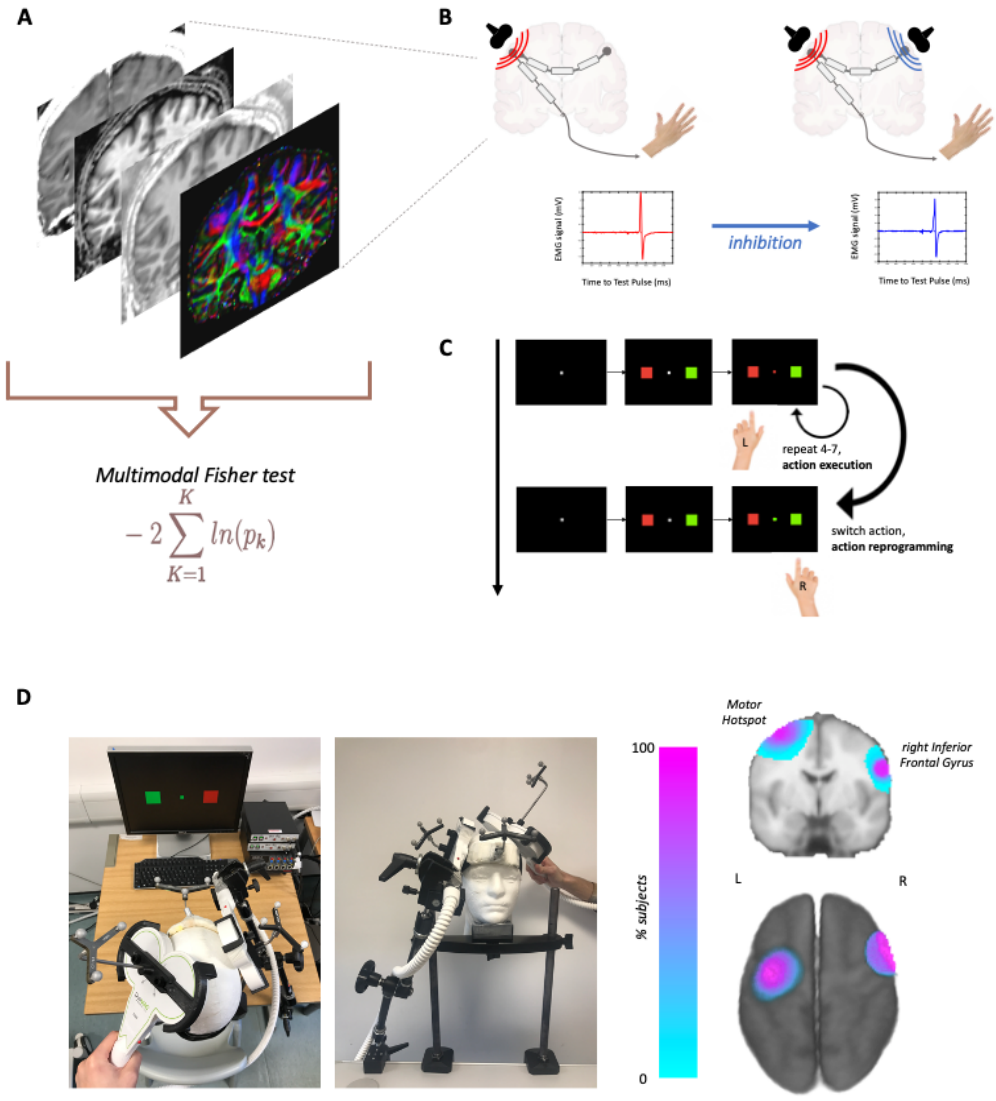

Figure 4.1: (Previous page.) **Non-invasive measurement of myelination and of cortico-cortical interactions during behaviour.** A. Multiple myelin-sensitive modalities from Multi-Parameter Mapping (MPM, top left) were collected and jointly analysed through multimodal Fisher tests. Motor-Evoked Potentials (MEPs, top right) were collected from the same participants during an action reprogramming task. Stimulation of premotor cortex during the task allowed to measure the modulatory effects of premotor cortex on MEPs driven by M1 stimulation B. Details of the action reprogramming task. C. Transcranial Magnetic Stimulation (TMS) set-up to induce MEPs and measure cortico-cortical interactions. Precise neuroanatomical targeting is achieved through continuous neuronavigation during stimulation, and confirmed with analysis of subject-specific TMS target locations.

We hypothesized that greater myelination of a long-range projection is associated with stronger effect on its target areas, and that this is associated with better behavioural performance. To test this hypothesis, we collected MPM-based multimodal markers of myelin, ppTMS-based, and behavioural measures in an action reprogramming task.

Multi-Parameter mapping allows to collect many markers that are known to be related to myelin (Figure 4.1A). Taken independently, each marker is sensitive to other features of the tissue (e.g. R2* is also sensitive to iron), so a Fisher test was used to find common patterns across all modalities. Since myelin is the only biological feature all sequences are sensitive to, we reasoned that any concordant, common trend in relationships with all these markers must signify strong evidence for a myelin-driven effect.

ppTMS was used to probe levels of directional interaction from PMv to M1 during the action reprogramming task (Figures 4.1B, 4.1C). In half of all TMS trials, participants were stimulated over M1 only, to determine their average MEP during single pulse stimulation. In the other half of trials, M1

stimulation was preceded by PMv stimulation, with the aim of quantifying the effect that activating PMv neurons would have on M1-driven MEPs. By taking a ratio between single pulse stimulation MEPs and PMv+M1 paired stimulation, we obtained a metric of the interaction between the two areas (Figure 4.1A).

### 4.4.2 Physiological measures of cortico-cortical interactions relate to myelination of the underlying long-range circuit

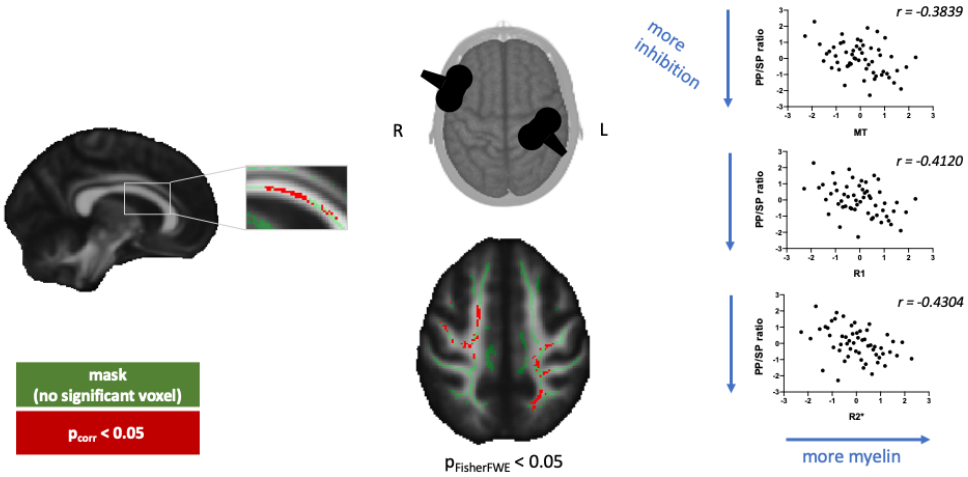


Figure 4.2: **Multimodal joint inference reveals concordant relationships between inter-hemispheric inhibition and myelin markers across modalities.** Significance threshold for Fisher test is set at 0.05 after correcting for family-wise error correction. Each data point is a single participant; scatterplots and Spearman correlation effect sizes are presented for post-hoc visualisation of the correlations, rather than for statistical inference.

We find that people with the most inhibition from PMv to M1, as measured by ppTMS, also have higher levels of myelin markers in white matter, with correlations especially prominent in MT, R1 and R2* (Figure 4.2). FA was also analysed, but no significant correlation with ppTMS was observed. The areas where this effect is significant are spatially asymmetric. In the left hemisphere, they cluster posteriorly, under the average location of the M1 coil; in the right hemisphere, they cluster slightly more anteriorly, under the average location of the PMv coil. Finally, the significant clusters in both hemispheres are connected by a cluster crossing the midline in the corpus callosum. This hints that myelination of the tract being stimulated may be uniquely important for PMv's inhibition of M1 during action reprogramming.

To probe the specificity of the relationship between myelination and cortico-cortical interactions, we then ask whether this observed relationship is unique to the physiological interactions between cortical areas, or whether myelination also relates to local physiological inhibition in M1, or to behavioural performance during action reprogramming (Supplementary Results, Figure 4.5). To test this, we use joint inference again and find that behavioural switch cost during the action reprogramming task does not significantly relate to myelin markers ($p_{\mathrm{FisherFWE}} < 0.05$). To obtain a more fine-grained picture of complex dynamics in primary motor cortex, we also look at task-dependent modulation of M1 excitability and find that its excitability significantly decreases during action reprogramming trials compared to action execution trials (Wilcoxon matched-pairs test, $p < 0.001$). However, inter-individual differences in this metric of task-dependent M1 modulation

do not relate to inter-individual differences in white matter myelin ($p_{FisherFWE}$ <0.05).

### 4.4.3 Physiological dynamics mediate the link between myelin markers and action reprogramming behaviour

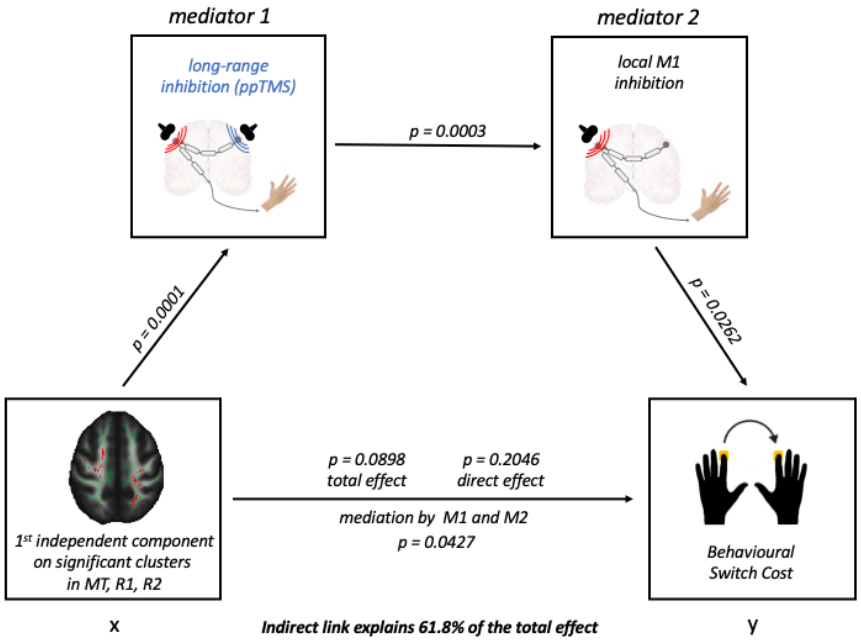


Figure 4.3: **Motor network physiology links myelination to switching behaviour.** A mediation analysis reveals an indirect link between the myelin-related measure of inter-hemispheric inhibition and switch cost, a metric of performance during the action reprogramming task. The 95% boostrapped CI for the indirect effect of sequential mediation of M1 and M2 is -.29 to -0.02, which overall explained 61.8% of the total effect (Right panel).

It has been established by previous literature that cortico-cortical interactions are constrained by structural features of cortico-cortical connections (Grandjean et al., 2017, Hermundstad et al., 2013). Moreover, cortico-cortical

connectivity shapes dynamics of individual brain areas, and in turn individual brain areas perform computations that directly regulate behavioural output. This is especially clear in the case of primary motor cortex (M1), whose computations directly determine movement (Churchland and Shenoy, 2007, Elsayed et al., 2016) and are input-driven (Sauerbrei et al., 2020). Therefore, we take advantage of the well-established circuit properties of the motor network to hypothesize that cortico-cortical interactions would relate to local cortical dynamics, and that in turn local cortical dynamics would relate to motor behaviour.

In support of this hypothesis (Supplementary Results, Figure 4.6), we find that inhibition from PMv to M1, as measured by ppTMS, correlates with task-dependent M1 modulation (r= -0.5245, p <0.0001), and that task-dependent M1 modulation correlates with behavioural output, as captured by switch cost (r= -0.3096, p=0.0202), but we find no relationship between ppTMS inhibition and switch cost (r=0.1925, p=0.1551). Moreover, as mentioned previously, myelination correlates specifically with inhibition from PMv to M1, but not with task-dependent physiological modulation of M1, nor with behavioural switch cost ($p_{\mathrm{FisherFWE}}$ >0.05, Supplementary Results, Figure 4.5).

Given our strong, directional, a priori hypotheses on how myelination, physiology and behaviour would relate to each other, we formalise these relationships in a single statistical model, by means of a 2-mediator mediation analysis. In cross-sectional designs, mediation analysis does not replace causal or pseudo-causal approaches, but is a powerful tool to test statisti-

cal inter-dependence between variables in a hypothesis-driven way, as we do here. In accordance with our hypothesis, we find that cortico-cortical interactions (mediator 1 or M1) and local M1 dynamics (mediator 2 or M2) sequentially mediate the link between myelination and action reprogramming behaviour ($p = 0.0427$, 95% boostrapped CI: -.29 to -0.02, indirect link explaining 61.8% of the total effect). Furthermore, we also confirmed this link using a traditional 1-mediator mediation analysis (Supplementary Results, Figure 4.7).

### 4.4.4 Physiological measures of cortico-cortical interactions do not correlate with demographic factors and features of M1 physiology

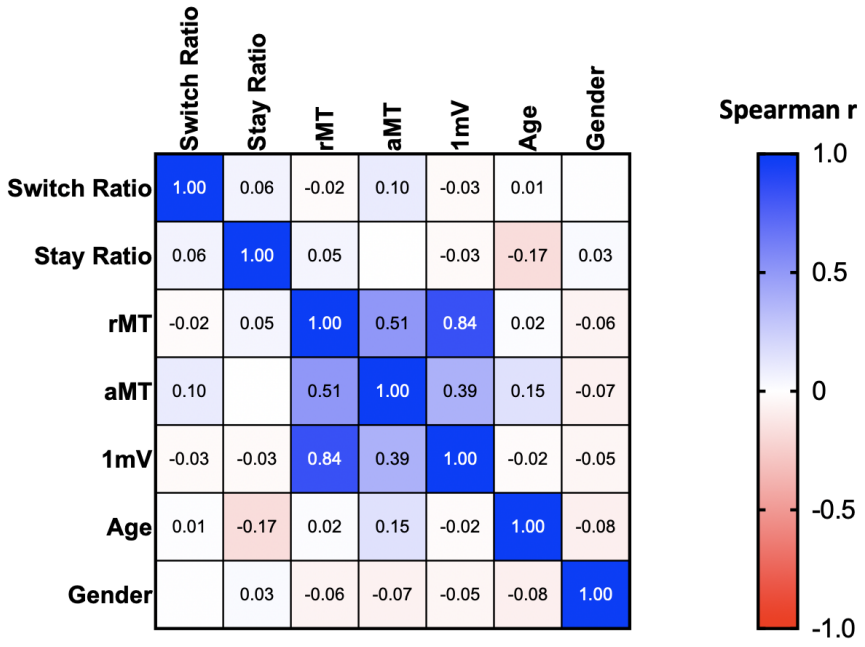


Figure 4.4: **Correlations between physiological measures of cortico-cortical interactions, demographic factors and features of M1 physiology.** We report Spearman r correlation values for correlations of all possible pairs between: switch ratio, stay ratio, resting Motor Threshold (rMT), active Motor Threshold (aMT), 1mV, age and gender. We find no significant correlation for the switch ratio metric across any tests.

To test whether the PP/SP ratio in switch trials relates to non-specific individual differences across subjects, we test correlations between switch ratio, demographic factors, and features of primary motor cortex physiology (Fig-

ure 5). We find that switch ratio does not correlate with resting Motor Threshold (rMT, r= -0.2, p=0.87), active Motor Threshold (aMT, r=0.10, p=0.46) or 1mV (r=-0.3, p=0.82) measures. We also find that age and gender are not correlated with any other physiological metric, and in particular not with PP/SP ratio in switch trials (age: r=0.01, p=0.94; gender: r=0.004, p=0.98).

## 4.5 Discussion

In the current study, we focused on the relationship between myelination of a circuit and the downstream effects that levels of myelination may have on physiology of that circuit, as well as the resulting behaviour. We find a link between metrics of physiological interactions between two brain areas and metrics of white matter myelination in the tract connecting the two areas. This relationship proves highly specific. It is common across multiple modalities, but a whole-brain voxelwise analysis reveals it to be localised to areas of the pathways stimulated by ppTMS. Moreover, multimodal myelin markers do not relate to a cortex-dependent metric of physiology, nor to behavioural measures. We also demonstrate that metrics of cortico-cortical interactions are independent of demographic and other unspecific physiological factors. Taken together, these results argue for a specific link between the physiology of PMv to M1 projections, and their myelination.

It has been repeatedly suggested that variability of white matter in the general population holds explanatory value about individual differences in brain physiology (Boorman et al., 2007, Neubert et al., 2010), cognition (Matejko and Ansari, 2015), and behaviour (Boekel et al., 2015, Kanai and Rees, 2011). However, what features of white matter may be driving this meaningful variability is less well understood. In recent years, white matter myelination has come to prominence as an underappreciated regulator of brain function, with studies demonstrating new roles such as trophic support of axons (Nave, 2010) (Fünfschilling et al., 2012) but also plastic potential

(Sampaio-Baptista et al., 2013). Therefore, it would make sense for inter-individual variability in myelin to play an important role in cognition and behaviour, and potentially to underpin the previously reported relevance of white matter variability to wide-ranging behaviours. To the best of our knowledge, this study is the first demonstration that variability in myelination holds meaningful explanatory information about physiological and behavioural processes, and opens the door to further studies exploring inter-individual variability of myelination in humans.

Although the study highlights a robust relationship between the amount of myelin in a tract and its physiological properties, it is difficult to interpret which morphological aspects of a tract that may be driving this effect. Levels of myelination in a voxel are influenced by a variety of factors, including myelin thickness, number of oligodendrocytes, length of Nodes of Ranvier (NoR), and axon packaging (Walhovd et al., 2014). As a simplified example, a voxel with high MT could reflect a high number of myelinated axons, or thicker myelin sheaths on each axon (Kaller et al., 2017, Walhovd et al., 2014, Zatorre et al., 2012). Recent work has also highlighted the contributions that NoRs may play in dynamically regulating functional axonal properties (Arancibia-Carcamo et al., 2017, Dutta et al., 2018, Ford et al., 2015, Lazari et al., 2018), which our results are compatible with. To further the previous example, two voxels with the exact same number of myelin sheets and oligodendrocytes may have different MT and R2* values if one of the voxels has shorter NoRs, therefore allowing more myelin to cluster within the same 3D volume. In summary, our study is compatible with mul-

tiple morphological interpretations, but cannot distinguish between them. Future studies will be able to use our findings to build upon them and tackle these biologically-driven questions by 'reverse-translation' to rodent studies, where tools such as immunohistochemistry and Electron Microscopy would be able to answer more detailed cellular questions.

A key limitation of the study is that it employs non-invasive, MR-based metrics of myelination to quantify myelin. Drawing one-to-one relationships between biophysical signals detected from MR and the underlying biology is notoriously problematic (Walhovd et al., 2014, Zatorre et al., 2012), and we took several steps to maximise the biological interpretability of our findings. Rather than focusing on an individual myelin marker, we collected a suite of four different myelin markers, each with a different profile of biophysical sensitivity. We also used a joint inference framework when carrying out statistical analyses, so that we would only consider effects that are common across modalities. This minimises the risk that the link we discovered here is driven by other biological features of white matter: MT is also sensitive to oedema (Cook et al., 2004), and R2* is also sensitive to vasculature (Weisskoff and Kiihne, 1992), but the only known signal that they both pick up is from tissue myelination. Although it comes with limitations, using non-invasive markers of myelination allows to gather insights and test hypotheses in humans that would be otherwise restricted to preclinical studies in animal models. In particular, taking this approach has allowed us to identify a new link between human behaviour and myelination that would have been inaccessible through invasive histology.

A foundational assumption of many *in vitro* studies of axonal properties is that the same principles that apply to relationships between an axon's morphology and its physiological properties play out in similar ways at a larger scale in axon bundles within white matter tracts. The current results provide further confirmation of this assumption. Previous studies have found that increased myelination increases conduction velocity and information transmission between neurons. Here, by probing cortico-cortical circuits with macroscopic methods, we show that a similar relationship exists for white matter tracts and cortex-to-cortex connectivity, whereby increased myelination of a tract also influences information transmission from one cortical area to another.

We studied brain-behaviour relationships in the context of a particular behavioral task – namely action reprogramming. Controlling what actions to execute, often termed 'cognitive control' (Neubert et al., 2010), is a key function of the brain, and is likely an agglomeration of a variety of parallel and diverse mechanisms (Chambers et al., 2006, Forstmann et al., 2008, MacDonald et al., 2000, Mars et al., 2007, Ridderinkhof et al., 2004). Here, we examined a specific component of 'cognitive control', i.e. action reprogramming (Isoda and Hikosaka, 2007). For the first time, we show that at least some components of cognitive control can be explained in terms of physiological interactions, which are in turn driven by microstructural properties of the underlying circuit. This constitutes a fundamental step forward in our understanding of the mechanisms underpinning cognitive control, and how we may be able to modulate them.

These results illustrate a mechanistic link binding myelination of long-range circuits to their physiology and to action reprogramming. They highlight, for the first time, that myelin's effects on axon conductance are also relevant at the larger spatial scales of tracts and translatable to the study of the live human brain. Taken together, this represents a first step towards translating studies on cellular-level properties of myelin to human-relevant knowledge, which is crucial to develop clinically-relevant knowledge of cortical circuits and to design therapeutic treatments aimed at modulating myelination.

## 4.6 Supplementary Results

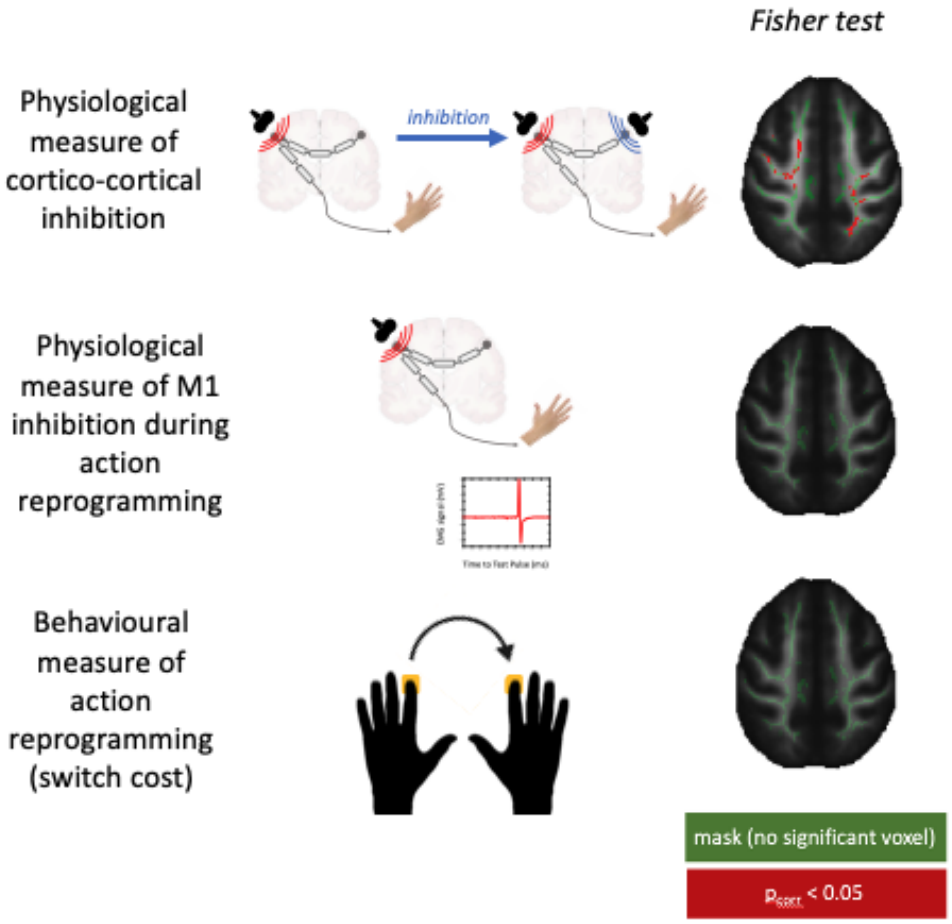


Figure 4.5: **Specificity of the relationship between white matter myelination and cortico-cortical interactions.** We use joint inference and find that unlike ppTMS-based measures of cortico-cortical interactions, behavioural switch cost during the action reprogramming task does not significantly relate to myelin markers ($p_{\mathrm{FisherFWE}} < 0.05$), nor does task-dependent M1 modulation ($p_{\mathrm{FisherFWE}} < 0.05$).

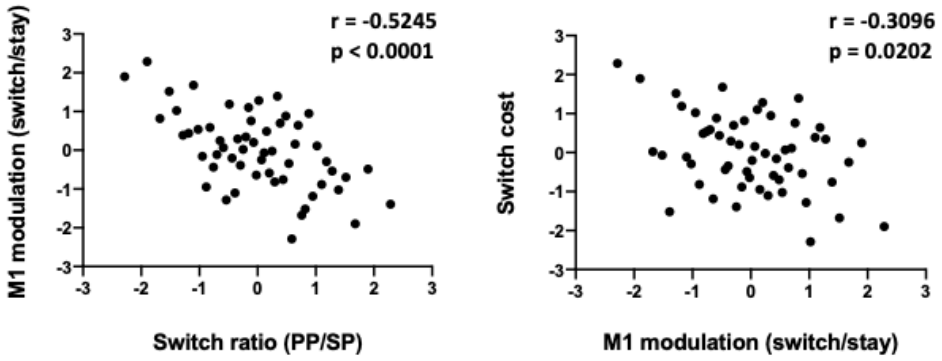


Figure 4.6: **Hypothesis-driven correlations between physiology and behaviour.** Inhibition from PMv to M1, as measured by ppTMS, correlates with task-dependent M1 modulation (r= -0.5245, p <0.0001, left panel). Moreover, task-dependent M1 modulation correlates with action reprogramming behaviour, as measured by switch cost (r= -0.3096, p=0.0202, right panel).

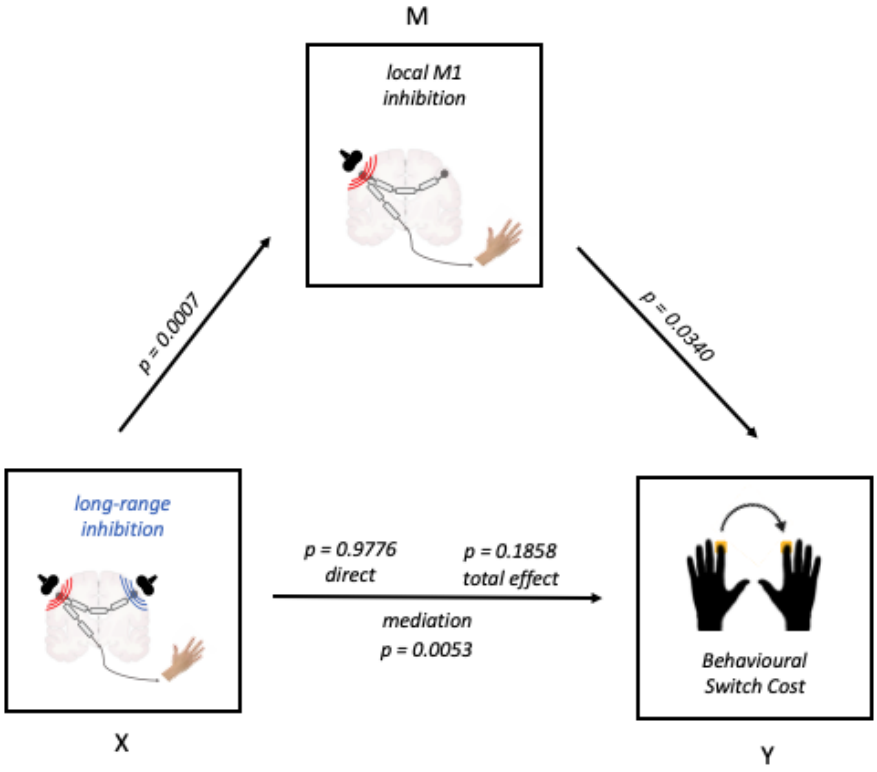


Figure 4.7: **1-mediator mediation analysis.** To complement the full 2-mediator analysis, we show that 1-mediator analysis (with no neuroimaging data) yields similar results. In this analysis, we use task-dependent M1 modulation as a mediator of the relationship between cortico-cortical interactions (ppTMS metric) and behaviour output (switch cost).

# Chapter 5: Inducing functional plasticity in a premotor-motor projection

## 5.1 Abstract

Despite widespread interest in the plasticity of myelinated long-range projections, tools to modulate them are lacking.

Here, we use a novel intervention, paired associative TMS (paTMS), to induce Hebbian-like plasticity in myelinated long-range projections. We assess paTMS in a pilot dataset (Study 1, n=12), an exploratory dataset (Study 2, n=17) and a confirmatory randomised blinded dataset (Study 3, n=34). Outcome measures such as behaviour and physiology are used across all studies to test the efficacy of the intervention.

In addition, studies 2 and 3 also use multimodal neuroimaging to tackle open questions about the rules governing plasticity of myelinated long-range projections. Microstructural myelin markers allow to ask whether myelin plasticity can occur through Hebbian-like mechanisms. Resting-state fMRI allows to ask whether Hebbian plasticity observed in studies in vitro also operates in vivo.

## 5.2 Introduction

While many questions about the physiology and plasticity of myelinated long-range projections remain open, most studies take indirect, correlational approaches to find answers (such as Chapter 3 and 4 in this thesis). Such indirect approaches are key to generating hypotheses and establishing links between brain-related phenomena. Nonetheless, causal interventions remain the gold standard to demonstrate that links established through correlation hold true, causal value, and that they can be manipulated and harnessed for real-life therapeutic applications.

Despite the widespread interest in plasticity of myelinated long-range projections, there is a dearth of tools to modulate them. An early tool used in the Non-Invasive Brain Stimulation (NIBS) literature has been Paired Associative Stimulation (PAS), i.e. a protocol that can induce potentiation of synaptic outputs from ascending cortical pathways to primary motor cortex (M1), by pairing stimulation of peripheral nerve fibers projecting to M1 with M1 stimulation (Stefan et al., 2000). This protocol has been used to successfully study Hebbian plasticity *in vivo* in humans, and to determine what factors influence it, from circadian rhythms to pathology (Huber et al., 2008, Suppa et al., 2017). However, this form of PAS cannot be extended to cortico-cortical pathways. Because of this limitation, PAS remains of limited use to test hypotheses related to behavioural outputs that are mediated by long-range projections and to commonly used MRI markers, such as resting-state fMRI and microstructural imaging, that are also known to be influenced

by features of myelinated projections.

Cortico-cortical PAS (ccPAS), also known as paired associative stimulation (paTMS), aims to stimulate two cortical areas with TMS in order to achieve PAS-like plasticity induction in cortico-cortical, rather than spinal pathways. In the past decade, a small but diverse body of work (summarised in Figure 5.1) has described effects of paTMS on a number of outcome measures, ranging from physiological (i.e. TMS-based) readouts (Arai et al., 2011, Buch et al., 2011, Koch et al., 2013, Rizzo et al., 2009), to behavioural (Chao et al., 2015, Chiappini et al., 2018, Fiori et al., 2018, Kohl et al., 2019, Nord et al., 2019, Romei et al., 2016), to neuroimaging-based readouts (Johnen et al., 2015, Veniero et al., 2013, Zibman et al., 2019). Although the literature has reported consistent effects of paTMS across all outcome metrics, many questions remain open.

One question concerns timing. Although it has been shown that plastic effects of paTMS are still present 3 hours after plasticity induction (Buch et al., 2011), it is unclear how long-lasting they are and whether they would still be present 24 hours later.

A second questions concerns what plasticity mechanisms may be involved in paTMS-induced plasticity. The Hebbian nature of the protocol makes it likely that its effects are underpinned by synaptic plasticity (Bi and Poo, 1998). This assumption is also compatible with a previous study highlighting increases between stimulated areas in functional connectivity (Johnen et al., 2015), which is thought to be sensitive to changes in synaptic strength (Logothetis et al., 2001, Mateo et al., 2017, Viswanathan and Freeman, 2007).

However, a plethora of plastic mechanisms exist in the brain, and it is unclear whether structural changes (in myelination, for instance) may also be involved (Sampaio-Baptista and Johansen-Berg, 2017), or whether synaptic changes lead to reorganisation of distributed cortico-cortical connectivity (Johnen et al., 2015).

A third question pertains to more practical aspects of paTMS. Although paTMS has been widely used to modulate intra-hemispheric circuits, we also know that interhemispheric circuits play key roles in the brain (Suárez et al., 2018). paTMS has been applied inter-hemispherically, but only to homotopic cortices, such as right M1 and left M1 (Rizzo et al., 2009), or right LPFC and left LPFC (Zibman et al., 2019). Therefore, it is still untested whether paTMS effects can be generalised to inter-hemispheric circuits.

Finally, the vast majority of paTMS studies report positive results, which raises questions about whether publication bias might have led to an overestimation of the efficacy of paTMS across outcome metrics (Hedges and Vevea, 1996, Murad et al., 2018). In addition, only a couple of previous studies have used blinded randomised-controlled designs to assess paTMS, and no previous study has reported confirmatory analyses on replication datasets (Figure 5.1). While seminal studies were designed to explore and tweak parameters of a new and understudied protocol, it is important to complement this early evidence with robust, confirmatory experimental designs in order to consolidate our knowledge of this key intervention to manipulate myelinated long-range projections.

Here, we aimed to assess the efficacy of inter-hemispheric paTMS on be-

haviour and physiological metrics. We also aimed to test immediate as well as 24-hour effects of paTMS to further define the duration of its action, and to replicate them in an independent sample in order to provide confirmatory evidence for the efficacy of the intervention. Finally, we complemented our experimental design with MR-based measures, in order to further understand mechanisms driving paTMS plasticity.

| Year | Authors | Inter-hemispheric | Randomised | Blinded | Anatomical areas | Duration of effect tested | Outcome measures | Confirmatory component? |
|---|---|---|---|---|---|---|---|---|
| 2009 | Rizzo et al | Yes (homotopic) | No | No | Left M1 and right M1 | 1 hour | Physiological | No |
| 2011 | Arai et al | No | No (one experiment) | ? | Right SMA to right M1; Left SMA to left M1 | 30 min | Physiological | No |
| 2011 | Buch et al | No | No | ? | Left PMv to left M1 | 3 hours | Physiological Behavioural | No |
| 2013 | Veniero et al | No | No | ? | Left PCC to left M1 | 5 min | Physiological Neuroimaging (EEG) | No |
| 2013 | Koch et al | No | No | ? | Left PCC to left M1 | 25 min | Physiological | No |
| 2015 | Chao et al | No | No | ? | Left PCC to left M1 | 60 min (2 and 24 hours also tested) | Behavioural Physiological | No |
| 2015 | Johnen et al. | No | No | ? | Left PMv to left M1 | 4 min | Physiological Neuroimaging (fMRI) | No |
| 2016 | Romei et al | No | Yes | ? | Left V5 to/from bilateral V1 | 60 min | Behavioural | No |
| 2018 | Fiori et al | No | Yes | Yes | Left PMv to left M1 | 30 min | Behavioural Physiological | No |
| 2018 | Chiappini et al | No | Yes | ? | Left V5 to/from bilateral V1 | 30 min | Behavioural | No |
| 2019 | Zibman et al. | Yes (homotopic) | No | ? | Right LPFC to/from left LPFC | 0 mins | Behavioural Neuroimaging (EEG) | No |
| 2019 | Nord et al. | No | Yes | ? | Right IPS to/from right LPFC | 30 mins | Behavioural | No |
| 2019 | Kohl et al. | No | Yes | ? | Right IFC to right preSMA | 30 mins | Behavioural | No |
| 2020 | Lazari DPhil thesis | Yes | Yes | Yes | Right PMv to left M1 | 24 hours | Behavioural Physiological Neuroimaging (multimodal) | Yes |

Figure 5.1: A detailed list of all previously published papers assessing the effectiveness of paTMS. The table summarises aspects of the experimental design (randomisation, blinding, confirmatory sample) as well as readout method (behavioural, physiological - i.e. TMS-based, or neuroimaging-based), timepoints assessed and locations targeted. The table was reproduced and modified from Gavine et al., (2019, MSc thesis, University of Oxford).

## 5.3 Materials and Methods

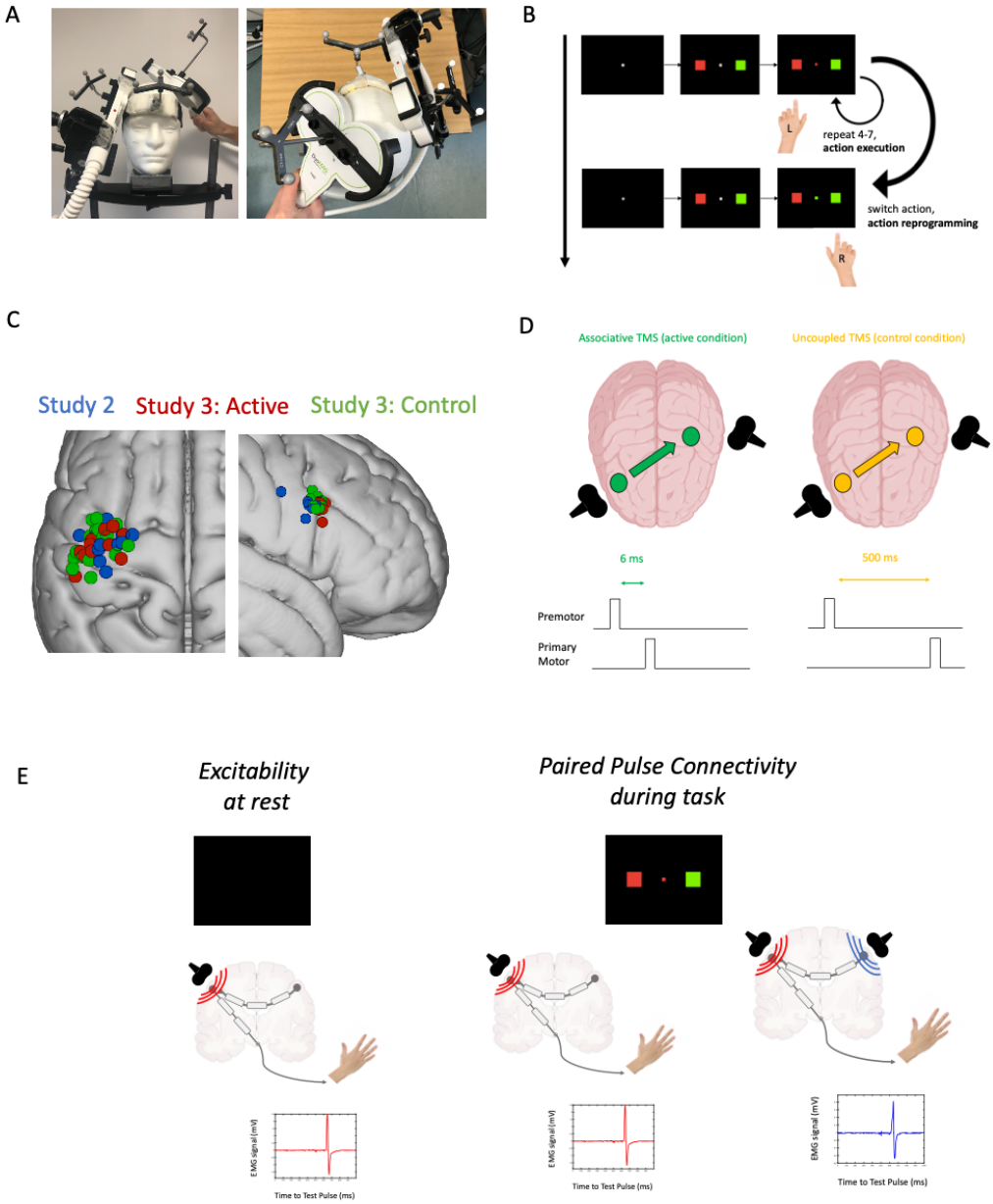

Figure 5.2: (Previous page.) Summary of experimental set-up. A. Photo of the neuronavigation set-up for the TMS session. B. Schematic of the action reprogramming task. C. Stimulation locations for participants in studies 2 and 3. D. Temporal patterns of rIFG and lM1 stimulation during active and control TMS protocols. E. Physiological outcome measures included measures of primary motor cortex excitability at rest, and measures of rIFG-lM1 connectivity during action execution.

### 5.3.1 Participants and experimental design

In study 1, 12 healthy participants (5 female, aged 22-37) underwent a single session of MRI and a single TMS session consisting of paired pulse TMS during task, paired associative TMS at rest, followed by another paired pulse TMS measurement during task. The MRI and TMS sessions took place on different days, but were matched for time-of-day (Figure 5.3).

In studies 2 and 3, participants underwent three consecutive days of testing (MRI, TMS, MRI+TMS respectively, see Figure 5.3). Each participant's sessions were matched to be at the same time of day to control for circadian effects. In study 2, 18 healthy participants (aged 18-32, 9 female) underwent a longitudinal MRI-TMS-MRI paradigm, and all participants experienced the plasticity-induction condition (paTMS). In study 3, 36 healthy participants (aged 19-30, 22 female) underwent a longitudinal MRI-TMS-MRI paradigm. Participants were randomly assigned either to the plasticity-induction condition (paTMS) or to the control stimulation condition (puTMS, details below).

All participants were screened for TMS and MRI safety, received monetary compensation for their participation, and gave their informed consent to participate in this study. All study procedures were reviewed and approved

by the local ethics committee at the University of Oxford (Central University Research Ethics Committee (CUREC)), and followed the Declaration of Helsinki.

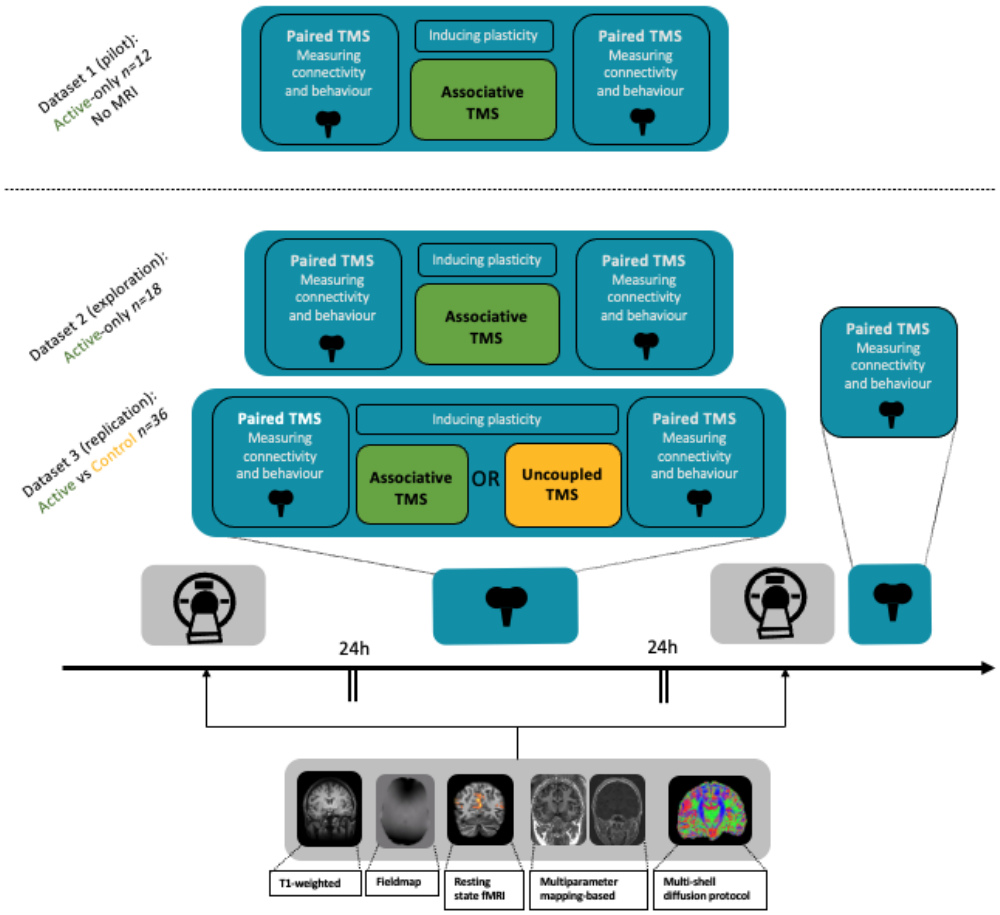


Figure 5.3: Summary of experimental design.

### 5.3.2 Magnetic Resonance Imaging (MRI) acquisition

In studies 2 and 3, participants underwent Magnetic Resonance Imaging (MRI) sessions 24 hours before and 24 hours after the TMS intervention. MRI

data were collected with a 3.0-T Prisma Magnetom Siemens scanner, software VE11B (Siemens Medical Systems, Erlangen, Germany). Participants were asked to keep their head still and to wear earplugs during scanning in order to reduce the impact of MRI-related noise.The sequences were collected as follows: T1-weighted image (T1w), resting-stated fMRI (rs-fMRI), Multi-Parameter Mapping (MPM) and Diffusion-Weighted Imaging (DWI). MRI scan pre-processing, analysis and statistical comparisons were performed using FMRIB Software Library (FSL, v6.0), except for the MPM quantitative map estimation step which was carried out using the hMRI toolbox implemented in Matlab-based SPM, as described in (Tabelow et al., 2019).

The T1w sequence had a TR of 1900 ms, TE of 3.96 ms, a 1mm isotropic resolution and a large Field of View (FOV, 256mm) to allow for the nose to be included in the image and thus facilitate neuronavigation later on in the paradigm. The sequence used GRAPPA with an acceleration factor of 2.

The rs-fMRI Echo-planar imaging (EPI) sequence had a TR of 750 ms and a TE of 29.00 ms. It had a 2mm isotropic resolution, FOV of 208 mm and employed fat saturation-based fat-suppression. The sequence had a multi-band factor 6 and used GRAPPA with acceleration factor 2. Participants were asked to keep their eyes open and let their mind wander during this sequence. The screen was kept black for the duration of this scan, and an eye tracker was used to ensure the participant was awake.

The MPM sequence (as per Weiskopf et al., 2013) included three multi-echo 3D FLASH (fast low-angle shot) scans with varying acquisition parameters, one radio frequency (RF, or B1+) transmit field map and one static

magnetic (B0) field map scan, for a total acquisition time of roughly 22 minutes. To correct for inter-scan motion, the position-specific receive coil sensitivity field was calculated and corrected for, as per Papp et al., 2016. The three types of FLASH scans were designed to be predominantly T1-, PD-, or MT-weighted by changing the flip angle and the presence of a pre-pulse: 8 echoes were predominantly Proton Density-weighted (TR = 25ms; flip angle = 6 degrees; TE = 2.3-18.4ms), 8 echoes were predominantly T1-weighted (TR = 25ms; flip angle = 21 degrees; TE = 2.3-18.4ms) and 6 echoes were predominantly Magnetisation Transfer-weighted (TR = 25ms; flip angle = 21 degrees; TE = 2.3-13.8ms). For MTw scans, excitation was preceded by off-resonance Gaussian MT pulse of 4 ms duration, nominal flip angle, 2 kHz frequency offset from water resonance. All FLASH scans had 1 mm isotropic resolution and field of view (FOV) of 256x224x176 mm. The B1 map was acquired through an echo-planar (EPI)-based sequence featuring spin and stimulated echoes (SE and STE) with varying flip angles, FOV of 192x192x256 mm and TR of 500 ms. The TE for SE was 37.06 ms, while the TE for STE was 68.28 ms. The B0 map was acquired to correct the B1 map for distortions and off-resonance effects. The B0 map sequence had a TR of 1020.0 ms, first TE of 10 ms, second TE of 12.46 ms, field of view (FOV) of 192x192x256 mm and read-out bandwidth of 260 Hz/pixel.

The diffusion-weighted Echo-planar imaging (EPI)sequence had TR=3070 ms, TE=85.00 ms, FOV=256mm, voxel size=1.5mm isotropic, multiband factor of 4. Diffusion scans were collected for two b-values (500 and 2000 $s/mm^2$), over 281 directions. An additional 23 volumes were acquired at

b=0, 15 in AP phase-encoding direction and 8 in the PA phase-encoding direction.

### 5.3.3 MRI preprocessing

All T1w images were preprocessed through a standard FreeSurfer pipeline (Fischl et al., 2004) to correct for bias field and achieve ACPC alignment (for use in Neuronavigation) and also to register them to MNI space through non-linear transformations (in preparation for further group-level analyses). In longitudinal analyses, great care was taken to calculate an unbiased structural mid-point between the two timepoints, and a custom-script based on (Scholz et al., 2009) was used for this purpose.

Automated custom pipelines based on existing FSL tools were developed for our diffusion sequence. The topup tool was run on average images of AP b0 volumes and PA b0 volumes. After applytopup was used to correct for the resulting susceptibility-induced off-resonance field, eddy was run (with flags optimised for multiband diffusion data) to correct for eddy currents and subject movement. A diffusion tensor model was fit to each voxel through DTIFIT, with flags optimised for multi-shell data processing, such as the –kurt option. Boundary-Based Registration was then used to calculate a DWI-to-T1w registration using AP b0 images (with high tissue boundary contrast), and then applied to the Fractional Anisotropy volume.

In order to register MPM volumes to FA volumes, we used the following steps. Boundary-Based Registration was used to calculate a DWI-to-T1w registration using AP b0 images (with high tissue boundary contrast). A

customised pipeline was used to ACPC align the MPM maps and register them to T1w space. At this stage, 1 participant was excluded as the MPM scan was heavily corrupted due to movement artefacts (study 2); 1 participant was excluded due to lower quality signal in the MPM scan, which resulted in poor registrations with other modalities (study 3, control condition); 1 participant was excluded due to a callosal abnormality (study 3, active condition). Once registration matrices for MPM-T1w and DWI-T1w were calculated, they were inverted, concatenated and applied as needed to bring MPM volumes into DWI space with minimal interpolation. For a separate analysis in MNI space, MPM volumes were also registered to MNI space by combining the registration between MPM volumes and midpoint T1w images with the registration between the midpoint T1w space and the MNI template; these volumes were then smoothed with gauss kernel of 3mm.

Preprocessing of rs-fMRI data was run in the FSL FEAT GUI, with parameters as follows: high pass filter cutoff of 100 s, MCFLIRT to correct for motion, smoothing at FWHM of 5mm, BBR registration, B0 unwarping with fieldmap (previously prepared with `fsl_preparefield_map`). Single session Multivariate Exploratory Linear Optimized Decomposition into Independent Components (MELODIC)-based Independent Component Analysis was used to extract components at the single subject level. As per (Griffanti et al., 2017), components were classified as noise or signal manually for the first few subjects, and the labels were then used to build a FIX-based classifier to denoise the data. Once all individual scans were pre-processed, they were fed into a group-level MELODIC-based Independent Component Analysis with

dimensionality of 30.

### 5.3.4 Statistical inference for MRI data

Group-level analyses for DWI and MPM data were carried out in a common space, by skeletonising the FA volumes with Tract-Based Spatial Statistics (TBSS), applying DWI-based skeletonisation transforms to MPM data in DWI space, and running *randomise* (5000 permutations) in each modality with the relevant repeated measure and unpaired t-test general linear model design. In addition, group-level analyses for MPM data were also run separately in MNI space, to exclude the possibility of voxel selection bias during the skeletonisation process. Exchangeability blocks were defined at the subject-level to avoid permutations being influenced by the non-independent, repeated measure data (Winkler et al., 2015). Group-level analyses for rs-fMRI data were carried out with dual regression, taking care to use exchangeability blocks in permutation-based steps.

### 5.3.5 Transcranial Magnetic Stimulation (TMS)

Two DuoMAG MP-Dual Paired Pulse TMS monophasic stimulators (DeyMed DuoMag, Rogue Resolutions Ltd.) were used to deliver pulses to two figure-eight coils, one 70mm-diameter coil over primary motor cortex (M1) and one 50mm-diameter coil over right inferior frontal gyrus (rIFG).

The 70mm/M1 coil was held by the main experimenter throughout the experiment. This coil was kept tangential to the skull and at roughly a 45° angle to the scalp's midline, resulting in a Posterior Anterior (PA) current di-

rection. The main experimenter changed between subjects but always stayed the same for each subject, to minimise variability in coil positioning.

The 50mm/rIFG coil was positioned in place using a clamp held by a Manfrotto Variable Friction Arm (Wex Photo Video, Calumet Photographic Limited) which was clamped to the same table as the chinrest. The position of the coil was determined through the participant's T1w image, and the coordinates were based on (Neubert et al., 2010), more specifically they were x = 58, y = 15, z = 30 in MNI (Montreal Neurological Institute) space. The angle of the rIFG coil was 0° relative to midline.

Participants sat on a chair and were asked to position their head on a chin rest in order to minimize head movement. During the plasticity induction protocol, they were provided with a pillow on which to relax both their hands. Before the start of any TMS stimulation, participants were asked not to move either hand voluntarily, but to relax and allow movements to occur when elicited by the stimulation. They were also asked to keep their feet relaxed and flat on the ground. They were asked to keep their head still on the chinrest and to not move too much. Finally, when watching images, they were asked to try not to fall asleep. The participants were free to move their body between sessions, but they were asked to move the hand with the electrodes as little as they could. All participants wore earplugs to reduce the effects of TMS-related clicking noise.

Neuronavigation was achieved through a Polaris camera and the Brainsight (Rogue Resolutions, Inc.) software. The participant was tracked through a headband with reflective spheres attached to it; the coils were tracked with

coil trackers that were re-calibrated at the beginning of each testing day. In addition, extensive hardware checks were performed before each session, including that the coils worked on a peripheral muscle, that cable connections were correctly in place, and importantly, a PicoScope6 (Pico Technology) was used to check the timing of the two pulses to ensure they were correct and identical between task and rest blocks at sub-millisecond precision (Figure 5.2A).

Online neuronavigation was used in all subjects to ensure the coil was targeting the cortical area of choice throughout the task. Moreover, a sample of the coil location was collected for each participant during the session, and analysed offline. An automated Brainsight tool was used to find the closest brain voxel to the sampled stimulation site. The coordinates for this voxel were then transformed in standard space to allow overlaying of stimulation sites from different participants. At this stage, a total of 41 stimulation locations were included, as 4 participants' stimulation locations failed to save due to software fault (2 in active-only study, 1 in active randomised and 1 in control randomised), and 5 participant's stimulation locations could not be automatically determined with Brainsight (2 in active-only, 2 in active randomised, 1 in control randomised). All stimulation sites across conditions (Figure 5.2C) were within 2 cm of target location, as described in previous publications (Buch et al., 2011, Johnen et al., 2015).

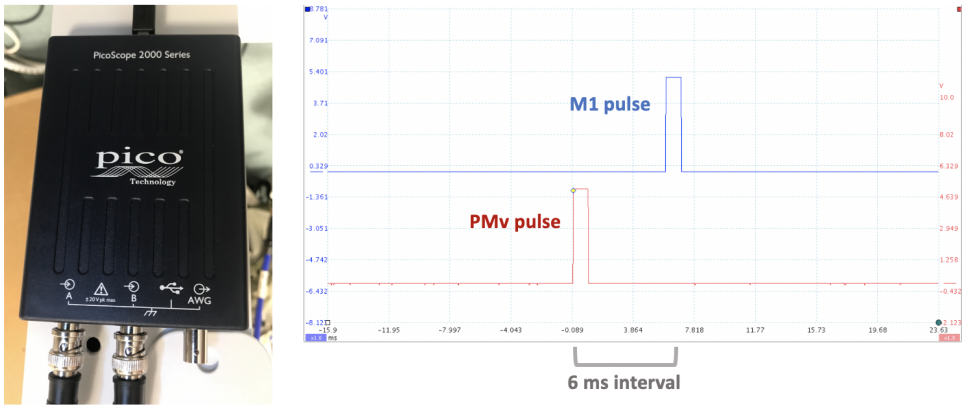


Figure 5.4: A picoscope was used to determine the accuracy of inter-pulse interval with millisecond precision.

### 5.3.6 Electromyography (EMG)

Electromyography (EMG) was recorded from the participant's right hand in a tendon-belly montage, aiming to record from the First Dorsal Interosseus muscle. After scrubbing the three electrode sites with alcohol wipes, 25-mm electrodes (Kendall Neonatal ECG Electrodes Puppydog) were applied. A ground electrode was placed on the hand's carpus and the exact location of the electrodes was carefully replicated across days for the same participant. In order, the EMG signal output was processed through a D440 amplifier (Digitimer), a Humbug Noise Eliminator, 50Hz (Digitimer) to notch-filter the data, and a CED micro1401 Mk.II A/D converter (Cambridge Electronic Design) to digitise the signal and relay it to a PC running Spike2 (Cambridge Electronic Design). Sampling rate was 5000 Hz, and bandpass filters were

set between 10 and 1000 Hz.

### 5.3.7 Motor hotspot determination

The M1 coil intensity was increased and slowly moved around over the left side of the scalp until a motor hotspot could be identified. Several criteria were applied to confirm the right coil location had been reached: reliability of the MEPs, smoothness of the MEP shape, selectivity of finger movement during MEPs, and degradation of MEP response as the coil moved away from the identified spot. Participants who failed to meet all motor hotspot criteria were excluded from further testing. The location of the motor hotspot was recorded through neuronavigation during the first session. After the first session, the recorded location was used to quickly re-confirm the motor hotspot; this also ensured the same motor hotspot was stimulated across sessions in multi-day protocols.

### 5.3.8 Parameter determination

After determining the location of the motor hotspot, three parameters were determined for each participant: the intensities for 1mV, resting motor threshold (rMT) and active motor threshold (aMT). For participants in study 3, and a subset of participants in study 2, 1mV, aMT and rMT were collected before the plasticity induction protocol, and 24 hours after.

1mV was determined as the intensity giving reliable and stable 1mV MEPs at rest over around 10 pulses; stability of the MEPs, rather than a precise mean value of 1mV across 10 pulses, was used as the key parameter

in determining 1mV intensity. rMT was determined as the intensity at which 5 out of 10 pulses give MEP responses greater than 0.05 mV.

After 1mV and rMT determination, a brief, standardised protocol was used to determine aMT as per (Stagg et al., 2011). A separate screen was moved towards the participant so that they could observe their own FDI EMG trace in real time from the chinrest. After the participants verbally confirmed they could see the screen, and they were asked to squeeze the thumb against the index finger as hard as they could a couple of times to determine their maximum contraction. A sliding line on the screen was then set to 20% of maximum muscle contraction, and participants were asked to try and keep their contraction levels around that line. The experimenters ensured this level of contraction did not cause fatigue but that it was also not too close to the noise level; if it did/was, maximum contraction was calculated once again. This FDI-contraction set-up allowed to measure the aMT, which we defined in this experiment as the intensity at which 5 out of 10 TMS pulses produced an MEP that was time-locked to the TMS pulse, and was followed by a cortical silent period (time-locking and presence of cortical silence period were chosen as criteria because MEP size is influenced by background muscle contraction during aMT). Presence of time-locked MEPs, rather than presence of cortical silent period, was used as the key parameter in determining aMT.

### 5.3.9 paired pulse TMS (ppTMS)

Participants underwent ppTMS during task before and immediately after the plasticity induction protocol. Participants in study 2 and 3 also underwent ppTMS 24 hours after the plasticity induction protocol. ppTMS was carried out by stimulating the motor hotspot at 1mV in half the trials, and carrying out the same stimulation, preceded by 6ms by a conditioning rIFG pulse at 110% of rMT. The pulses were always delivered 175ms after cue onset, and were randomly assigned in an equal fashion to stay vs switch trials and to right-hand vs left-hand trials (Figure 5.2E).

### 5.3.10 paired associative TMS (paTMS) and paired uncoupled TMS (puTMS)

Paired associative TMS (paTMS) and paired uncoupled TMS (puTMS) both consisted of 90 paired pulses, delivered at 0.1 Hz over a 15 minute period, without interruptions (Figure 5.2D). The M1 coil was set at a 1mV intensity, whereas the rIFG coil was set at a 110% rMT intensity. In paTMS, the paired pulses were 6ms apart, whereas in puTMS the pulses were 500 ms apart, in accordance with previous literature (Buch et al., 2011), (Johnen et al., 2015). paTMS and puTMS were always performed at rest, with the participant resting their hands on a pillow and watching a series of still images on a computer screen.

### 5.3.11 Motor Evoked Potential (MEP) analysis

EMG analysis focused on TMS-induced Motor-Evoked Potential (MEPs), and more specifically on the peak-to-peak amplitude of MEPs. MEP recording, preprocessing and analysis procedures were identical for all experiments. MEPs were identified based on recorded TMS timings, pre-processed in MATLAB (Version R2018b, Mathworks, MA, USA) and visualised for quality control purposes. Absent or unusually small MEPs (<0.2 mV) or unusually high MEP (>9 mV) were excluded from further analyses. Trials with incorrect, premature (<150 ms) and high-reaction-time (>800 ms) responses were also excluded from further analyses. Trials with significant 'precontraction' (i.e. muscle contraction above 0.4 mV in the 100 ms before the MEP and the test pulse) were also excluded. After preprocessing, MEP ratios (ppTMS/spTMS) were obtained from the the median normalised MEP for each condition.

### 5.3.12 Action Reprogramming Task

The Action Reprogramming task was implemented based on a task originally developed by (Isoda and Hikosaka, 2007) for monkeys and then adapted for use in human TMS studies by (Neubert et al., 2010). The task aimed to probe action execution and action reprogramming. Cues consisted of a central square (either red or green) with two 'flanker' squares (one red and one green). Participants were instructed to press the button on the side where the flanker colour matched the colour of the central square. The flankers

kept switching sides at random, whereas the central square was the same colour for 3-7 trials at the time (Figure 5.2B). This way, participants simply had to execute a movement when the central cue colour stayed the same ('stay trials'), but they had to inhibit the movement and carry out a different one in the trials where the central cue colour had switched ('switch trials'). Participants in study 1 underwent 2 sessions of the task (before and immediately after the plasticity induction protocol); participants in studies 2 and 3 underwent 3 sessions (before, immediately after, and 24 hours after the plasticity induction protocol). Each session consisted of a set of 112 switch trials and corresponding stay trials. Each session had 3 automatic breaks in between to ensure participants had a chance to rest if they wished to do so. Participants were told to be as fast and accurate as they could. Participants received detailed task instructions in paper format at the beginning of each session; in addition, the instructions were reiterated in a computer-based fashion at the beginning of the baseline task (full code available here: https://github.com/lazaral/paTMS_task). Before the baseline task, they undertook roughly 100 trials to make sure first that they understood the rules of the task, then that they had habituated to the task, and finally that they could tolerate TMS pulses while performing the task. Participants were pressing the two buttons with index fingers from their two hands, and were instructed to keep their hands relaxed between trials until the cue came in; they were occasionally reminded to keep their hands relaxed if a lot of muscle contractions were observed between trials.

### 5.3.13 Blinding

In study 3, after the baseline ppTMS block, participants were allocated to either active or control group at random through an algorithm aimed at minimizing variance in gender between active and control group (executed on the rando.la website). Subjects were blind to their experimental condition throughout the experiment. Experimenters were also blind to the condition during baseline testing; however, the obvious sound difference between paired associative TMS and paired uncoupled TMS made it impossible to achieve full blinding once the plasticity intervention had started taking place.

### 5.3.14 Discomfort and blinding assessment

At the end of the experiment, participants were administered a discomfort questionnaire and a questionnaire aimed at assessing blinding of the experiment.

The discomfort questionnaire was loosely based on (Meteyard and Holmes, 2018) and asked participants: to rate the level of distraction caused by the stimulation (from 0, "not distracting at all", to 10, "very distracting (I found it difficult to concentrate)"), how annoying were the TMS pulses (from 0, "not annoying at all", to 10, "very annoying (Unable to complete the task)"), and if there were any twitches, how strong were the muscle twitches from the TMS pulse (from 0, "no twiches", to 10, "a very strong cramp"). The twitch question was repeated for head and face. In order to minimise cueing in reporting of adverse effects, the participants were asked whether they had

experienced any other side effects of the stimulation. If the answer was yes, they were administered a second questionnaire, based on established literature on tDCS adverse effects (based on a systematic review by (Brunoni et al., 2011)), asking for levels of pain, headache, neck soreness, sleepiness, acute mood change, and with blank spaces to add other unforeseen potential side effects. In this second questionnaire, the participants were also asked to rate how strongly they thought each side effect they had experienced was related to TMS.

The blinding questionnaire was custom-made and adapted with careful consideration of the specific constraints of blinding for TMS conditions. The questionnaire explained that on the second day of the experiment, the participant had received 15 minutes of paired TMS while they were watching pictures on the screen. It then explained the the study contains two different patterns of paired TMS – an active pattern and a control pattern; and that they were randomly assigned to receive either an active pattern or a control pattern. After that, the participants were asked which pattern they thought they had received (active or control). They were also asked to rate, in percentage, how certain they were of the answer. Less than 50% confidence was registered as an 'I don't know' answer, and the scores were used to calculated an overall Bang's Blinding Index for the experiment (Bang et al., 2004).

To avoid biasing the participants, a script was developed to answer potential questions about blinding. The script was as follows: Q: 'What is the difference between active and control?' A: 'I can't give you any more information about the differences between conditions – please just answer as best

as you can. It is fine to guess if you don't know'. Q: 'I have no clue which one it is'. A: 'I can't give you any more information– please just answer as best as you can. It is fine to guess if you don't know'. Q: 'What does 'control' mean?' A: 'It has a similar meaning to 'placebo".

### 5.3.15 Statistical inference for TMS and behavioural data

Analyses of MEPs and Reaction Times were run in GraphPad Prism (GraphPad Software, La Jolla, California, US) with the exception of the ANCOVA analysis which was run in SPSS (SPSS Statistics, IBM Corp.). Parametric statistics was used for normal data, and non-parametric statistics were used for non-normal data. Longitudinal analyses between two time-points within a group, or between two groups, were run as matched-pair tests, whereas longitudinal analyses across all groups were run as one-way ANOVAs, with Dunn's multiple comparison tests as post-hoc tests. Longitudinal analyses across all groups which aimed to covary for additional factors were run as ANCOVAs. When testing whether ratios were significantly different from 1, a one-sample Wilcoxon test was used. Alpha level for statistical significance was set at 0.05 and all Confidence Intervals (CIs) were set at 95% confidence.

| | Active (*n=18*) | | Control (*n=18*) | |
|---|---|---|---|---|
| | *Mean* | *SD* | *Mean* | *SD* |
| Age | 25.167 | 3.240 | 23.722 | 2.824 |
| Handedness | 88.529 | 13.076 | 86.013 | 15.109 |
| Distraction | 4.056 | 2.235 | 5.333 | 1.847 |
| Annoyance | 3.722 | 2.347 | 3.944 | 2.100 |
| Head twitches | 2.389 | 2.279 | 1.667 | 2.196 |
| Face twitches | 1.000 | 1.715 | 1.278 | 1.904 |
| Bang's Blinding index | 0.111 | 0.458 | 0.000 | 0.460 |

| | Active | Control |
|---|---|---|
| | *# participants* | *# participants* |
| **Reported other side effects** | 3 | 1 |
| **Gender** | | |
| *female* | 12 | 10 |
| *male* | 6 | 8 |
| **Time of day** | | |
| *morning* | 6 | 11 |
| *afternoon* | 12 | 7 |

Figure 5.5: Participant attributes and experiences are well matched between active and control intervention in Study 3. Adverse effects are all on a scale from 1 to 10. The Distraction score, for example, runs from 1 ('not distracting at all') to 10 ('very distracting - I found it difficult to concentrate'). 4 participants in total in Study 3 reported 'Other side effects'. When further questioned on it, all reported headaches, and one pain. They all believed it was related to TMS, and one participant (active condition) believed it was specifically due to the chinrest during the stimulation.

## 5.4 Results

### 5.4.1 Study 1: Behavioural and physiological effects of paTMS

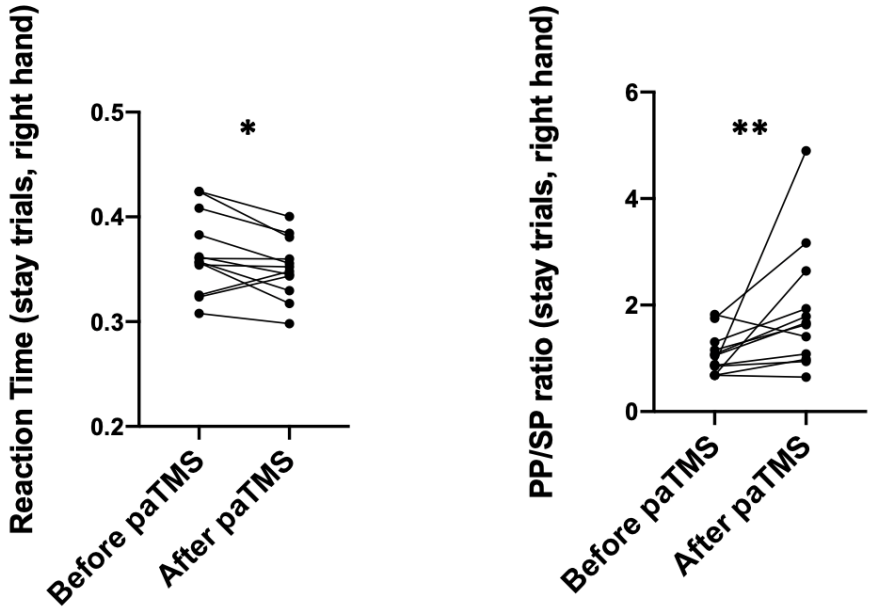


Figure 5.6: Preliminary evidence for efficacy of paTMS in a pilot sample of 12 participants. Each dot corresponds to the metric for an individual participant; metrics before and after paTMS for the same participant are connected by a line.

Study 1 (pilot) aimed to assess behavioural and physiological effects of paTMS on the interhemispheric circuit connecting right PMv to left M1. The results show that following paTMS, participants have significantly faster reaction times during stay trials (which aimed to measure action execution perfor-

mance, Figure 5.6, Wilcoxon matched-pairs rank test: 95% Confidence Interval of median of differences, -0.02763 to -0.0005164; p=0.0269) and significantly higher PP/SP ratio, a metric of physiological connectivity (see Methods), in the same trial condition ( Figure 5.6, Wilcoxon matched-pairs rank test: 95% Confidence Interval of median of differences, 0.08757 to 1.414; p=0.0068).

### 5.4.2 Studies 2 and 3: Behavioural and physiological effects of paTMS

Studies 2 (exploration) and 3 (confirmation) aimed to replicate and extend the findings from Study 1. Compared to study 1, studies 2 and 3 also had a 24h post-paTMS time-point for behavioural and physiological data, during which data on excitability at rest was also collected (which had not been collected in Study 1).

Effects of paTMS on behavioural measures from Studies 2 and 3 were assessed using ANOVAs on expression/baseline ratios (where expression is immediately after plasticity induction) and considering 3 groups: Active 1 (paTMS group, study 2), Active 2 (paTMS group, study 3) and Control (puTMS, study 3). To confirm which group differences were driving the effect, post-hoc tests were run between each individual group for significant ANOVAs. Further, to confirm the direction of time-related effects, one-sample Wilcoxon test were run on ratios for individual groups (where ratios higher than 1 reflect an increase of the measure, and ratios under 1 reflect a decrease in the measure).

Analysis of stay trial RTs (action execution) found faster reaction times following paTMS, as indicated by the expression/baseline ratios being less than 1 in the Active groups (one-sample Wilcoxon test: Active 1 CI of -0.08730 to -0.02070 and p = 0.0033; Active 2 CI of -0.1003 to -0.005973 and p = 0.0063). This result replicates the pilot findings in the paTMS group in study 1. However, no significant effect of group was found (one-way ANOVA effect of group: $F(2, 51)=1.100$, $p=0.5769$), showing that this effect was not specific to the paTMS intervention.

Analysis of switch trials (action reprogramming) revealed a significant effect of group (one-way ANOVA effect of group: $F(2, 51)=4.377$, $p=0.0178$) and post-hoc tests showed both active groups differed from control (Active 2 vs Control p = 0.0280; Active 1 vs Control p = 0.0447). This reflected a slowing down of reaction time in the Control group (expression/baseline ratios greater than 1 in a one-sample Wilcoxon test: CI -0.009631 to 0.1146; p = 0.0150) that was counteracted by paTMS in the Active groups, which showed no change in RTs (ratios close to 1, one-sample Wilcoxon test for Active 1: CI of -0.02296 to 0.03960, p = 0.9843; one-sample Wilcoxon test for Active 2: CI of -0.05365 to 0.05296; p = 0.8209).

To test whether the effect of group in the ANOVA analysis of switch trials was driven by overall changes in all RTs, or whether it was specific to action reprogramming, we then used an ANCOVA considering the same measures as before (expression/baseline ratios of switch trial RTs) and considering the same 3 groups (Active 1, Active 2 and Control), but additionally covarying by the expression/baseline ratio in stay trial RTs. Similarly to the results of

the ANOVA, the results show an effect of group (one-way ANCOVA effect of group: $F(2, 51)=4.373$, $p=0.018$), demonstrating that the effects on switch trial RT are specific to action reprogramming.

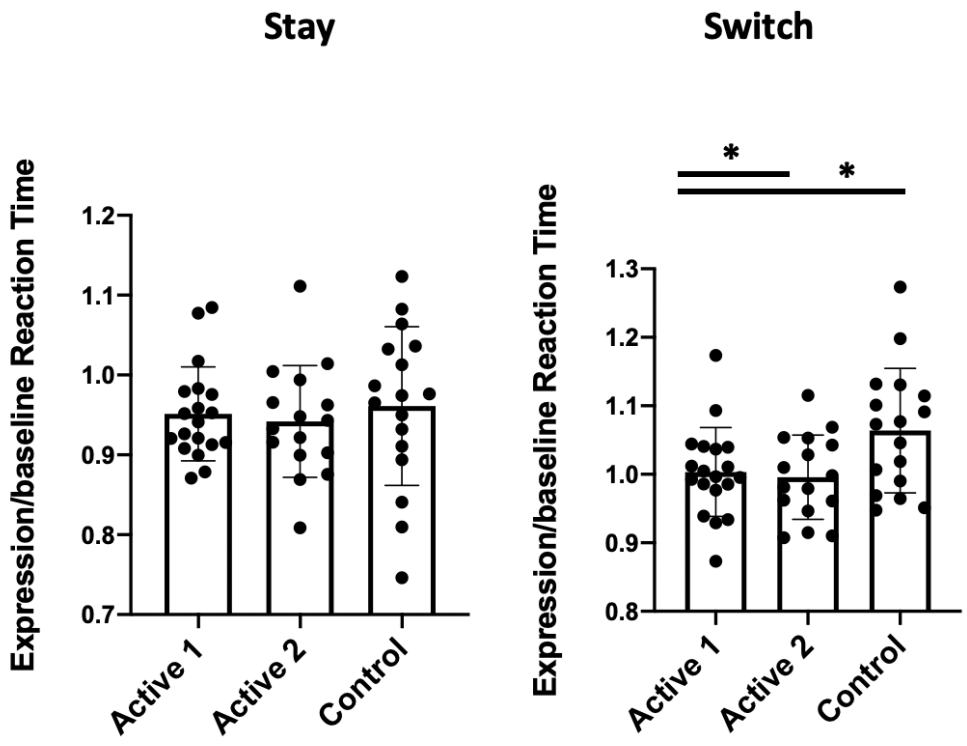


Figure 5.7: Effects of paTMS on action reprogramming behaviour in Study 2 and 3. Bar plot shows mean +/- Standard Error of the Mean (SEM). Each dot corresponds to an individual participant.

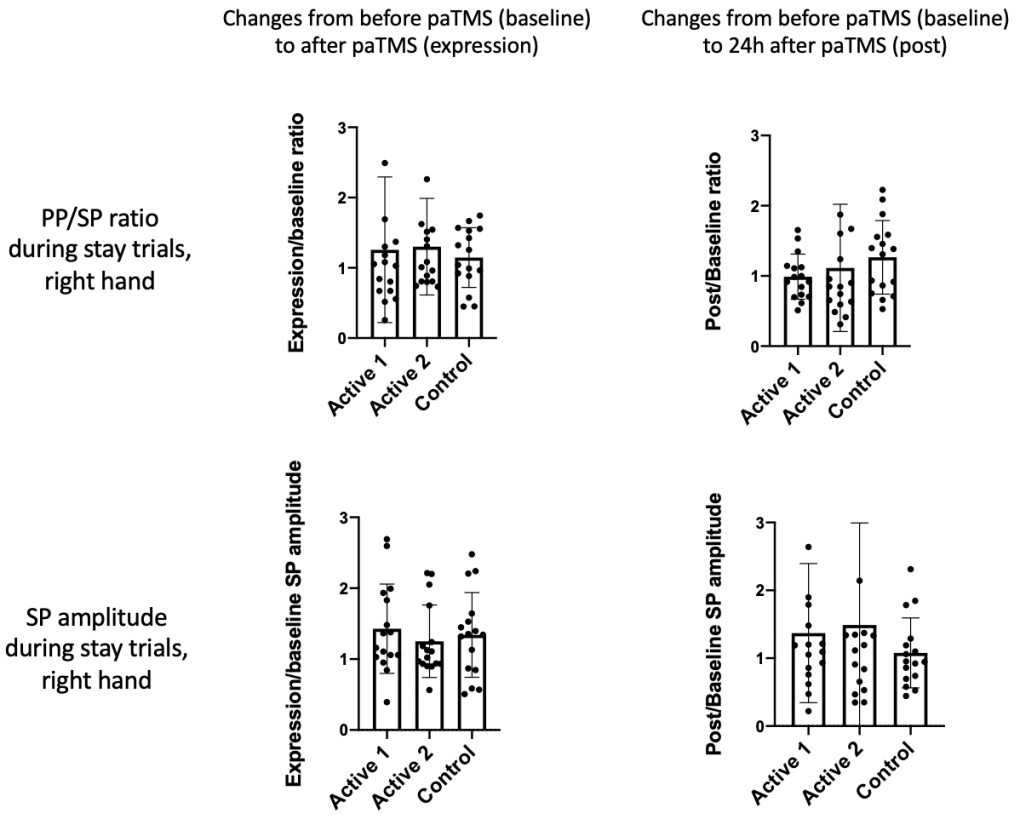


Figure 5.8: paTMS fails to induce robust changes in metrics based on Paired Pulse TMS. Bar plot shows mean +/- Standard Error of the Mean (SEM). Each dot corresponds to an individual participant. Top left panel: two data points above 3 not displayed, one in Active 1 and one in Active 2.Top right panel: one data points above 3 not displayed, in Active 2. Bottom right panel: three data points above 3 not displayed, one in Active 1, two in Active 2.

Effects of paTMS on paired pulse measures from Studies 2 and 3 were assessed using ANOVAs on expression/baseline ratios (where expression is immediately after plasticity induction) and post/baseline ratios (where post is 24 hours after plasticity induction). 3 groups were considered in the ANOVA: Active 1 (paTMS group, study 2), Active 2 (paTMS group, study 3) and

Control (puTMS, study 3).

Analysis of PP/SP ratio found no group differences, either between Baseline and Expression ($F(2, 47)=0.6964$, $p=0.7059$) or between Baseline and Post ($F(2, 47)=3.031$, $p=0.2197$). To probe whether this was confounded by SP amplitude changes, we also tested for group differences in mean SP amplitudes but find no evidence for this (Baseline vs Expression: $F(2, 47)=1.053$, $p=0.5391$; Baseline vs Post: $F(2, 47)=0.5912$, $p=0.7441$).

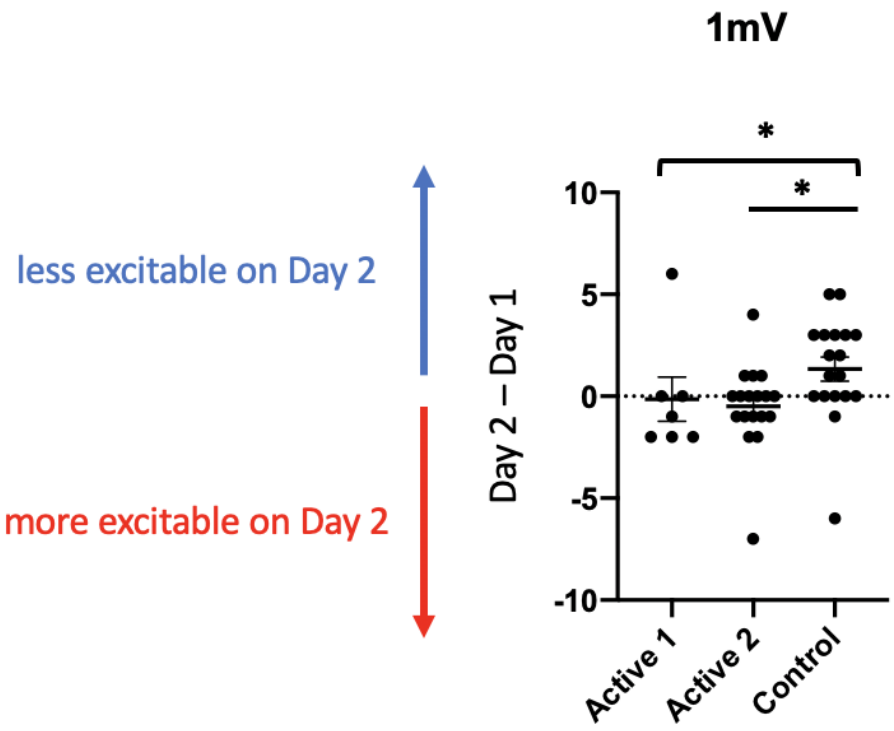


Figure 5.9: paTMS induces increases in M1 excitability. Each dot corresponds to an individual participant.

Effects of paTMS on excitability at rest were then assessed using ANOVAs

on post/baseline ratios (where post is 24 hours after plasticity induction) and considering 3 groups: Active 1 (paTMS group, study 2), Active 2 (paTMS group, study 3) and Control (puTMS, study 3). To confirm which group differences were driving the effect, post-hoc tests were run between each individual group for significant ANOVAs. Further, to confirm the direction of time-related effects, one-sample Wilcoxon test were run on ratios for individual groups (where ratios higher than 1 reflect an increase of the measure, and ratios under 1 reflect a decrease in the measure).

We find a significant effect of group on M1 excitability changes (one-way ANOVA, $F(2, 42) = 8.747$, $p = 0.0126$; post-hoc Active 2 vs Control $p = 0.0294$; post-hoc Active 1 vs Control = 0.0639). In particular, the Control group shows time-related decreases in cortical excitability (ratios over 1, one-sample Wilcoxon test for Control: CI of 0 to 3, $p = 0.0303$), possibly due to habituation, whereas participants who receive paTMS show no change in cortical excitability (ratios close to 1, one-sample Wilcoxon test for Active 1: CI of -2 to 6, $p = 0.5625$; one-sample Wilcoxon test for Active 2: CI of -1 to 0, $p = 0.2681$), suggesting paTMS increases corticospinal excitability at rest over 24 hours.

### 5.4.3 paTMS effects on microstructural MRI measures

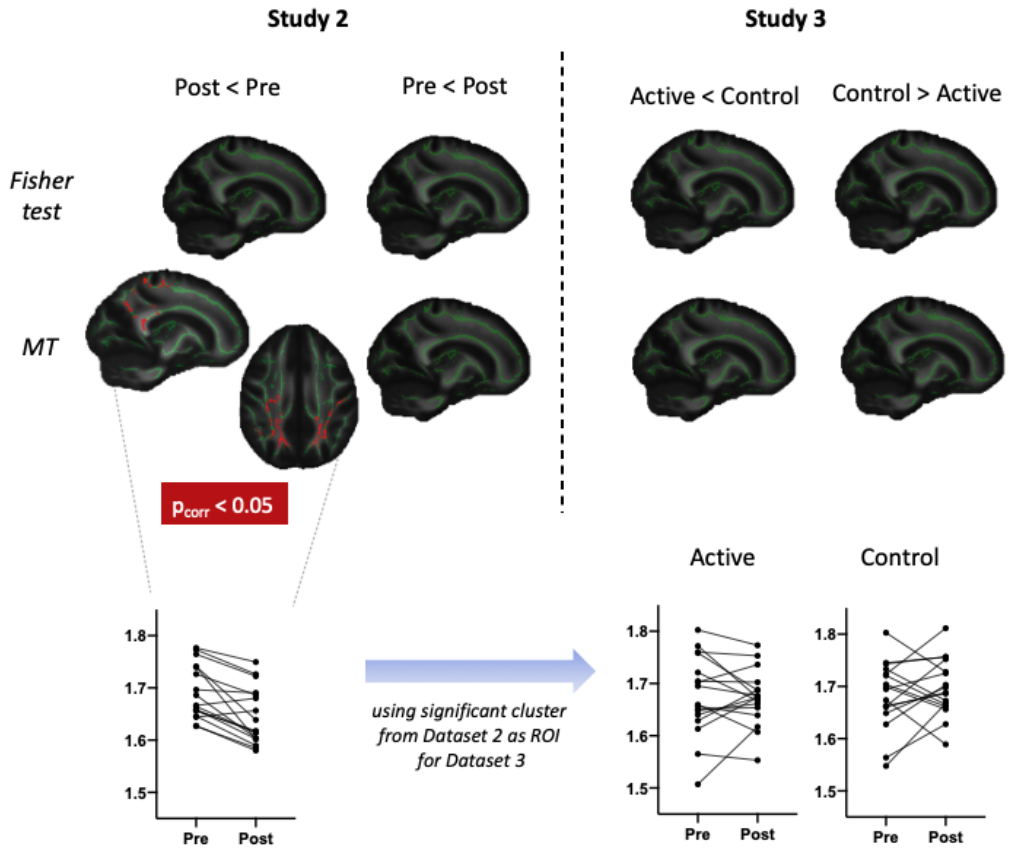


Figure 5.10: No consistent effects of paTMS on microstructure in a voxelwise analysis of white matter. Each dot corresponds to the metric for an individual participant (extracted from the significant cluster); metrics before and after paTMS for the same participant are connected by a line.

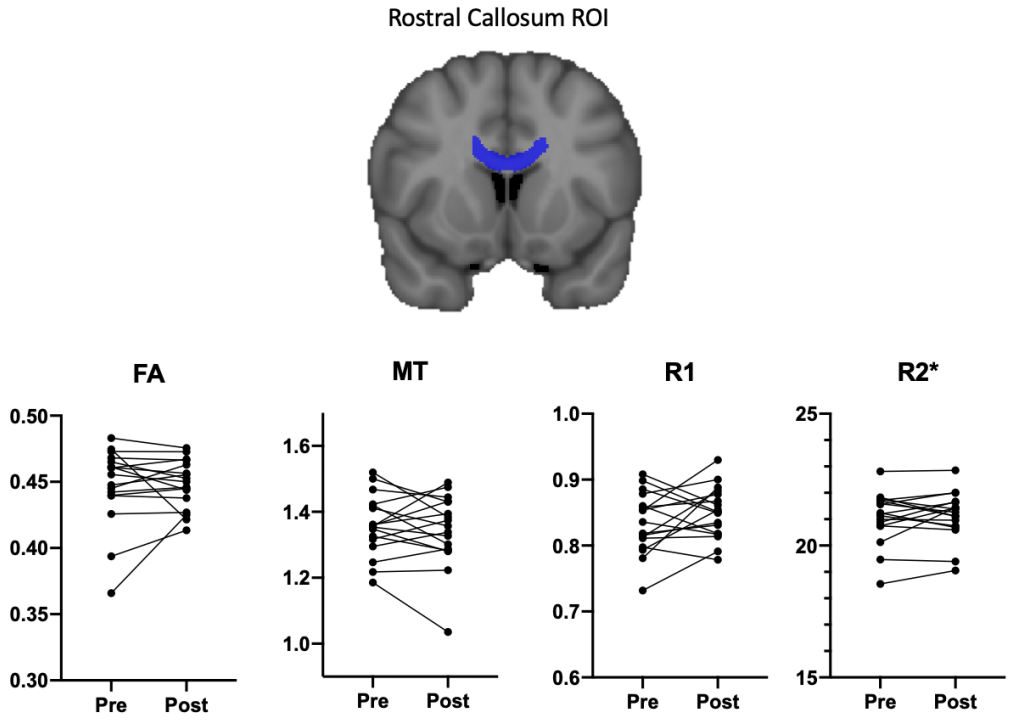


Figure 5.11: No consistent effects of paTMS on microstructure in an ROI analysis of white matter. Each dot corresponds to the metric for an individual participant; metrics before and after paTMS for the same participant are connected by a line.

Studies 2 and 3 aimed to probe the plastic mechanisms induced by paTMS by quantifying tissue microstructure through DWI and MPM scans before and after the intervention. Exploratory analyses from Study 2 find a significant decrease in MT values following paTMS (significant cluster of $p_{corr}$ <0.05 in Figure 5.10; peak $p_{corr}$=0.019). These results, however, are not reproduced in Study 3 (Wilcoxon matched-pairs rank test on mean MT in significant cluster from Study 2 in Active condition of Study 3, CI of -0.02986 to 0.02384, p = 0.8151; CI of -0.02932 to 0.03306 and p = 0.7819 in Control condition of

Study 3).

To verify these results were not driven by specific voxels selected during skeletonisation, we then repeated the analysis for MPM data in MNI space. Here, we find the same pattern of results as Figure 5.10 (results not shown in figures): exploratory analyses from Study 2 find a significant decrease in MT values following paTMS (significant cluster of $p_{corr} < 0.05$; peak $p_{corr} = 0.010091$), which is not reproduced in Study 3 (Wilcoxon matched-pairs rank test on mean MT in significant cluster from Study 2 in Active condition of Study 3, CI of -0.03059 to 0.02721, p = 0.8176; in Control condition of Study 3, CI of -0.03157 to 0.05758, p = 0.3529).

We then followed up these whole-brain analyses with a hypothesis-driven approach. As the fibers stimulated are known to connect right IFG and left M1 interhemispherically, one would expect a change in their myelination to be observed in the corpus callosum. Therefore, we carried out an ROI analysis of atlas-defined rostral Corpus Callosum voxels, taking the mean value for all microstructural markers within the ROI. The results further shows that no reproducible white matter changes take places following paTMS in Study 2 (Wilcoxon matched-pairs rank tests, FA: p=0.8900, MT: p=0.5477, R1: p=0.2435; R2*: p=0.7467).

### 5.4.4 paTMS effects on rs-fMRI measures

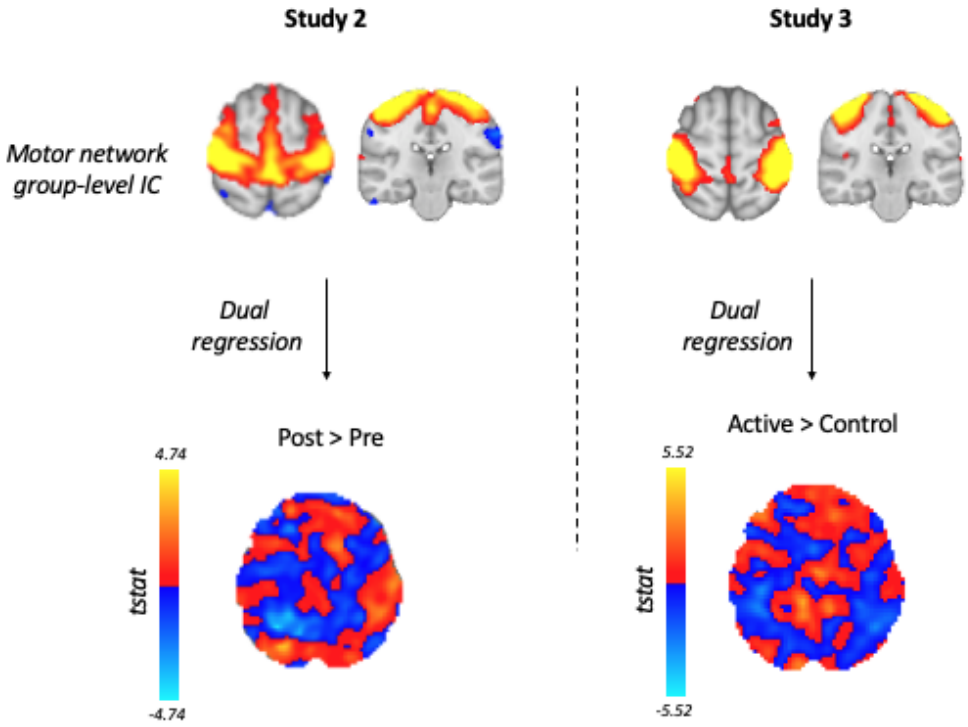


Figure 5.12: Dual regression shows no consistent effects of paTMS on connectivity of the motor network.

Studies 2 and 3 also aimed to investigate the plastic mechanisms induced by paTMS by quantifying connectivity in the motor network with rs-fMRI scans before and after the intervention. As shown in Figure 5.12, group-level ICA on both datasets yields similar motor networks in studies 2 and 3. To test for changes in the connectivity of this network, dual regression was run on the motor network ICA of each study. In both studies, dual regression does not identify changes in connectivity for the motor network (Figure 5.12).

## 5.5 Discussion

A key aim of the chapter was to evaluate efficacy and mechanisms of paired associative TMS (paTMS) interventions, as a way to broaden the evidence base for much-needed protocols to modulate myelinated long-range projections.

Regarding the first question about timing of paTMS-induced plasticity effects, we find that physiological effects persist 24 hours after paTMS. This result is compatible with a previous report that paTMS effects are still present 3 hours after plasticity induction (Buch et al., 2011). However, another study found no physiological effects of paTMS 24 hours after testing (Chao et al., 2015). One potential reason for this could be that the previous study by (Chao et al., 2015), with a sample size of 12, might have been slightly underpowered to detect a small, long-lasting effect of paTMS on noisy physiological metrics. A second reason might have to do with anatomical differences between the studies. The study by (Chao et al., 2015) stimulated projections linking Posterior Parietal Cortex (PCC) to M1, and found no behavioural effect. This hints that there may be critical differences in paTMS outcomes which are dependent on the anatomical site of stimulation, which is often the case in NIBS (Castrillon et al., 2020). In terms of 24-hour effects, we did not find a significant behavioural effect, but the strong effect of time on behavioural performance, likely driven by over-training, could have overshadowed behavioural 24 hour effects.

Two additional questions regarding paTMS as a tool to induce plasticity

regarded (a) whether plasticity could be induced in interhemispheric projections and (b) whether plasticity effects were robust and could be reproduced in confirmatory efforts. The behavioural and physiological effects hint that the answer to both questions is yes. The fact that behavioural effects were consistently found across studies (pilot, exploration and confirmation studies) makes is clear that these effects are reproducible, and can be induced with an inter-hemispheric paradigm. This is the first confirmatory demonstration of paTMS, and the first demonstration that paTMS works in non-homotopic interhemispheric circuits.

A key question, of crucial relevance to the thesis aims, is what the mechanisms underlying paTMS may be. The studies presented here aimed to elucidate this issue through multimodal imaging, but the results are inconclusive.

In particular, initial results from Study 2 seemed to provide evidence towards an effect of paTMS on myelin, whereby paTMS induced broad decreases in MTR – a marker of myelination - in multiple white matter tracts. This would be compatible with much of the previous literature on myelination. First, paTMS is a low-frequency (0.1 Hz) stimulation protocol, and a similar protocol, also at 0.1 Hz, has previously been shown to reduce myelination in vitro (Stevens et al., 1998). Second, recent work has shown that OPCs receive input from distant areas (Mount et al., 2019), which would be compatible with the spatially broad, bilateral decreases in myelination observed in Study 2.

However, these effects failed to replicate in Study 3. There are several

reasons why this could be the case. Inconsistencies in experimental protocols are often claimed to be potential causes for non-replication of published studies (Berg, 2019), but the paradigm was kept the same across all 3 studies, even using the same equipment, thus excluding this possibility.

While n=17 is a typical sample size in longitudinal intervention studies, there is little literature on performing power calculations for longitudinal neuroimaging studies (Mumford, 2012, Steen et al., 2007), especially for those employing novel MR sequences (De Santis et al., 2014). Therefore, one possibility is that all the studies used here may be slightly underpowered to detect the effect of interest, thus leading to a higher likelihood of spurious false positives (Button et al., 2013).

Another explanation for failure to replicate the result in Study 3 relates to assumptions of the analyses that were carried out. Throughout the thesis, a consistent analysis approach was taken by registering MPM scans to their DWI correspondent, and carrying out a common skeletonisation across modalities (Smith et al., 2006). This approach was favoured as it allows to carry out multimodal voxelwise analyses that are not affect by volumetric effects, which is known to be important for DWI (Smith et al., 2006). However, this approach assumes that the relevant voxels from MPM scans will be in the voxels with the highest FA values. For example, if a similar effect as Study 2 was present in Study 3, but not in peak-FA voxels, then our analyses would not have detected it. Therefore, future analyses could focus on multimodal ICA-based fusion of the data (Groves et al., 2011), thus foregoing the need to registering all modalities to a common space.

Regardless of the exact reason why Studies 2 and 3 show different results despite their identical experimental protocols, the results of this chapter really highlight the importance that confirmatory studies have to develop a solid knowledge base in neuroscience (Munafò et al., 2017), and argue for a more extensive uptake of confirmatory study designs.

This result follows up on a large emerging literature highlighting the role that neuronal activity plays in regulating active myelination during adulthood. Previous studies have found that inducing neuronal activity induces myelination, whether this is done by electrical (Li et al., 2010), optogenetic (Gibson et al., 2014), chemogenetic (Mitew et al., 2018), or transcranial magnetic (Cullen et al., 2019) stimulation. Therefore, the lack of overall effects of paTMS on white matter across all conditions is somewhat surprising. A potential explanation is that the intervention was too short. Previous papers typically induce neuronal activity in brief daily sessions carried out each day for 1 or 2 weeks: for example, the paper by (Cullen et al., 2019) found changes in myelin following TMS, but they delivered TMS for 14 consecutive days. Our rationale for choosing a single TMS session was that results from rodent studies (Gibson et al., 2014) indicate that optogenetics induces OPC proliferation already 24 hours after the first 30-minute stimulation session, which means we expected some white matter changes to be present. In addition, paTMS is a rather new NIBS protocol, and as such it is still not known whether it would be safe to deliver it more than once a week. A more plausible explanation is that our myelin markers might have failed to detect existing myelin changes. A major difference compared to previous studies is

that our protocol was carried out in humans, and myelin changes were measured indirectly through MRI. Therefore, it is possible that although paTMS induces myelin plasticity, our MR modalities of choice might not have enough sensitivity to detect it.

Finally, the study also used resting-state fMRI to test whether changes in motor network connectivity may be a potential mechanism underlying the physiological and behavioural effects of paTMS. In both datasets, we find no evidence that paTMS induces changes in motor network connectivity. This is in line with a previous study by (Johnen et al., 2015), finding that paTMS does not induce immediate functional changes that are observable with resting-state fMRI. This previous study probed effects of paTMS 4 minutes after plasticity induction; here, we extend the finding to a 24 hour time-point, which implies motor network connectivity is robust to paTMS stimulation, independently of the timescale on which this is assessed.

There are several reasons why resting-state fMRI might not be able to detect changes following paTMS. First, it could be that changes in synaptic connectivity do take place, but by a small magnitude that is not accessible with coarse methods like fMRI. Second, it could be that changes are most detectable when the network in question is engaged. This interpretation is certainly supported by the findings in (Johnen et al., 2015), which show changes in connectivity of the motor network with fMRI, but only during task. Third, it is possible that functional changes in the brain following paTMS are more distributed, and not restricted to the motor network. Taken together, these studies indicate that paTMS is unlikely to modulate

macroscopic brain networks, and that the mechanisms underlying paTMS-induced behavioural and physiological changes are likely more fine-grained, distributed, or state-dependent.

In conclusion, this chapter provides strong evidence for a robust, 24h effect of paTMS on behaviour and physiology of the motor network. This represents an important step forward, as future studies can build on this knowledge base to further harness paTMS in the study of myelinated long-range projections. However, the mechanisms underlying these paTMS effects remain unclear.

# General Discussion

This thesis aimed to further our understanding of brain plasticity, and in particular of the plasticity in myelinated long-range projections. Three studies were presented, which attempted to answer key questions in the growing field of myelin research.

## 6.1 Overall Comments on Chapter 3 and 4

Before we can study the plastic potential of myelin, it is important to first understand what relationship myelin has to physiology and behaviour. The first two empirical chapters (Chapter 3 and Chapter 4) deal exactly with this question.

Chapter 3 used a cross-sectional, pre-registered dataset to probe whether white matter myelination shapes behaviour. The answer seems to be that this is not the case. In most of Chapter 3, as well as in part of Chapter 4, negative tests are reported on multimodal correlations between myelin markers and behavioural performance, providing strong overall evidence that inter-individual variation in myelin does not have a direct, consistent effect on human behaviour.

At first glance, this might seem in contrast with a lot of literature from the past decade. After all, multiple relationships have been reported between white matter volume and behaviour, as well as between white matter microstructure and behaviour. Several factors could explain this discrepancy. First, it could be that features of white matter other than myelin (e.g.

axon caliber, etc.) may explain variability in behaviour (Perge et al., 2012). Second, it could be that different white-matter behaviour correlations are underpinned by different features of myelinated axon morphology, for example myelin thickness vs length of Nodes of Ranvier (Kaller et al., 2017).

An additional explanation for the lack of myelin-behaviour relationships may be that myelin directly influences brain physiology, which in turn then influences behaviour. In Chapter 4, we find evidence that this may be the case: myelin influences behaviour, but does so indirectly, by influencing physiological processes. In this framework, it makes sense that there is no straightforward relationship between myelination in a given tract and behavioural output: after all, behaviour arises from complex interactions between several brain networks, and myelin levels of a given tract may only influence the physiology of that specific tract.

## 6.2 Overall Comments on Chapter 5

A main aim of this thesis has also been to answer broader questions about myelin plasticity. The first question we set out to answer in Chapter 5 was about whether there is a spike-timing-dependent plasticity effect for myelin plasticity. The results show that despite preliminary evidence for this in one dataset, we find that no robust, reproducible evidence that myelin plasticity is spike-timing-dependent.

This could be because of several reasons. While the study we carried out builds on a now large literature on the effects that neuronal firing can

have on myelination during adulthood (Cullen et al., 2019, Gibson et al., 2014, Li et al., 2010, Mitew et al., 2018), all previous studies have used immunohistochemistry-based histology and Electron Microscopy to study myelination. Therefore, while we know that MR metrics can be sensitive enough to pick up behaviourally-induced white matter changes Sampaio-Baptista et al. (2019a, 2013, 2019b), Scholz et al. (2009), it may be possible that relatively fine-grained changes in myelin, such as the ones induced by neuronal activity interventions, might be missed in MRI.

An open issue in the literature on myelin plasticity is the one of timing. We now know a wide range of plasticity mechanisms take place in white matter (Kaller et al., 2017), but these are likely to unfold over different timescales, and the specifics of timing for these different plasticity mechanisms is still uncertain(Almeida and Lyons, 2017). Therefore, a key source of uncertainty in myelin plasticity studies is often when exactly to collect each timepoint. In Chapter 5, we opted for a 24 hour timepoint, as it was the earliest timepoint where multiple stands of evidence agreed white matter changes would have taken place (Gibson et al., 2014, Xiao et al., 2016). Therefore, it is unlikely that we might have missed the right time to observe myelin changes. However, it is possible that our single-session intervention was not enough to induce the changes, and studies such as (Cullen et al., 2019) have hinted that several sessions may be needed to induce myelin changes non-invasively, although this has not been directly tested. Unfortunately, it is at present not possible to do multiple TMS sessions for paTMS, as safety data on multi-session paTMS is lacking. Moreover, we have also shown that it does have

long-lasting effects, which will make it harder to argue for using multiple sessions of paTMS in healthy participants in the future.

Taken together, these observations can yield some recommendations for future studies aiming to measure myelin plasticity. For studies expecting relatively small effects, histology-based approaches in preclinical models might be more sensitive than MR-based metrics collected in humans. Optogenetics-based interventions, for instance, may be harnessed to ask similar questions to Chapter 5, thus allowing direct, microscopic observation of potential myelin changes. Such experiments do however have downsides: they need higher power, as invasive methodologies are intrinsically incompatible with longitudinal experimental designs, and they need a higher number of control conditions, to control for invasive effects of viral injections and light delivery.

Another important recommendation for future myelin plasticity studies is to consider multiple plasticity-induction sessions. Where possible, carrying out multiple plasticity induction sessions would increase the chances of inducing myelin plasticity. Moreover, a variety of timepoints should be collected where possible, both to circumvent the current uncertainty on timing of myelin plasticity as well as to build a body of knowledge that could reduce such uncertainty in future studies.

## 6.3 Future Directions

A key tenet of this thesis has been that the study of myelinated long-range projections needs to be increasingly more causal, and for this to be achieved,

better intervention tools should be developed to modulate myelinated long-range projections.

The results from Chapter 5 highlight a key problem with developing novel interventions to stimulate specific cortico-cortical projections: brain stimulation protocols often have off-target, non-specific effects. In our case, we found that non-specific M1 excitability changes are induced by Hebbian protocols. This is compatible with in vitro evidence that Hebbian protocols are accompanied by changes in post-synaptic neuronal excitability (Frick et al., 2004). Therefore, even stimulation protocols aiming to reproduce biologically-relevant patterns of brain activity may end up having unintended off-target effects, which is important to keep in mind when designing interventions to modulate long-range projections.

Another key concern when developing new NIBS protocols is balancing efficacy with safety. We know from rodent studies that multiple sessions of optogenetics (Gibson et al., 2014) or of TMS (Cullen et al., 2019) are most likely to yield stable myelin changes, but very little is known about the safety limits for paTMS. As we do not know how long the after-effects of paTMS last (and in fact, Chapter 5 show they may last more than 24 hours), it is at present still controversial whether carrying out multiple paTMS sessions within the same week would be safe, and whether the effects of multiple sessions would have synergistic effects or would counteract each other because of homeostatic effects. Understanding the safety profile of multi-session paTMS interventions, and their effects on the brain, will also be crucial if we are to translate brain stimulation interventions to the clinic, where most success-

ful TMS trials to date involve multi-week TMS interventions (George et al., 2000). Surprisingly, there is very little literature on the effectiveness and mechanisms of NIBS (not only paTMS, but also rTMS and tDCS) interventions when they are delivered over multiple days, as they often are in the clinic, and this is a key question that future studies should aim to address.

In terms of safety, the parameter space of possible paTMS protocols is definitely under-explored, beyond just the number of paTMS sessions that can be delivered to an individual participant. Just to mention two examples, frequency of stimulation is typically kept low (0.1-0.5 Hz depending on the study), as so is length (maximum 15 minutes). We know from safety studies on single-site TMS that higher frequencies, and higher TMS session durations, are still safe (Rossi et al., 2009), but dual-site TMS plasticity interventions are a relatively uncharted territory. Therefore, future studies might want to consider aligning dual-site TMS protocol parameters with single-site TMS protocols, but to do so while still well within safety limits and in a careful manner.

To complement all the methodological points made above, one additional future direction that studies on myelinated long-range projections may want to take is to make the scientific process even more 'open'. As summarised in Chapter 2, each experimental chapter in the thesis has taken one or another measure to ensure reproducibility of the results. However, further measures could be taken. For example, we know that confirmatory studies are the highest standard of evidence in neuroscience, but only two of the studies presented here had a confirmatory component. Optimal study design of-

ten clashes with practicalities: in Chapter 4 we analysed the largest-ever cohort of Paired Pulse TMS data (n=56), and replicating such a result in an independent cohort would have been wildly not feasible. Moreover, pre-registering TMS studies is challenging and still not common practice, which impeded pre-registration of Chapter 4. In the future, setting standards for pre-registration of TMS (and NIBS studies more in general) may help the field progress and make studies such as the one in Chapter 4 confirmatory. In addition, sharing of data and code should be prioritized in the future.

## 6.4 Open questions on myelin plasticity

This thesis aimed to answer questions on the rules shaping myelin plasticity. The focus has been specifically on whether myelin plasticity is spike-timing-dependent in nature. However, many other questions on the rules governing myelin plasticity are still open.

A key open issue relates to the existence of bidirectional myelin plasticity effects. To further the comparison with synaptic plasticity that was drawn in Chapter 1, we know that synapses undergo decreases as well as increases in their efficacy. We also know that homeostatic mechanisms take place, whereby an overall increase in synaptic strengths and firing rates can be counterbalanced with a broad decrease in synaptic efficacy to maintain equilibrium within the circuit. By contrast, little to nothing is know about whether myelin plasticity can be bidirectional (Lazari et al., 2018). Most studies have demonstrated increases in myelin, but inactivity-dependent de-

creases in myelination remain purely speculative and will certainly be the subject of many upcoming studies.

Whether myelin plasticity is *necessary* for any behavioural and/or physiological change to take place in the brain, is also a matter of recent focus in the myelination literature. While many studies have now confirmed that neuronal activity and behavioural interventions can induce myelin changes, relatively few studies have explored the issue of whether changes in myelination are causally necessary in physiological and/or behavioural change, as opposed to being a mere by-product of other plasticity mechanisms, such Long-Term Potentiation (LTP). Seminal studies have shown that myelin changes are needed for motor training (McKenzie et al., 2014), as well as fear conditioning (Pan et al., 2020) and memory consolidation (Steadman et al., 2020). As the study of the rules and factors shaping myelin plasticity continues, it is important to recognise that many studies, such as the ones in this thesis, are not able to causally disentangle the effects of synaptic and myelin plasticity on physiology and behaviour.

Another open question regards how adaptive myelination is integrated into intrinsic myelination programmes during development. Developmental myelination has been known to occur for decades, and an influential model in the field has contrasted the well-established phenomenon of intrinsic myelination, taking place during development, with the under-studied concept of adaptive myelination, taking place during adulthood (Bechler et al., 2018). However, little is known about the trajectory of intrinsic myelination across the brain during development, and whether developmental myelin plasticity

follows similar principles as adult myelin plasticity (Ziegler et al., 2019). Recent studies have found developmental myelination to also have an adaptive component (Etxeberria et al., 2016, Makinodan et al., 2012, Sinclair et al., 2017), thus opening new questions on how adaptive and intrinsic myelination programmes are integrated, and whether myelin plasticity may be contributing to sensitive periods during development (Fuhrmann et al., 2015, Hartley and Lee, 2015, Makinodan et al., 2012).

Finally, this thesis has explored the role of myelination in physiology and plasticity mostly in the motor domain. Although there is increasing evidence that myelin and oligodendrocytes might be implicated in many neuropsychiatric disorders (Khanbabaei et al., 2019, Phan et al., 2020, Zerbi et al., 2018), the importance of myelin in mental health-related problems is relatively under-explored. While previous studies have highlighted that myelin plasticity plays a key role in response to stress and adversity (Lehmann et al., 2017, Liu et al., 2012, Makinodan et al., 2012), and can be an effective drug target in models of depressions (Liu et al., 2016, Su et al., 2018), the extent to which myelination and white matter microstructure may be useful in diagnosing and treating psychiatric disorders is still under-researched.

# Bibliography

# References

Almeida, R. G. and Lyons, D. A. (2017). On myelinated axon plasticity and neuronal circuit formation and function. *Journal of Neuroscience*, 37(42):10023–10034.

Arai, N., Müller-Dahlhaus, F., Murakami, T., Bliem, B., Lu, M.-K., Ugawa, Y., and Ziemann, U. (2011). State-dependent and timing-dependent bidirectional associative plasticity in the human sma-m1 network. *Journal of Neuroscience*, 31(43):15376–15383.

Arancibia-Carcamo, I. L., Ford, M. C., Cossell, L., Ishida, K., Tohyama, K., and Attwell, D. (2017). Node of ranvier length as a potential regulator of myelinated axon conduction speed. *Elife*, 6:e23329.

Argyridis, I., Li, W., Johnson, G. A., and Liu, C. (2014). Quantitative magnetic susceptibility of the developing mouse brain reveals microstructural changes in the white matter. *Neuroimage*, 88:134–142.

Aung, W. Y., Mar, S., and Benzinger, T. L. (2013). Diffusion tensor mri as a biomarker in axonal and myelin damage. *Imaging in medicine*, 5(5):427.

Bai, R., Stewart, C. V., Plenz, D., and Basser, P. J. (2016). Assessing the sensitivity of diffusion mri to detect neuronal activity directly. *Proceedings of the National Academy of Sciences*, 113(12):E1728–E1737.

Bandettini, P. A., Wong, E. C., Hinks, R. S., Tikofsky, R. S., and Hyde, J. S. (1992). Time course epi of human brain function during task activation. *Magnetic resonance in medicine*, 25(2):390–397.

Bang, H., Ni, L., and Davis, C. E. (2004). Assessment of blinding in clinical trials. *Controlled clinical trials*, 25(2):143–156.

Bannerman, D., Good, M., Butcher, S., Ramsay, M., and Morris, R. (1995). Distinct components of spatial learning revealed by prior training and nmda receptor blockade. *Nature*, 378(6553):182.

Barker, A. T., Jalinous, R., and Freeston, I. L. (1985). Non-invasive magnetic stimulation of human motor cortex. *The Lancet*, 325(8437):1106–1107.

Basser, P. J., Mattiello, J., and LeBihan, D. (1994). Mr diffusion tensor spectroscopy and imaging. *Biophysical journal*, 66(1):259–267.

Bathelt, J., Johnson, A., Zhang, M., and Astle, D. E. (2019). The cingulum as a marker of individual differences in neurocognitive development. *Scientific reports*, 9(1):2281.

Bäumer, T., Schippling, S., Kroeger, J., Zittel, S., Koch, G., Thomalla, G., Rothwell, J., Siebner, H., Orth, M., and Münchau, A. (2009). Inhibitory and facilitatory connectivity from ventral premotor to primary motor cortex in healthy humans at rest–a bifocal tms study. *Clinical Neurophysiology*, 120(9):1724–1731.

Beaulieu, C. (2002). The basis of anisotropic water diffusion in the nervous system–a technical review. *NMR in Biomedicine: An International Journal Devoted to the Development and Application of Magnetic Resonance In Vivo*, 15(7-8):435–455.

Bechler, M. E., Swire, M., and ffrench Constant, C. (2018). Intrinsic and adaptive myelination?a sequential mechanism for smart wiring in the brain. *Developmental neurobiology*, 78(2):68–79.

Begley, C. G. and Ellis, L. M. (2012). Drug development: Raise standards for preclinical cancer research. *Nature*, 483(7391):531.

Behrens, T. E., Woolrich, M. W., Jenkinson, M., Johansen-Berg, H., Nunes, R. G., Clare, S., Matthews, P. M., Brady, J. M., and Smith, S. M. (2003). Characterization and propagation of uncertainty in diffusion-weighted mr imaging. *Magnetic Resonance in Medicine: An Official Journal of the International Society for Magnetic Resonance in Medicine*, 50(5):1077–1088.

Belliveau, J., Kennedy, D., McKinstry, R., Buchbinder, B., Weisskoff, R., Cohen, M., Vevea, J., Brady, T., and Rosen, B. (1991). Functional mapping of the human visual cortex by magnetic resonance imaging. *Science*, 254(5032):716–719.

Berg, J. (2019). Replication challenges.

Berlucchi, G. and Buchtel, H. A. (2009). Neuronal plasticity: historical roots and evolution of meaning. *Experimental brain research*, 192(3):307–319.

Bezukladova, S., Tuisku, J., Matilainen, M., Vuorimaa, A., Nylund, M., Smith, S., Sucksdorff, M., Mohammadian, M., Saunavaara, V., Laaksonen, S., et al. (2020). Insights into disseminated ms brain pathology with multimodal diffusion tensor and pet imaging. *Neurology-Neuroimmunology Neuroinflammation*, 7(3).

Bi, G.-q. and Poo, M.-m. (1998). Synaptic modifications in cultured hippocampal neurons: dependence on spike timing, synaptic strength, and postsynaptic cell type. *Journal of neuroscience*, 18(24):10464–10472.

Bliss, T. V. and Lømo, T. (1973). Long-lasting potentiation of synaptic transmission in the dentate area of the anaesthetized rabbit following stimulation of the perforant path. *The Journal of physiology*, 232(2):331–356.

Boekel, W., Wagenmakers, E.-J., Belay, L., Verhagen, J., wn, S., and Forstmann, B. U. (2015). A purely confirmatory replication study of structural brain-behavior correlations. *Cortex*, 66:115–133.

Boorman, E. D., O'Shea, J., Sebastian, C., Rushworth, M. F., and Johansen-Berg, H. (2007). Individual differences in white-matter microstructure reflect variation in functional connectivity during choice. *Current Biology*, 17(16):1426–1431.

Boussaoud, D., Tanné-Gariépy, J., Wannier, T., and Rouiller, E. M. (2005). Callosal connections of dorsal versus ventral premotor areas in the macaque monkey: a multiple retrograde tracing study. *BMC neuroscience*, 6(1):67.

Brunoni, A. R., Amadera, J., Berbel, B., Volz, M. S., Rizzerio, B. G., and Fregni, F. (2011). A systematic review on reporting and assessment of adverse effects associated with transcranial direct current stimulation. *International Journal of Neuropsychopharmacology*, 14(8):1133–1145.

Buch, E. R., Johnen, V. M., Nelissen, N., O'Shea, J., and Rushworth, M. F. (2011). Noninvasive associative plasticity induction in a corticocortical pathway of the human brain. *Journal of Neuroscience*, 31(48):17669–17679.

Buch, E. R., Mars, R. B., Boorman, E. D., and Rushworth, M. F. (2010). A network centered on ventral premotor cortex exerts both facilitatory and inhibitory control over primary motor cortex during action reprogramming. *Journal of Neuroscience*, 30(4):1395–1401.

Button, K. S., Ioannidis, J. P., Mokrysz, C., Nosek, B. A., Flint, J., Robinson, E. S., and Munafò, M. R. (2013). Power failure: why small sample size undermines the reliability of neuroscience. *Nature Reviews Neuroscience*, 14(5):365.

Callaghan, M. F., Freund, P., Draganski, B., Anderson, E., Cappelletti, M., Chowdhury, R., Diedrichsen, J., FitzGerald, T. H., Smittenaar, P., Helms, G., et al. (2014). Widespread age-related differences in the human brain microstructure revealed by quantitative magnetic resonance imaging. *Neurobiology of aging*, 35(8):1862–1872.

Carpenter, S. (2012). Psychology's bold initiative.

Castrillon, G., Sollmann, N., Kurcyus, K., Razi, A., Krieg, S. M., and Riedl, V. (2020). The physiological effects of noninvasive brain stimulation fundamentally differ across the human cortex. *Science Advances*, 6(5):eaay2739.

Cercignani, M. and Bouyagoub, S. (2018). Brain microstructure by multimodal mri: Is the whole greater than the sum of its parts? *Neuroimage*, 182:117–127.

Chambers, C. D., Bellgrove, M. A., Stokes, M. G., Henderson, T. R., Garavan, H., Robertson, I. H., Morris, A. P., and Mattingley, J. B. (2006). Executive ?brake failure? following deactivation of human frontal lobe. *Journal of cognitive neuroscience*, 18(3):444–455.

Chang, E. H., Argyelan, M., Aggarwal, M., Chandon, T.-S. S., Karlsgodt, K. H., Mori, S., and Malhotra, A. K. (2017). The role of myelination in measures of white matter integrity: combination of diffusion tensor imaging and two-photon microscopy of clarity intact brains. *Neuroimage*, 147:253–261.

Chao, C.-C., Karabanov, A. N., Paine, R., Carolina de Campos, A., Kukke, S. N., Wu, T., Wang, H., and Hallett, M. (2015). Induction of motor associative plasticity in the posterior parietal cortex–primary motor network. *Cerebral Cortex*, 25(2):365–373.

Chen, C.-C., Gilmore, A., and Zuo, Y. (2014). Study motor skill learning by single-pellet reaching tasks in mice. *JoVE (Journal of Visualized Experiments)*, (85):e51238.

Chenevert, T. L., Brunberg, J. A., and Pipe, J. G. (1990). Anisotropic diffusion in human white matter: demonstration with mr techniques in vivo. *Radiology*, 177(2):401–405.

Chéreau, R., Saraceno, G. E., Angibaud, J., Cattaert, D., and Nägerl, U. V. (2017). Superresolution imaging reveals activity-dependent plasticity of axon morphology linked to changes in action potential conduction velocity. *Proceedings of the National Academy of Sciences*, 114(6):1401–1406.

Chiappini, E., Silvanto, J., Hibbard, P. B., Avenanti, A., and Romei, V. (2018). Strengthening functionally specific neural pathways with transcranial brain stimulation. *Current Biology*, 28(13):R735–R736.

Churchland, M. M. and Shenoy, K. V. (2007). Temporal complexity and heterogeneity of single-neuron activity in premotor and motor cortex. *Journal of neurophysiology*, 97(6):4235–4257.

Civardi, C., Cantello, R., Asselman, P., and Rothwell, J. C. (2001). Transcranial magnetic stimulation can be used to test connections to primary motor areas from frontal and medial cortex in humans. *Neuroimage*, 14(6):1444–1453.

Cleveland, G., Chang, D., Hazlewood, C., and Rorschach, H. (1976). Nuclear magnetic resonance measurement of skeletal muscle: anisotrophy of the diffusion coefficient of the intracellular water. *Biophysical journal*, 16(9):1043–1053.

Cook, L. L., Foster, P. J., Mitchell, J. R., and Karlik, S. J. (2004). In vivo 4.0-t magnetic resonance investigation of spinal cord inflammation, demyelination, and axonal damage in chronic-progressive experimental allergic encephalomyelitis. *Journal of Magnetic Resonance Imaging: An Official Journal of the International Society for Magnetic Resonance in Medicine*, 20(4):563–571.

Cullen, C. L., Senesi, M., Tang, A. D., Clutterbuck, M. T., Auderset, L., O'Rourke, M. E., Rodger, J., and Young, K. M. (2019). Low-intensity transcranial magnetic stimulation promotes the survival and maturation of newborn oligodendrocytes in the adult mouse brain. *Glia*, 67(8):1462–1477.

Damadian, R. (1971). Tumor detection by nuclear magnetic resonance. *Science*, 171(3976):1151–1153.

Davare, M., Lemon, R., and Olivier, E. (2008). Selective modulation of interactions between ventral premotor cortex and primary motor cortex during precision grasping in humans. *The Journal of physiology*, 586(11):2735–2742.

Davare, M., Rothwell, J. C., and Lemon, R. N. (2010). Causal connectivity between the human anterior intraparietal area and premotor cortex during grasp. *Current Biology*, 20(2):176–181.

De Crespigny, A., Roberts, T., Kucharcyzk, J., and Moseley, M. (1993). Im-

proved sensitivity to magnetic susceptibility contrast. *Magnetic resonance in medicine*, 30(1):135–137.

De Santis, S., Drakesmith, M., Bells, S., Assaf, Y., and Jones, D. K. (2014). Why diffusion tensor mri does well only some of the time: variance and covariance of white matter tissue microstructure attributes in the living human brain. *Neuroimage*, 89:35–44.

Deloire-Grassin, M., Brochet, B., Quesson, B., Delalande, C., Dousset, V., Canioni, P., and Petry, K. (2000). In vivo evaluation of remyelination in rat brain by magnetization transfer imaging. *Journal of the neurological sciences*, 178(1):10–16.

Demerens, C., Stankoff, B., Logak, M., Anglade, P., Allinquant, B., Couraud, F., Zalc, B., and Lubetzki, C. (1996). Induction of myelination in the central nervous system by electrical activity. *Proceedings of the National Academy of Sciences*, 93(18):9887–9892.

Deoni, S. C., Rutt, B. K., Arun, T., Pierpaoli, C., and Jones, D. K. (2008). Gleaning multicomponent t1 and t2 information from steady-state imaging data. *Magnetic Resonance in Medicine: An Official Journal of the International Society for Magnetic Resonance in Medicine*, 60(6):1372–1387.

Di Lazzaro, V., Oliviero, A., Meglio, M., Cioni, B., Tamburrini, G., Tonali, P., and Rothwell, J. (2000). Direct demonstration of the effect of lorazepam on the excitability of the human motor cortex. *Clinical neurophysiology*, 111(5):794–799.

Di Pino, G., Pellegrino, G., Assenza, G., Capone, F., Ferreri, F., Formica, D., Ranieri, F., Tombini, M., Ziemann, U., Rothwell, J. C., et al. (2014). Modulation of brain plasticity in stroke: a novel model for neurorehabilitation. *Nature Reviews Neurology*, 10(10):597.

Doran, M., Hajnal, J. V., Van, N. B., King, M. D., Young, I. R., and Bydder, G. M. (1990). Normal and abnormal white matter tracts shown by mr imaging using directional diffusion weighted sequences. *Journal of computer assisted tomography*, 14(6):865–873.

Dousset, V., Brochet, B., Vital, A., Gross, C., Benazzouz, A., Boullerne, A., Bidabe, A.-M., Gin, A.-M., and Caille, J.-M. (1995). Lysolecithin-induced demyelination in primates: preliminary in vivo study with mr and magnetization transfer. *American journal of neuroradiology*, 16(2):225–231.

Dousset, V., Grossman, R. I., Ramer, K. N., Schnall, M. D., Young, L. H., Gonzalez-Scarano, F., Lavi, E., and Cohen, J. A. (1992). Experimental allergic encephalomyelitis and multiple sclerosis: lesion characterization with magnetization transfer imaging. *Radiology*, 182(2):483–491.

Dutta, D. J., Woo, D. H., Lee, P. R., Pajevic, S., Bukalo, O., Huffman, W. C., Wake, H., Basser, P. J., SheikhBahaei, S., Lazarevic, V., et al. (2018). Regulation of myelin structure and conduction velocity by perinodal astrocytes. *Proceedings of the National Academy of Sciences*, 115(46):11832–11837.

Dyke, K., Pépés, S. E., Chen, C., Kim, S., Sigurdsson, H. P., Draper, A., Husain, M., Nachev, P., Gowland, P. A., Morris, P. G., et al. (2017). Comparing gaba-dependent physiological measures of inhibition with proton magnetic resonance spectroscopy measurement of gaba using ultra-high-field mri. *Neuroimage*, 152:360–370.

Elsayed, G. F., Lara, A. H., Kaufman, M. T., Churchland, M. M., and Cunningham, J. P. (2016). Reorganization between preparatory and movement population responses in motor cortex. *Nature communications*, 7(1):1–15.

Etxeberria, A., Hokanson, K. C., Dao, D. Q., Mayoral, S. R., Mei, F., Redmond, S. A., Ullian, E. M., and Chan, J. R. (2016). Dynamic modulation of myelination in response to visual stimuli alters optic nerve conduction velocity. *Journal of Neuroscience*, 36(26):6937–6948.

Farr, T. D. and Whishaw, I. Q. (2002). Quantitative and qualitative impairments in skilled reaching in the mouse (mus musculus) after a focal motor cortex stroke. *Stroke*, 33(7):1869–1875.

Feinberg, D. A., Moeller, S., Smith, S. M., Auerbach, E., Ramanna, S., Glasser, M. F., Miller, K. L., Ugurbil, K., and Yacoub, E. (2010). Multiplexed echo planar imaging for sub-second whole brain fmri and fast diffusion imaging. *PloS one*, 5(12).

Ferbert, A., Priori, A., Rothwell, J., Day, B., Colebatch, J., and Marsden, C. (1992). Interhemispheric inhibition of the human motor cortex. *The Journal of physiology*, 453(1):525–546.

Fiori, F., Chiappini, E., and Avenanti, A. (2018). Enhanced action performance following tms manipulation of associative plasticity in ventral premotor-motor pathway. *NeuroImage*, 183:847–858.

Fischl, B., Salat, D. H., Van Der Kouwe, A. J., Makris, N., Ségonne, F., Quinn, B. T., and Dale, A. M. (2004). Sequence-independent segmentation of magnetic resonance images. *Neuroimage*, 23:S69–S84.

Ford, M. C., Alexandrova, O., Cossell, L., Stange-Marten, A., Sinclair, J., Kopp-Scheinpflug, C., Pecka, M., Attwell, D., and Grothe, B. (2015). Tuning of ranvier node and internode properties in myelinated axons to adjust action potential timing. *Nature communications*, 6:8073.

Forstmann, B. U., Jahfari, S., Scholte, H. S., Wolfensteller, U., van den Wildenberg, W. P., and Ridderinkhof, K. R. (2008). Function and structure of the right inferior frontal cortex predict individual differences in response inhibition: a model-based approach. *Journal of Neuroscience*, 28(39):9790–9796.

Fox, M. D., Halko, M. A., Eldaief, M. C., and Pascual-Leone, A. (2012). Measuring and manipulating brain connectivity with resting state functional connectivity magnetic resonance imaging (fcmri) and transcranial magnetic stimulation (tms). *Neuroimage*, 62(4):2232–2243.

Fralix, T. A., Ceckler, T. L., Wolff, S. D., Simon, S. A., and Balaban, R. S. (1991). Lipid bilayer and water proton magnetization transfer: effect of cholesterol. *Magnetic resonance in medicine*, 18(1):214–223.

Frick, A., Magee, J., and Johnston, D. (2004). Ltp is accompanied by an enhanced local excitability of pyramidal neuron dendrites. *Nature neuroscience*, 7(2):126–135.

Fuhrmann, D., Knoll, L. J., and Blakemore, S.-J. (2015). Adolescence as a sensitive period of brain development. *Trends in cognitive sciences*, 19(10):558–566.

Fünfschilling, U., Supplie, L. M., Mahad, D., Boretius, S., Saab, A. S., Edgar, J., Brinkmann, B. G., Kassmann, C. M., Tzvetanova, I. D., Möbius, W., et al. (2012). Glycolytic oligodendrocytes maintain myelin and long-term axonal integrity. *Nature*, 485(7399):517.

George, M. S., Nahas, Z., Molloy, M., Speer, A. M., Oliver, N. C., Li, X.-B., Arana, G. W., Risch, S. C., and Ballenger, J. C. (2000). A controlled trial of daily left prefrontal cortex tms for treating depression. *Biological psychiatry*, 48(10):962–970.

Gibson, E. M., Purger, D., Mount, C. W., Goldstein, A. K., Lin, G. L., Wood, L. S., Inema, I., Miller, S. E., Bieri, G., Zuchero, J. B., et al. (2014). Neuronal activity promotes oligodendrogenesis and adaptive myelination in the mammalian brain. *Science*, 344(6183):1252304.

Giedd, J. N., Raznahan, A., Alexander-Bloch, A., Schmitt, E., Gogtay, N., and Rapoport, J. L. (2015). Child psychiatry branch of the national institute of mental health longitudinal structural magnetic resonance imaging study of human brain development. *Neuropsychopharmacology*, 40(1):43.

Glasser, M. F., Goyal, M. S., Preuss, T. M., Raichle, M. E., and Van Essen, D. C. (2014). Trends and properties of human cerebral cortex: correlations with cortical myelin content. *Neuroimage*, 93:165–175.

Glasser, M. F. and Van Essen, D. C. (2011). Mapping human cortical areas in vivo based on myelin content as revealed by t1-and t2-weighted mri. *Journal of Neuroscience*, 31(32):11597–11616.

Goldman, L. and Albus, J. S. (1968). Computation of impulse conduction in myelinated fibers; theoretical basis of the velocity-diameter relation. *Biophysical journal*, 8(5):596–607.

Gooijers, J. and Swinnen, S. (2014). Interactions between brain structure and behavior: the corpus callosum and bimanual coordination. *Neuroscience & Biobehavioral Reviews*, 43:1–19.

Gøtzsche, P. C. and Ioannidis, J. P. (2012). Content area experts as authors: helpful or harmful for systematic reviews and meta-analyses? *BMj*, 345:e7031.

Grandjean, J., Zerbi, V., Balsters, J. H., Wenderoth, N., and Rudin, M. (2017). Structural basis of large-scale functional connectivity in the mouse. *Journal of Neuroscience*, 37(34):8092–8101.

Gratton, C., Laumann, T. O., Nielsen, A. N., Greene, D. J., Gordon, E. M., Gilmore, A. W., Nelson, S. M., Coalson, R. S., Snyder, A. Z., Schlaggar, B. L., et al. (2018). Functional brain networks are dominated by stable

group and individual factors, not cognitive or daily variation. *Neuron*, 98(2):439–452.

Griffanti, L., Douaud, G., Bijsterbosch, J., Evangelisti, S., Alfaro-Almagro, F., Glasser, M. F., Duff, E. P., Fitzgibbon, S., Westphal, R., Carone, D., et al. (2017). Hand classification of fmri ica noise components. *Neuroimage*, 154:188–205.

Groppa, S., Werner-Petroll, N., Münchau, A., Deuschl, G., Ruschworth, M. F., and Siebner, H. R. (2012). A novel dual-site transcranial magnetic stimulation paradigm to probe fast facilitatory inputs from ipsilateral dorsal premotor cortex to primary motor cortex. *Neuroimage*, 62(1):500–509.

Groves, A. R., Beckmann, C. F., Smith, S. M., and Woolrich, M. W. (2011). Linked independent component analysis for multimodal data fusion. *Neuroimage*, 54(3):2198–2217.

Groves, A. R., Smith, S. M., Fjell, A. M., Tamnes, C. K., Walhovd, K. B., Douaud, G., Woolrich, M. W., and Westlye, L. T. (2012). Benefits of multi-modal fusion analysis on a large-scale dataset: life-span patterns of inter-subject variability in cortical morphometry and white matter microstructure. *Neuroimage*, 63(1):365–380.

Grubb, M. S., Shu, Y., Kuba, H., Rasband, M. N., Wimmer, V. C., and Bender, K. J. (2011). Short-and long-term plasticity at the axon initial segment. *Journal of Neuroscience*, 31(45):16049–16055.

Grussu, F., Schneider, T., Tur, C., Yates, R. L., Tachrount, M., Ianuş, A., Yiannakas, M. C., Newcombe, J., Zhang, H., Alexander, D. C., et al. (2017). Neurite dispersion: a new marker of multiple sclerosis spinal cord pathology? *Annals of clinical and translational neurology*, 4(9):663–679.

Grydeland, H., Vértes, P. E., Váša, F., Romero-Garcia, R., Whitaker, K., Alexander-Bloch, A. F., Bjørnerud, A., Patel, A. X., Sederevičius, D., Tamnes, C. K., et al. (2018). Waves of maturation and senescence in micro-structural mri markers of human cortical myelination over the lifespan. *Cerebral Cortex*, 29(3):1369–1381.

Guillery, R. W. (2004). Observations of synaptic structures: origins of the neuron doctrine and its current status. *Philosophical Transactions of the Royal Society B: Biological Sciences*, 360(1458):1281–1307.

Haacke, E. M., Mittal, S., Wu, Z., Neelavalli, J., and Cheng, Y.-C. (2009). Susceptibility-weighted imaging: technical aspects and clinical applications, part 1. *American Journal of Neuroradiology*, 30(1):19–30.

Hallett, M. (2007). Transcranial magnetic stimulation: a primer. *Neuron*, 55(2):187–199.

Harkins, K. D., Dula, A. N., and Does, M. D. (2012). Effect of intercompartmental water exchange on the apparent myelin water fraction in multiexponential t2 measurements of rat spinal cord. *Magnetic resonance in medicine*, 67(3):793–800.

Hartley, C. A. and Lee, F. S. (2015). Sensitive periods in affective development: Nonlinear maturation of fear learning. *Neuropsychopharmacology*, 40(1):50–60.

Hayes, A. F. (2013). Introduction to mediation, moderation, and conditional process analysis: A regression-based approach. 2013. *New York: Guilford*, 1609182308.

Heath, F., Hurley, S. A., Johansen-Berg, H., and Sampaio-Baptista, C. (2018). Advances in noninvasive myelin imaging. *Developmental neurobiology*, 78(2):136–151.

Hebb, D. O. and Hebb, D. (1949). *The organization of behavior*, volume 65. Wiley New York.

Hedges, L. V. and Vevea, J. L. (1996). Estimating effect size under publication bias: Small sample properties and robustness of a random effects selection model. *Journal of Educational and Behavioral Statistics*, 21(4):299–332.

Helms, G., Dathe, H., and Dechent, P. (2008). Quantitative flash mri at 3t using a rational approximation of the ernst equation. *Magnetic Resonance in Medicine: An Official Journal of the International Society for Magnetic Resonance in Medicine*, 59(3):667–672.

Helms, G., Draganski, B., Frackowiak, R., Ashburner, J., and Weiskopf, N. (2009). Improved segmentation of deep brain grey matter structures using magnetization transfer (mt) parameter maps. *Neuroimage*, 47(1):194–198.

Hermundstad, A. M., Bassett, D. S., Brown, K. S., Aminoff, E. M., Clewett, D., Freeman, S., Frithsen, A., Johnson, A., Tipper, C. M., Miller, M. B., et al. (2013). Structural foundations of resting-state and task-based functional connectivity in the human brain. *Proceedings of the National Academy of Sciences*, 110(15):6169–6174.

Hill, R. A., Li, A. M., and Grutzendler, J. (2018). Lifelong cortical myelin plasticity and age-related degeneration in the live mammalian brain. *Nature neuroscience*, 21(5):683.

Horowitz, A., Barazany, D., Tavor, I., Yovel, G., and Assaf, Y. (2015). Response to the comments on the paper by horowitz et al.(2014). *Brain Structure and Function*, 220(3):1791–1792.

Huber, R., Määttä, S., Esser, S. K., Sarasso, S., Ferrarelli, F., Watson, A., Ferreri, F., Peterson, M. J., and Tononi, G. (2008). Measures of cortical plasticity after transcranial paired associative stimulation predict changes in electroencephalogram slow-wave activity during subsequent sleep. *Journal of Neuroscience*, 28(31):7911–7918.

Huettel, S. A., Song, A. W., McCarthy, G., et al. (2004). *Functional magnetic resonance imaging*, volume 1. Sinauer Associates Sunderland, MA.

Hughes, E. G., Orthmann-Murphy, J. L., Langseth, A. J., and Bergles, D. E. (2018). Myelin remodeling through experience-dependent oligodendrogenesis in the adult somatosensory cortex. *Nature neuroscience*, 21(5):696.

Husain, F. T., Medina, R. E., Davis, C. W., Szymko-Bennett, Y., Simonyan, K., Pajor, N. M., and Horwitz, B. (2011). Neuroanatomical changes due to hearing loss and chronic tinnitus: a combined vbm and dti study. *Brain research*, 1369:74–88.

Ilmoniemi, R. J., Virtanen, J., Ruohonen, J., Karhu, J., Aronen, H. J., Näätänen, R., and Katila, T. (1997). Neuronal responses to magnetic stimulation reveal cortical reactivity and connectivity. *Neuroreport*, 8(16):3537–3540.

Ioannidis, J. P. (2005). Why most published research findings are false. *PLoS medicine*, 2(8):e124.

Isoda, M. and Hikosaka, O. (2007). Switching from automatic to controlled action by monkey medial frontal cortex. *Nature neuroscience*, 10(2):240.

Jbabdi, S., Sotiropoulos, S. N., Savio, A. M., Graña, M., and Behrens, T. E. (2012). Model-based analysis of multishell diffusion mr data for tractography: how to get over fitting problems. *Magnetic resonance in medicine*, 68(6):1846–1855.

Jenny, A. (1979). Commissural projections of the cortical hand motor area in monkeys. *Journal of Comparative Neurology*, 188(1):137–145.

Johansen-Berg, H. (2010). Behavioural relevance of variation in white matter microstructure. *Current opinion in neurology*, 23(4):351–358.

Johansen-Berg, H., Della-Maggiore, V., Behrens, T. E., Smith, S. M., and Paus, T. (2007). Integrity of white matter in the corpus callosum correlates with bimanual co-ordination skills. *Neuroimage*, 36:T16–T21.

Johnen, V. M., Neubert, F.-X., Buch, E. R., Verhagen, L., O'Reilly, J. X., Mars, R. B., and Rushworth, M. F. (2015). Causal manipulation of functional connectivity in a specific neural pathway during behaviour and at rest. *Elife*, 4:e04585.

Kaller, M. S., Lazari, A., Blanco-Duque, C., Sampaio-Baptista, C., and Johansen-Berg, H. (2017). Myelin plasticity and behaviour?connecting the dots. *Current opinion in neurobiology*, 47:86–92.

Kanai, R. and Rees, G. (2011). The structural basis of inter-individual differences in human behaviour and cognition. *Nature Reviews Neuroscience*, 12(4):231.

Kanwisher, N. (2017). The quest for the ffa and where it led. *Journal of Neuroscience*, 37(5):1056–1061.

Kaplan, R. M. and Irvin, V. L. (2015). Likelihood of null effects of large nhlbi clinical trials has increased over time. *PloS one*, 10(8):e0132382.

Khanbabaei, M., Hughes, E., Ellegood, J., Qiu, L. R., Yip, R., Dobry, J., Murari, K., Lerch, J. P., Rho, J. M., and Cheng, N. (2019). Precocious myelination in a mouse model of autism. *Translational psychiatry*, 9(1):1–14.

Kleim, J. A., Barbay, S., Cooper, N. R., Hogg, T. M., Reidel, C. N., Remple, M. S., and Nudo, R. J. (2002). Motor learning-dependent synaptogenesis is localized to functionally reorganized motor cortex. *Neurobiology of learning and memory*, 77(1):63–77.

Kleim, J. A., Hogg, T. M., VandenBerg, P. M., Cooper, N. R., Bruneau, R., and Remple, M. (2004). Cortical synaptogenesis and motor map reorganization occur during late, but not early, phase of motor skill learning. *Journal of Neuroscience*, 24(3):628–633.

Kleim, J. A., Markham, J. A., Vij, K., Freese, J. L., Ballard, D. H., and Greenough, W. T. (2007). Motor learning induces astrocytic hypertrophy in the cerebellar cortex. *Behavioural brain research*, 178(2):244–249.

Koch, G., Franca, M., Del Olmo, M. F., Cheeran, B., Milton, R., Sauco, M. A., and Rothwell, J. C. (2006). Time course of functional connectivity between dorsal premotor and contralateral motor cortex during movement selection. *Journal of Neuroscience*, 26(28):7452–7459.

Koch, G., Ponzo, V., Di Lorenzo, F., Caltagirone, C., and Veniero, D. (2013). Hebbian and anti-hebbian spike-timing-dependent plasticity of human cortico-cortical connections. *Journal of Neuroscience*, 33(23):9725–9733.

Kohl, S., Hannah, R., Rocchi, L., Nord, C. L., Rothwell, J., and Voon, V. (2019). Cortical paired associative stimulation influences response inhibi-

tion: cortico-cortical and cortico-subcortical networks. *Biological psychiatry*, 85(4):355–363.

Kolasinski, J., Makin, T. R., Logan, J. P., Jbabdi, S., Clare, S., Stagg, C. J., and Johansen-Berg, H. (2016). Perceptually relevant remapping of human somatotopy in 24 hours. *Elife*, 5:e17280.

Kriegeskorte, N., Simmons, W. K., Bellgowan, P. S., and Baker, C. I. (2009). Circular analysis in systems neuroscience: the dangers of double dipping. *Nature neuroscience*, 12(5):535.

Kwong, K. K., Belliveau, J. W., Chesler, D. A., Goldberg, I. E., Weisskoff, R. M., Poncelet, B. P., Kennedy, D. N., Hoppel, B. E., Cohen, M. S., and Turner, R. (1992). Dynamic magnetic resonance imaging of human brain activity during primary sensory stimulation. *Proceedings of the National Academy of Sciences*, 89(12):5675–5679.

Lang, E. J. and Rosenbluth, J. (2003). Role of myelination in the development of a uniform olivocerebellar conduction time. *Journal of neurophysiology*, 89(4):2259–2270.

Langer, N., Hänggi, J., Müller, N., Simmen, H.-P., and Jäncke, L. (2012). Effects of limb immobilization on brain plasticity. *Neurology*, 78(3):182–188.

Langkammer, C., Schweser, F., Krebs, N., Deistung, A., Goessler, W., Scheurer, E., Sommer, K., Reishofer, G., Yen, K., Fazekas, F., et al. (2012).

Quantitative susceptibility mapping (qsm) as a means to measure brain iron? a post mortem validation study. *Neuroimage*, 62(3):1593–1599.

Lankford, C. L. and Does, M. D. (2013). On the inherent precision of mcdespot. *Magnetic resonance in medicine*, 69(1):127–136.

Lansner, A. (2009). Associative memory models: from the cell-assembly theory to biophysically detailed cortex simulations. *Trends in neurosciences*, 32(3):178–186.

Laule, C., Vavasour, I. M., Kolind, S. H., Li, D. K., Traboulsee, T. L., Moore, G. W., and MacKay, A. L. (2007). Magnetic resonance imaging of myelin. *Neurotherapeutics*, 4(3):460–484.

Lauterbur, P. C. (1973). Image formation by induced local interactions: examples employing nuclear magnetic resonance. *nature*, 242(5394):190–191.

Lazari, A., Koudelka, S., and Sampaio-Baptista, C. (2018). Experience-related reductions of myelin and axon diameter in adulthood. *Journal of neurophysiology*, 120(4):1772–1775.

Le, D. B., Turner, R., and Douek, P. (1993). Is water diffusion restricted in human brain white matter? an echo-planar nmr imaging study. *Neuroreport*, 4(7):887–890.

Lee, Y., Morrison, B. M., Li, Y., Lengacher, S., Farah, M. H., Hoffman, P. N., Liu, Y., Tsingalia, A., Jin, L., Zhang, P.-W., et al. (2012). Oligodendroglia

metabolically support axons and contribute to neurodegeneration. *Nature*, 487(7408):443.

Lehmann, M. L., Weigel, T. K., Elkahloun, A. G., and Herkenham, M. (2017). Chronic social defeat reduces myelination in the mouse medial prefrontal cortex. *Scientific reports*, 7:46548.

Lerch, J. P., van der Kouwe, A. J., Raznahan, A., Paus, T., Johansen-Berg, H., Miller, K. L., Smith, S. M., Fischl, B., and Sotiropoulos, S. N. (2017). Studying neuroanatomy using mri. *Nature Neuroscience*, 20(3):314.

Levesque, I. R. and Pike, G. B. (2009). Characterizing healthy and diseased white matter using quantitative magnetization transfer and multicomponent t2 relaxometry: A unified view via a four-pool model. *Magnetic Resonance in Medicine: An Official Journal of the International Society for Magnetic Resonance in Medicine*, 62(6):1487–1496.

Li, Q., Brus-Ramer, M., Martin, J. H., and McDonald, J. W. (2010). Electrical stimulation of the medullary pyramid promotes proliferation and differentiation of oligodendrocyte progenitor cells in the corticospinal tract of the adult rat. *Neuroscience letters*, 479(2):128–133.

Li, W., Wu, B., Batrachenko, A., Bancroft-Wu, V., Morey, R. A., Shashi, V., Langkammer, C., De Bellis, M. D., Ropele, S., Song, A. W., et al. (2014). Differential developmental trajectories of magnetic susceptibility in human brain gray and white matter over the lifespan. *Human brain mapping*, 35(6):2698–2713.

Li, W., Wu, B., and Liu, C. (2011). Quantitative susceptibility mapping of human brain reflects spatial variation in tissue composition. *Neuroimage*, 55(4):1645–1656.

Licht, T., Goshen, I., Avital, A., Kreisel, T., Zubedat, S., Eavri, R., Segal, M., Yirmiya, R., and Keshet, E. (2011). Reversible modulations of neuronal plasticity by vegf. *Proceedings of the National Academy of Sciences*, 108(12):5081–5086.

Liebetanz, D. and Merkler, D. (2006). Effects of commissural de-and remyelination on motor skill behaviour in the cuprizone mouse model of multiple sclerosis. *Experimental neurology*, 202(1):217–224.

Lin, Y., Wang, J., Wu, C., Wai, Y., Yu, J., and Ng, S. (2008). Diffusion tensor imaging of the auditory pathway in sensorineural hearing loss: changes in radial diffusivity and diffusion anisotropy. *Journal of Magnetic Resonance Imaging: An Official Journal of the International Society for Magnetic Resonance in Medicine*, 28(3):598–603.

Liu, C., Li, W., Johnson, G. A., and Wu, B. (2011). High-field (9.4 t) mri of brain dysmyelination by quantitative mapping of magnetic susceptibility. *Neuroimage*, 56(3):930–938.

Liu, J., Dietz, K., DeLoyht, J. M., Pedre, X., Kelkar, D., Kaur, J., Vialou, V., Lobo, M. K., Dietz, D. M., Nestler, E. J., et al. (2012). Impaired adult myelination in the prefrontal cortex of socially isolated mice. *Nature neuroscience*, 15(12):1621.

Liu, J., Dupree, J. L., Gacias, M., Frawley, R., Sikder, T., Naik, P., and Casaccia, P. (2016). Clemastine enhances myelination in the prefrontal cortex and rescues behavioral changes in socially isolated mice. *Journal of Neuroscience*, 36(3):957–962.

Lodygensky, G. A., Marques, J. P., Maddage, R., Perroud, E., Sizonenko, S. V., Hüppi, P. S., and Gruetter, R. (2012). In vivo assessment of myelination by phase imaging at high magnetic field. *Neuroimage*, 59(3):1979–1987.

Logothetis, N. K., Pauls, J., Augath, M., Trinath, T., and Oeltermann, A. (2001). Neurophysiological investigation of the basis of the fmri signal. *Nature*, 412(6843):150–157.

Lutti, A., Dick, F., Sereno, M. I., and Weiskopf, N. (2014). Using high-resolution quantitative mapping of r1 as an index of cortical myelination. *Neuroimage*, 93:176–188.

MacDonald, A. W., Cohen, J. D., Stenger, V. A., and Carter, C. S. (2000). Dissociating the role of the dorsolateral prefrontal and anterior cingulate cortex in cognitive control. *Science*, 288(5472):1835–1838.

Mackay, A., Whittall, K., Adler, J., Li, D., Paty, D., and Graeb, D. (1994). In vivo visualization of myelin water in brain by magnetic resonance. *Magnetic resonance in medicine*, 31(6):673–677.

Magri, C., Schridde, U., Murayama, Y., Panzeri, S., and Logothetis, N. K.

(2012). The amplitude and timing of the bold signal reflects the relationship between local field potential power at different frequencies. *Journal of Neuroscience*, 32(4):1395–1407.

Makinodan, M., Rosen, K. M., Ito, S., and Corfas, G. (2012). A critical period for social experience–dependent oligodendrocyte maturation and myelination. *science*, 337(6100):1357–1360.

Mandillo, S., Heise, I., Garbugino, L., Tocchini-Valentini, G. P., Giuliani, A., Wells, S., and Nolan, P. M. (2014). Early motor deficits in mouse disease models are reliably uncovered using an automated home-cage wheel-running system: a cross-laboratory validation. *Disease models & mechanisms*, 7(3):397–407.

Mangeat, G., Govindarajan, S. T., Mainero, C., and Cohen-Adad, J. (2015). Multivariate combination of magnetization transfer, t2* and b0 orientation to study the myelo-architecture of the in vivo human cortex. *NeuroImage*, 119:89–102.

Mansfield, P. (1977). Multi-planar image formation using nmr spin echoes. *Journal of Physics C: Solid State Physics*, 10(3):L55.

Marques, S., Zeisel, A., Codeluppi, S., van Bruggen, D., Falcão, A. M., Xiao, L., Li, H., Häring, M., Hochgerner, H., Romanov, R. A., et al. (2016). Oligodendrocyte heterogeneity in the mouse juvenile and adult central nervous system. *Science*, 352(6291):1326–1329.

Mars, R. B., Klein, M. C., Neubert, F.-X., Olivier, E., Buch, E. R., Boorman, E. D., and Rushworth, M. F. (2009). Short-latency influence of medial frontal cortex on primary motor cortex during action selection under conflict. *Journal of Neuroscience*, 29(21):6926–6931.

Mars, R. B., Piekema, C., Coles, M. G., Hulstijn, W., and Toni, I. (2007). On the programming and reprogramming of actions. *Cerebral Cortex*, 17(12):2972–2979.

Matejko, A. A. and Ansari, D. (2015). Drawing connections between white matter and numerical and mathematical cognition: a literature review. *Neuroscience & Biobehavioral Reviews*, 48:35–52.

Mateo, C., Knutsen, P. M., Tsai, P. S., Shih, A. Y., and Kleinfeld, D. (2017). Entrainment of arteriole vasomotor fluctuations by neural activity is a basis of blood-oxygenation-level-dependent ?resting-state? connectivity. *Neuron*, 96(4):936–948.

Matthews, P. and Jezzard, P. (2004). Functional magnetic resonance imaging. *Journal of Neurology, Neurosurgery & Psychiatry*, 75(1):6–12.

McKenzie, I. A., Ohayon, D., Li, H., De Faria, J. P., Emery, B., Tohyama, K., and Richardson, W. D. (2014). Motor skill learning requires active central myelination. *science*, 346(6207):318–322.

Meijer, J. H. and Robbers, Y. (2014). Wheel running in the wild. *Proceedings of the Royal Society B: Biological Sciences*, 281(1786):20140210.

Melbourne, A., Eaton-Rosen, Z., De Vita, E., Bainbridge, A., Cardoso, M. J., Price, D., Cady, E., Kendall, G. S., Robertson, N. J., Marlow, N., et al. (2014). Multi-modal measurement of the myelin-to-axon diameter g-ratio in preterm-born neonates and adult controls. In *International Conference on Medical Image Computing and Computer-Assisted Intervention*, pages 268–275. Springer.

Mensch, S., Baraban, M., Almeida, R., Czopka, T., Ausborn, J., El Manira, A., and Lyons, D. A. (2015). Synaptic vesicle release regulates myelin sheath number of individual oligodendrocytes in vivo. *Nature neuroscience*, 18(5):628.

Merton, P. and Morton, H. (1980). Stimulation of the cerebral cortex in the intact human subject. *Nature*, 285(5762):227–227.

Meteyard, L. and Holmes, N. (2018). Tms smart–scalp mapping of annoyance ratings and twitches caused by transcranial magnetic stimulation. *Journal of neuroscience methods*, 299:34–44.

Metz, G. A. and Whishaw, I. Q. (2000). Skilled reaching an action pattern: stability in rat (rattus norvegicus) grasping movements as a function of changing food pellet size. *Behavioural brain research*, 116(2):111–122.

Metzler-Baddeley, C., Jones, D. K., Steventon, J., Westacott, L., Aggleton, J. P., and O'Sullivan, M. J. (2012). Cingulum microstructure predicts cognitive control in older age and mild cognitive impairment. *Journal of Neuroscience*, 32(49):17612–17619.

Micheva, K. D., Wolman, D., Mensh, B. D., Pax, E., Buchanan, J., Smith, S. J., and Bock, D. D. (2016). A large fraction of neocortical myelin ensheathes axons of local inhibitory neurons. *elife*, 5:e15784.

Milham, M. P., Craddock, R. C., Son, J. J., Fleischmann, M., Clucas, J., Xu, H., Koo, B., Krishnakumar, A., Biswal, B. B., Castellanos, F. X., et al. (2018). Assessment of the impact of shared brain imaging data on the scientific literature. *Nature communications*, 9.

Mitew, S., Gobius, I., Fenlon, L. R., McDougall, S. J., Hawkes, D., Xing, Y. L., Bujalka, H., Gundlach, A. L., Richards, L. J., Kilpatrick, T. J., et al. (2018). Pharmacogenetic stimulation of neuronal activity increases myelination in an axon-specific manner. *Nature communications*, 9(1):306.

Moeller, S., Yacoub, E., Olman, C. A., Auerbach, E., Strupp, J., Harel, N., and Uğurbil, K. (2010). Multiband multislice ge-epi at 7 tesla, with 16-fold acceleration using partial parallel imaging with application to high spatial and temporal whole-brain fmri. *Magnetic resonance in medicine*, 63(5):1144–1153.

Moore, J. W., Joyner, R. W., Brill, M. H., Waxman, S. D., and Najar-Joa, M. (1978). Simulations of conduction in uniform myelinated fibers. relative sensitivity to changes in nodal and internodal parameters. *Biophysical journal*, 21(2):147–160.

Moore, S., Meschkat, M., Ruhwedel, T., Tzvetanova, I. D., Trevisiol, A., Battefeld, A., Kusch, K., Kole, M., Strenzke, N., Möbius, W., et al. (2019). A

role of oligodendrocytes in information processing independent of conduction velocity. *bioRxiv*, page 736975.

Moseley, M., Cohen, Y., Mintorovitch, J., Chileuitt, L., Shimizu, H., Kucharczyk, J., Wendland, M., and Weinstein, P. (1990a). Early detection of regional cerebral ischemia in cats: comparison of diffusion-and t2-weighted mri and spectroscopy. *Magnetic resonance in medicine*, 14(2):330–346.

Moseley, M. E., Cohen, Y., Kucharczyk, J., Mintorovitch, J., Asgari, H., Wendland, M., Tsuruda, J., and Norman, D. (1990b). Diffusion-weighted mr imaging of anisotropic water diffusion in cat central nervous system. *Radiology*, 176(2):439–445.

Moser, E. I., Krobert, K. A., Moser, M.-B., and Morris, R. G. (1998). Impaired spatial learning after saturation of long-term potentiation. *Science*, 281(5385):2038–2042.

Mount, C. W., Yalçın, B., Cunliffe-Koehler, K., and Monje, M. (2019). Monosynaptic tracing maps brain-wide afferent oligodendrocyte precursor cell connectivity. *bioRxiv*, page 669572.

Muellbacher, W., Ziemann, U., Boroojerdi, B., and Hallett, M. (2000). Effects of low-frequency transcranial magnetic stimulation on motor excitability and basic motor behavior. *Clinical Neurophysiology*, 111(6):1002–1007.

Mueller, J. K., Grigsby, E. M., Prevosto, V., Petraglia III, F. W., Rao, H., Deng, Z.-D., Peterchev, A. V., Sommer, M. A., Egner, T., Platt,

M. L., et al. (2014). Simultaneous transcranial magnetic stimulation and single-neuron recording in alert non-human primates. *Nature neuroscience*, 17(8):1130.

Muetzel, R. L., Collins, P. F., Mueller, B. A., Schissel, A. M., Lim, K. O., and Luciana, M. (2008). The development of corpus callosum microstructure and associations with bimanual task performance in healthy adolescents. *Neuroimage*, 39(4):1918–1925.

Müller-Dahlhaus, F., Ziemann, U., and Classen, J. (2010). Plasticity resembling spike-timing dependent synaptic plasticity: the evidence in human cortex. *Frontiers in synaptic neuroscience*, 2:34.

Mumford, J. A. (2012). A power calculation guide for fmri studies. *Social cognitive and affective neuroscience*, 7(6):738–742.

Munafò, M. R., Nosek, B. A., Bishop, D. V., Button, K. S., Chambers, C. D., Du Sert, N. P., Simonsohn, U., Wagenmakers, E.-J., Ware, J. J., and Ioannidis, J. P. (2017). A manifesto for reproducible science. *Nature Human Behaviour*, 1(1):0021.

Murad, M. H., Chu, H., Lin, L., and Wang, Z. (2018). The effect of publication bias magnitude and direction on the certainty in evidence. *BMJ evidence-based medicine*, 23(3):84–86.

Nave, K.-A. (2010). Myelination and support of axonal integrity by glia. *Nature*, 468(7321):244.

Neubert, F.-X., Mars, R. B., Buch, E. R., Olivier, E., and Rushworth, M. F. (2010). Cortical and subcortical interactions during action reprogramming and their related white matter pathways. *Proceedings of the National Academy of Sciences*, 107(30):13240–13245.

Nichols, T. E., Das, S., Eickhoff, S. B., Evans, A. C., Glatard, T., Hanke, M., Kriegeskorte, N., Milham, M. P., Poldrack, R. A., Poline, J.-B., et al. (2017). Best practices in data analysis and sharing in neuroimaging using mri. *Nature neuroscience*, 20(3):299.

Nord, C. L., Popa, T., Smith, E., Hannah, R., Donamayor, N., Weidacker, K., Bays, P. M., Rothwell, J., and Voon, V. (2019). The effect of frontoparietal paired associative stimulation on decision-making and working memory. *cortex*, 117:266–276.

Nord, C. L., Valton, V., Wood, J., and Roiser, J. P. (2017). Power-up: A reanalysis of'power failure'in neuroscience using mixture modeling. *Journal of Neuroscience*, 37(34):8051–8061.

Nosek, B. A., Ebersole, C. R., DeHaven, A. C., and Mellor, D. T. (2018). The preregistration revolution. *Proceedings of the National Academy of Sciences*, 115(11):2600–2606.

Ogawa, S., Lee, T.-M., Kay, A. R., and Tank, D. W. (1990). Brain magnetic resonance imaging with contrast dependent on blood oxygenation. *proceedings of the National Academy of Sciences*, 87(24):9868–9872.

Oldfield, R. C. (1971). The assessment and analysis of handedness: the edinburgh inventory. *Neuropsychologia*, 9(1):97–113.

O'Shea, J., Johansen-Berg, H., Trief, D., Göbel, S., and Rushworth, M. F. (2007). Functionally specific reorganization in human premotor cortex. *Neuron*, 54(3):479–490.

Ou, X., Sun, S.-W., Liang, H.-F., Song, S.-K., and Gochberg, D. F. (2009). Quantitative magnetization transfer measured pool-size ratio reflects optic nerve myelin content in ex vivo mice. *Magnetic Resonance in Medicine: An Official Journal of the International Society for Magnetic Resonance in Medicine*, 61(2):364–371.

Pajevic, S., Basser, P. J., and Fields, R. D. (2014). Role of myelin plasticity in oscillations and synchrony of neuronal activity. *Neuroscience*, 276:135–147.

Papp, D., Callaghan, M. F., Meyer, H., Buckley, C., and Weiskopf, N. (2016). Correction of inter-scan motion artifacts in quantitative r1 mapping by accounting for receive coil sensitivity effects. *Magnetic resonance in medicine*, 76(5):1478–1485.

Pauling, L. and Coryell, C. D. (1936). The magnetic properties and structure of hemoglobin, oxyhemoglobin and carbonmonoxyhemoglobin. *Proceedings of the National Academy of Sciences*, 22(4):210–216.

Pelletier, J., Habib, M., Lyon-Caen, O., Salamon, G., Poncet, M., and Khalil,

R. (1993). Functional and magnetic resonance imaging correlates of callosal involvement in multiple sclerosis. *Archives of Neurology*, 50(10):1077–1082.

Perge, J. A., Niven, J. E., Mugnaini, E., Balasubramanian, V., and Sterling, P. (2012). Why do axons differ in caliber? *Journal of Neuroscience*, 32(2):626–638.

Phan, B. N., Bohlen, J. F., Davis, B. A., Ye, Z., Chen, H.-Y., Mayfield, B., Sripathy, S. R., Page, S. C., Campbell, M. N., Smith, H. L., et al. (2020). A myelin-related transcriptomic profile is shared by pitt–hopkins syndrome models and human autism spectrum disorder. *Nature neuroscience*, 23(3):375–385.

Picciotto, M. (2018). Analytical transparency and reproducibility in human neuroimaging studies.

Poldrack, R. A. (2019). The costs of reproducibility. *Neuron*, 101(1):11–14.

Poldrack, R. A., Baker, C. I., Durnez, J., Gorgolewski, K. J., Matthews, P. M., Munafò, M. R., Nichols, T. E., Poline, J.-B., Vul, E., and Yarkoni, T. (2017). Scanning the horizon: towards transparent and reproducible neuroimaging research. *Nature Reviews Neuroscience*, 18(2):115.

Reardon, P., Seidlitz, J., Vandekar, S., Liu, S., Patel, R., Park, M. T. M., Alexander-Bloch, A., Clasen, L. S., Blumenthal, J. D., Lalonde, F. M., et al. (2018). Normative brain size variation and brain shape diversity in humans. *Science*, 360(6394):1222–1227.

Reis, J., Swayne, O. B., Vandermeeren, Y., Camus, M., Dimyan, M. A., Harris-Love, M., Perez, M. A., Ragert, P., Rothwell, J. C., and Cohen, L. G. (2008). Contribution of transcranial magnetic stimulation to the understanding of cortical mechanisms involved in motor control. *The Journal of physiology*, 586(2):325–351.

Rhyu, I., Bytheway, J., Kohler, S., Lange, H., Lee, K., Boklewski, J., McCormick, K., Williams, N., Stanton, G., Greenough, W., et al. (2010). Effects of aerobic exercise training on cognitive function and cortical vascularity in monkeys. *Neuroscience*, 167(4):1239–1248.

Ridderinkhof, K. R., Ullsperger, M., Crone, E. A., and Nieuwenhuis, S. (2004). The role of the medial frontal cortex in cognitive control. *science*, 306(5695):443–447.

Rioult-Pedotti, M.-S., Friedman, D., Hess, G., and Donoghue, J. P. (1998). Strengthening of horizontal cortical connections following skill learning. *Nature neuroscience*, 1(3):230.

Rioult-Pedotti, M.-S., Pekanovic, A., Atiemo, C. O., Marshall, J., and Luft, A. R. (2015). Dopamine promotes motor cortex plasticity and motor skill learning via plc activation. *PloS one*, 10(5):e0124986.

Rizzo, V., Siebner, H., Morgante, F., Mastroeni, C., Girlanda, P., and Quartarone, A. (2009). Paired associative stimulation of left and right human motor cortex shapes interhemispheric motor inhibition based on a hebbian mechanism. *Cerebral cortex*, 19(4):907–915.

Roberts, R. E., Anderson, E. J., and Husain, M. (2013). White matter microstructure and cognitive function. *The Neuroscientist*, 19(1):8–15.

Robinson, E. C., Garcia, K., Glasser, M. F., Chen, Z., Coalson, T. S., Makropoulos, A., Bozek, J., Wright, R., Schuh, A., Webster, M., et al. (2018). Multimodal surface matching with higher-order smoothness constraints. *NeuroImage*, 167:453–465.

Romei, V., Chiappini, E., Hibbard, P. B., and Avenanti, A. (2016). Empowering reentrant projections from v5 to v1 boosts sensitivity to motion. *Current Biology*, 26(16):2155–2160.

Romero, M. C., Davare, M., Armendariz, M., and Janssen, P. (2019). Neural effects of transcranial magnetic stimulation at the single-cell level. *Nature communications*, 10(1):1–11.

Rossi, S., Hallett, M., Rossini, P. M., Pascual-Leone, A., of TMS Consensus Group, S., et al. (2009). Safety, ethical considerations, and application guidelines for the use of transcranial magnetic stimulation in clinical practice and research. *Clinical neurophysiology*, 120(12):2008–2039.

Rushton, W. (1951). A theory of the effects of fibre size in medullated nerve. *The Journal of physiology*, 115(1):101–122.

Saab, A. S., Tzvetavona, I. D., Trevisiol, A., Baltan, S., Dibaj, P., Kusch, K., Möbius, W., Goetze, B., Jahn, H. M., Huang, W., et al. (2016). Oligodendroglial nmda receptors regulate glucose import and axonal energy metabolism. *Neuron*, 91(1):119–132.

Saenz, M. and Fine, I. (2010). Topographic organization of v1 projections through the corpus callosum in humans. *Neuroimage*, 52(4):1224–1229.

Sakimura, K., Kutsuwada, T., Ito, I., Manabe, T., Takayama, C., Kushiya, E., Yagi, T., Aizawa, S., Inoue, Y., Sugiyama, H., et al. (1995). Reduced hippocampal ltp and spatial learning in mice lacking nmda receptor $\varepsilon 1$ subunit. *Nature*, 373(6510):151.

Salami, M., Itami, C., Tsumoto, T., and Kimura, F. (2003). Change of conduction velocity by regional myelination yields constant latency irrespective of distance between thalamus and cortex. *Proceedings of the National Academy of Sciences*, 100(10):6174–6179.

Sampaio-Baptista, C., De Weijer, A., Van Der Toorn, A., Otte, W. M., Winkler, A. M., Lazari, A., Salvan, P., Bannerman, D. M., Dijkhuizen, R. M., and Johansen-Berg, H. (2019a). Skill acquisition increases myelination and strengthens functional connectivity in the sensorimotor circuit of the adult rat. *BioRxiv*, page 661546.

Sampaio-Baptista, C. and Johansen-Berg, H. (2017). White matter plasticity in the adult brain. *Neuron*, 96(6):1239–1251.

Sampaio-Baptista, C., Khrapitchev, A. A., Foxley, S., Schlagheck, T., Scholz, J., Jbabdi, S., DeLuca, G. C., Miller, K. L., Taylor, A., Thomas, N., et al. (2013). Motor skill learning induces changes in white matter microstructure and myelination. *Journal of Neuroscience*, 33(50):19499–19503.

Sampaio-Baptista, C., Vallès, A., Khrapitchev, A. A., Akkermans, G., Winkler, A. M., Foxley, S., Sibson, N. R., Roberts, M., Miller, K., Diamond, M. E., et al. (2019b). Experience alterations in white matter structure and myelin-related gene expression in adult rats. *BioRxiv*, page 532572.

Samsonov, A., Alexander, A. L., Mossahebi, P., Wu, Y.-C., Duncan, I. D., and Field, A. S. (2012). Quantitative mr imaging of two-pool magnetization transfer model parameters in myelin mutant shaking pup. *Neuroimage*, 62(3):1390–1398.

Saucier, D. and Cain, D. P. (1995). Spatial learning without nmda receptor-dependent long-term potentiation. *Nature*, 378(6553):186.

Sauerbrei, B. A., Guo, J.-Z., Cohen, J. D., Mischiati, M., Guo, W., Kabra, M., Verma, N., Mensh, B., Branson, K., and Hantman, A. W. (2020). Cortical pattern generation during dexterous movement is input-driven. *Nature*, 577(7790):386–391.

Schalomon, P. M. and Wahlsten, D. (2002). Wheel running behavior is impaired by both surgical section and genetic absence of the mouse corpus callosum. *Brain research bulletin*, 57(1):27–33.

Schauf, C. and Davis, F. A. (1974). Impulse conduction in multiple sclerosis: a theoretical basis for modification by temperature and pharmacological agents. *Journal of Neurology, Neurosurgery & Psychiatry*, 37(2):152–161.

Schilling, K. G., Janve, V., Gao, Y., Stepniewska, I., Landman, B. A., and

Anderson, A. W. (2018). Histological validation of diffusion mri fiber orientation distributions and dispersion. *Neuroimage*, 165:200–221.

Scholz, J., Klein, M. C., Behrens, T. E., and Johansen-Berg, H. (2009). Training induces changes in white-matter architecture. *Nature neuroscience*, 12(11):1370.

Schweser, F., Deistung, A., Sommer, K., and Reichenbach, J. R. (2012). Disentangling contributions from iron and myelin architecture to brain tissue magnetic susceptibility by using quantitative susceptibility mapping (qsm). In *Proc. Int. Soc. Magn. Reson. Med*, volume 20, page 409.

Setsompop, K., Gagoski, B. A., Polimeni, J. R., Witzel, T., Wedeen, V. J., and Wald, L. L. (2012). Blipped-controlled aliasing in parallel imaging for simultaneous multislice echo planar imaging with reduced g-factor penalty. *Magnetic resonance in medicine*, 67(5):1210–1224.

Shemer, A., Erny, D., Jung, S., and Prinz, M. (2015). Microglia plasticity during health and disease: an immunological perspective. *Trends in immunology*, 36(10):614–624.

Shore, D. I., Gray, K., Spry, E., and Spence, C. (2005). Spatial modulation of tactile temporal-order judgments. *Perception*, 34(10):1251–1262.

Siebner, H. R., Hartwigsen, G., Kassuba, T., and Rothwell, J. C. (2009). How does transcranial magnetic stimulation modify neuronal activity in the brain? implications for studies of cognition. *Cortex*, 45(9):1035–1042.

Sinclair, J. L., Fischl, M. J., Alexandrova, O., He$\beta$, M., Grothe, B., Leibold, C., and Kopp-Scheinpflug, C. (2017). Sound-evoked activity influences myelination of brainstem axons in the trapezoid body. *Journal of Neuroscience*, 37(34):8239–8255.

Sisti, H. M., Geurts, M., Gooijers, J., Heitger, M. H., Caeyenberghs, K., Beets, I. A., Serbruyns, L., Leemans, A., and Swinnen, S. P. (2012). Microstructural organization of corpus callosum projections to prefrontal cortex predicts bimanual motor learning. *Learning & Memory*, 19(8):351–357.

Sled, J. G. and Pike, G. B. (2001). Quantitative imaging of magnetization transfer exchange and relaxation properties in vivo using mri. *Magnetic Resonance in Medicine: An Official Journal of the International Society for Magnetic Resonance in Medicine*, 46(5):923–931.

Smith, R. S. and Koles, Z. J. (1970). Myelinated nerve fibers: computed effect of myelin thickness on conduction velocity. *American Journal of Physiology-Legacy Content*, 219(5):1256–1258.

Smith, S. M., Jenkinson, M., Johansen-Berg, H., Rueckert, D., Nichols, T. E., Mackay, C. E., Watkins, K. E., Ciccarelli, O., Cader, M. Z., Matthews, P. M., et al. (2006). Tract-based spatial statistics: voxelwise analysis of multi-subject diffusion data. *Neuroimage*, 31(4):1487–1505.

Snaidero, N. and Simons, M. (2014). Myelination at a glance.

Spitzer, S. O., Sitnikov, S., Kamen, Y., Evans, K. A., Kronenberg-Versteeg, D., Dietmann, S., de Faria Jr, O., Agathou, S., and Káradóttir, R. T.

(2019). Oligodendrocyte progenitor cells become regionally diverse and heterogeneous with age. *Neuron*, 101(3):459–471.

Stagg, C., Bestmann, S., Constantinescu, A., Moreno Moreno, L., Allman, C., Mekle, R., Woolrich, M., Near, J., Johansen-Berg, H., and Rothwell, J. (2011). Relationship between physiological measures of excitability and levels of glutamate and gaba in the human motor cortex. *The Journal of physiology*, 589(23):5845–5855.

Steadman, P. E., Xia, F., Ahmed, M., Mocle, A. J., Penning, A. R., Geraghty, A. C., Steenland, H. W., Monje, M., Josselyn, S. A., and Frankland, P. W. (2019). Disruption of oligodendrogenesis impairs memory consolidation in adult mice. *Neuron*.

Steadman, P. E., Xia, F., Ahmed, M., Mocle, A. J., Penning, A. R., Geraghty, A. C., Steenland, H. W., Monje, M., Josselyn, S. A., and Frankland, P. W. (2020). Disruption of oligodendrogenesis impairs memory consolidation in adult mice. *Neuron*, 105(1):150–164.

Stedehouder, J., Couey, J. J., Brizee, D., Hosseini, B., Slotman, J. A., Dirven, C., Shpak, G., Houtsmuller, A., and Kushner, S. (2017). Fast-spiking parvalbumin interneurons are frequently myelinated in the cerebral cortex of mice and humans. *Cerebral Cortex*, 27(10):5001–5013.

Steen, R., Hamer, R., and Lieberman, J. (2007). Measuring brain volume by mr imaging: impact of measurement precision and natural variation on

sample size requirements. *American journal of neuroradiology*, 28(6):1119–1125.

Stefan, K., Kunesch, E., Cohen, L. G., Benecke, R., and Classen, J. (2000). Induction of plasticity in the human motor cortex by paired associative stimulation. *Brain*, 123(3):572–584.

Stehling, M. K., Turner, R., and Mansfield, P. (1991). Echo-planar imaging: magnetic resonance imaging in a fraction of a second. *Science*, 254(5028):43–50.

Stevens, B., Tanner, S., and Fields, R. D. (1998). Control of myelination by specific patterns of neural impulses. *Journal of Neuroscience*, 18(22):9303–9311.

Stikov, N., Campbell, J. S., Stroh, T., Lavelée, M., Frey, S., Novek, J., Nuara, S., Ho, M.-K., Bedell, B. J., Dougherty, R. F., et al. (2015). In vivo histology of the myelin g-ratio with magnetic resonance imaging. *Neuroimage*, 118:397–405.

Stüber, C., Morawski, M., Schäfer, A., Labadie, C., Wähnert, M., Leuze, C., Streicher, M., Barapatre, N., Reimann, K., Geyer, S., et al. (2014). Myelin and iron concentration in the human brain: a quantitative study of mri contrast. *Neuroimage*, 93:95–106.

Stueber, C., Morawski, M., Schäfer, A., Labadie, C., Wähnert, M., Leuze, C., Streicher, M., Barapatre, N., Reimann, K., Geyer, S., et al. (2014).

Myelin and iron concentration in the human brain: a quantitative study of mri contrast. *Neuroimage*, 93:95–106.

Su, W.-J., Zhang, T., Jiang, C.-L., and Wang, W. (2018). Clemastine alleviates depressive-like behavior through reversing the imbalance of microglia-related pro-inflammatory state in mouse hippocampus. *Frontiers in cellular neuroscience*, 12:412.

Suárez, R., Paolino, A., Fenlon, L. R., Morcom, L. R., Kozulin, P., Kurniawan, N. D., and Richards, L. J. (2018). A pan-mammalian map of interhemispheric brain connections predates the evolution of the corpus callosum. *Proceedings of the National Academy of Sciences*, 115(38):9622–9627.

Sui, J., Huster, R., Yu, Q., Segall, J. M., and Calhoun, V. D. (2014). Function–structure associations of the brain: evidence from multimodal connectivity and covariance studies. *Neuroimage*, 102:11–23.

Sullivan, E. V., Rosenbloom, M. J., Desmond, J. E., and Pfefferbaum, A. (2001). Sex differences in corpus callosum size: relationship to age and intracranial size. *Neurobiology of aging*, 22(4):603–611.

Sun, H., Walsh, A. J., Lebel, R. M., Blevins, G., Catz, I., Lu, J.-Q., Johnson, E. S., Emery, D. J., Warren, K. G., and Wilman, A. H. (2015). Validation of quantitative susceptibility mapping with perls' iron staining for subcortical gray matter. *Neuroimage*, 105:486–492.

Suppa, A., Quartarone, A., Siebner, H., Chen, R., Di Lazzaro, V., Del Giudice, P., Paulus, W., Rothwell, J., Ziemann, U., and Classen, J. (2017). The associative brain at work: evidence from paired associative stimulation studies in humans. *Clinical Neurophysiology*, 128(11):2140–2164.

Tabelow, K., Balteau, E., Ashburner, J., Callaghan, M. F., Draganski, B., Helms, G., Kherif, F., Leutritz, T., Lutti, A., Phillips, C., et al. (2019). hmri–a toolbox for quantitative mri in neuroscience and clinical research. *NeuroImage*.

Tagoe, T., Barker, M., Jones, A., Allcock, N., and Hamann, M. (2014). Auditory nerve perinodal dysmyelination in noise-induced hearing loss. *Journal of Neuroscience*, 34(7):2684–2688.

Takahashi, M., Hackney, D. B., Zhang, G., Wehrli, S. L., Wright, A. C., O'Brien, W. T., Uematsu, H., Wehrli, F. W., and Selzer, M. E. (2002). Magnetic resonance microimaging of intraaxonal water diffusion in live excised lamprey spinal cord. *Proceedings of the National Academy of Sciences*, 99(25):16192–16196.

Takeuchi, N., Chuma, T., Matsuo, Y., Watanabe, I., and Ikoma, K. (2005). Repetitive transcranial magnetic stimulation of contralesional primary motor cortex improves hand function after stroke. *Stroke*, 36(12):2681–2686.

Tavor, I., Jones, O. P., Mars, R., Smith, S., Behrens, T., and Jbabdi, S. (2016). Task-free mri predicts individual differences in brain activity during task performance. *Science*, 352(6282):216–220.

Tennant, K. A., Adkins, D. L., Scalco, M. D., Donlan, N. A., Asay, A. L., Thomas, N., Kleim, J. A., and Jones, T. A. (2012). Skill learning induced plasticity of motor cortical representations is time and age-dependent. *Neurobiology of learning and memory*, 98(3):291–302.

Thomas, A. G., Dennis, A., Rawlings, N. B., Stagg, C. J., Matthews, L., Morris, M., Kolind, S. H., Foxley, S., Jenkinson, M., Nichols, T. E., et al. (2016). Multi-modal characterization of rapid anterior hippocampal volume increase associated with aerobic exercise. *Neuroimage*, 131:162–170.

Todorow, M., DeSouza, J. F., Banwell, B. L., and Till, C. (2014). Interhemispheric cooperation in global–local visual processing in pediatric multiple sclerosis. *Journal of clinical and experimental neuropsychology*, 36(2):111–126.

Tofts, P., Cercignani, M., Tozer, D., Symms, M., Davies, G., Ramani, A., and Barker, G. (2005). Tozer et al. quantitative magnetization transfer mapping of bound protons in multiple sclerosis, magn reson med 2003; 50: 83-91. *Magnetic Resonance in Medicine: An Official Journal of the International Society for Magnetic Resonance in Medicine*, 53(2):492–493.

Tomassy, G. S., Berger, D. R., Chen, H.-H., Kasthuri, N., Hayworth, K. J., Vercelli, A., Seung, H. S., Lichtman, J. W., and Arlotta, P. (2014). Distinct profiles of myelin distribution along single axons of pyramidal neurons in the neocortex. *Science*, 344(6181):319–324.

Tomassy, G. S., Dershowitz, L. B., and Arlotta, P. (2016). Diversity matters: a revised guide to myelination. *Trends in cell biology*, 26(2):135–147.

Tournier, J.-D., Calamante, F., and Connelly, A. (2007). Robust determination of the fibre orientation distribution in diffusion mri: non-negativity constrained super-resolved spherical deconvolution. *Neuroimage*, 35(4):1459–1472.

Tsien, J. Z., Huerta, P. T., and Tonegawa, S. (1996). The essential role of hippocampal ca1 nmda receptor–dependent synaptic plasticity in spatial memory. *Cell*, 87(7):1327–1338.

Tunik, E., Frey, S. H., and Grafton, S. T. (2005). Virtual lesions of the anterior intraparietal area disrupt goal-dependent on-line adjustments of grasp. *Nature neuroscience*, 8(4):505–511.

Turner, E. H., Matthews, A. M., Linardatos, E., Tell, R. A., and Rosenthal, R. (2008). Selective publication of antidepressant trials and its influence on apparent efficacy. *New England Journal of Medicine*, 358(3):252–260.

van Eijsden, P., Otte, W. M., Saskia van der Hel, W., van Nieuwenhuizen, O., Dijkhuizen, R. M., de Graaf, R. A., and Braun, K. P. (2011). In vivo diffusion tensor imaging and ex vivo histologic characterization of white matter pathology in a post–status epilepticus model of temporal lobe epilepsy. *Epilepsia*, 52(4):841–845.

Veniero, D., Ponzo, V., and Koch, G. (2013). Paired associative stimula-

tion enforces the communication between interconnected areas. *Journal of Neuroscience*, 33(34):13773–13783.

Verhoeven, K., De Jonghe, P., Van de Putte, T., Nelis, E., Zwijsen, A., Verpoorten, N., De Vriendt, E., Jacobs, A., Van Gerwen, V., Francis, A., et al. (2003). Slowed conduction and thin myelination of peripheral nerves associated with mutant rho guanine-nucleotide exchange factor 10. *The American Journal of Human Genetics*, 73(4):926–932.

Viswanathan, A. and Freeman, R. D. (2007). Neurometabolic coupling in cerebral cortex reflects synaptic more than spiking activity. *Nature neuroscience*, 10(10):1308–1312.

Wager, T. D., Davidson, M. L., Hughes, B. L., Lindquist, M. A., and Ochsner, K. N. (2008). Prefrontal-subcortical pathways mediating successful emotion regulation. *Neuron*, 59(6):1037–1050.

Walhovd, K. B., Johansen-Berg, H., and Karadottir, R. T. (2014). Unraveling the secrets of white matter–bridging the gap between cellular, animal and human imaging studies. *Neuroscience*, 276:2–13.

Wang, H., Liang, Y., Fan, W., Zhou, X., Huang, M., Shi, G., Yu, H., and Shen, G. (2019). Dti study on rehabilitation of the congenital deafness auditory pathway and speech center by cochlear implantation. *European Archives of Oto-Rhino-Laryngology*, 276(9):2411–2417.

Waxman, S. G. (1980). Determinants of conduction velocity in myelinated

nerve fibers. *Muscle & Nerve: Official Journal of the American Association of Electrodiagnostic Medicine*, 3(2):141–150.

Weber, F., Do, J. P. H., Chung, S., Beier, K. T., Bikov, M., Doost, M. S., and Dan, Y. (2018). Regulation of rem and non-rem sleep by periaqueductal gabaergic neurons. *Nature communications*, 9(1):354.

Wedeen, V. J., Hagmann, P., Tseng, W.-Y. I., Reese, T. G., and Weisskoff, R. M. (2005). Mapping complex tissue architecture with diffusion spectrum magnetic resonance imaging. *Magnetic resonance in medicine*, 54(6):1377–1386.

Weiskopf, N., Lutti, A., Helms, G., Novak, M., Ashburner, J., and Hutton, C. (2011). Unified segmentation based correction of r1 brain maps for rf transmit field inhomogeneities (unicort). *Neuroimage*, 54(3):2116–2124.

Weiskopf, N., Suckling, J., Williams, G., Correia, M. M., Inkster, B., Tait, R., Ooi, C., Bullmore, E. T., and Lutti, A. (2013). Quantitative multi-parameter mapping of r1, pd*, mt, and r2* at 3t: a multi-center validation. *Frontiers in neuroscience*, 7:95.

Weisskoff, R. M. and Kiihne, S. (1992). Mri susceptometry: image-based measurement of absolute susceptibility of mr contrast agents and human blood. *Magnetic resonance in medicine*, 24(2):375–383.

Werhahn, K. J., Kunesch, E., Noachtar, S., Benecke, R., and Classen, J. (1999). Differential effects on motorcortical inhibition induced by blockade of gaba uptake in humans. *The Journal of physiology*, 517(2):591–597.

Whishaw, I. Q. and Tomie, J.-A. (1989). Olfaction directs skilled forelimb reaching in the rat. *Behavioural brain research*, 32(1):11–21.

Wicherts, J. M., Borsboom, D., Kats, J., and Molenaar, D. (2006). The poor availability of psychological research data for reanalysis. *American Psychologist*, 61(7):726.

Winkler, A. M., Ridgway, G. R., Webster, M. A., Smith, S. M., and Nichols, T. E. (2014). Permutation inference for the general linear model. *Neuroimage*, 92:381–397.

Winkler, A. M., Webster, M. A., Brooks, J. C., Tracey, I., Smith, S. M., and Nichols, T. E. (2016). Non-parametric combination and related permutation tests for neuroimaging. *Human brain mapping*, 37(4):1486–1511.

Winkler, A. M., Webster, M. A., Vidaurre, D., Nichols, T. E., and Smith, S. M. (2015). Multi-level block permutation. *Neuroimage*, 123:253–268.

Winston, G. P., Vos, S. B., Caldairou, B., Hong, S.-J., Czech, M., Wood, T. C., Wastling, S. J., Barker, G. J., Bernhardt, B. C., Bernasconi, N., et al. (2020). Microstructural imaging in temporal lobe epilepsy: Diffusion imaging changes relate to reduced neurite density. *NeuroImage: Clinical*, page 102231.

Wolff, S. D. and Balaban, R. S. (1989). Magnetization transfer contrast (mtc) and tissue water proton relaxation in vivo. *Magnetic resonance in medicine*, 10(1):135–144.

Wolters, A., Sandbrink, F., Schlottmann, A., Kunesch, E., Stefan, K., Cohen, L. G., Benecke, R., and Classen, J. (2003). A temporally asymmetric hebbian rule governing plasticity in the human motor cortex. *Journal of neurophysiology*, 89(5):2339–2345.

Wolters, A., Schmidt, A., Schramm, A., Zeller, D., Naumann, M., Kunesch, E., Benecke, R., Reiners, K., and Classen, J. (2005). Timing-dependent plasticity in human primary somatosensory cortex. *The Journal of physiology*, 565(3):1039–1052.

Wood, T. C., Simmons, C., Hurley, S. A., Vernon, A. C., Torres, J., Dell?Acqua, F., Williams, S. C., and Cash, D. (2016). Whole-brain ex-vivo quantitative mri of the cuprizone mouse model. *PeerJ*, 4:e2632.

Xiao, L., Ohayon, D., McKenzie, I. A., Sinclair-Wilson, A., Wright, J. L., Fudge, A. D., Emery, B., Li, H., and Richardson, W. D. (2016). Rapid production of new oligodendrocytes is required in the earliest stages of motor-skill learning. *Nature neuroscience*, 19(9):1210.

Yarnykh, V. L. (2002). Pulsed z-spectroscopic imaging of cross-relaxation parameters in tissues for human mri: theory and clinical applications. *Magnetic Resonance in Medicine: An Official Journal of the International Society for Magnetic Resonance in Medicine*, 47(5):929–939.

Yeung, M. S., Zdunek, S., Bergmann, O., Bernard, S., Salehpour, M., Alkass, K., Perl, S., Tisdale, J., Possnert, G., Brundin, L., et al. (2014). Dynamics

of oligodendrocyte generation and myelination in the human brain. *Cell*, 159(4):766–774.

Zatorre, R. J., Fields, R. D., and Johansen-Berg, H. (2012). Plasticity in gray and white: neuroimaging changes in brain structure during learning. *Nature neuroscience*, 15(4):528–536.

Zerbi, V., Ielacqua, G. D., Markicevic, M., Haberl, M. G., Ellisman, M. H., A-Bhaskaran, A., Frick, A., Rudin, M., and Wenderoth, N. (2018). Dysfunctional autism risk genes cause circuit-specific connectivity deficits with distinct developmental trajectories. *Cerebral Cortex*, 28(7):2495–2506.

Zhang, H., Schneider, T., Wheeler-Kingshott, C. A., and Alexander, D. C. (2012). Noddi: practical in vivo neurite orientation dispersion and density imaging of the human brain. *Neuroimage*, 61(4):1000–1016.

Zhao, X., Lynch Jr, J. G., and Chen, Q. (2010). Reconsidering baron and kenny: Myths and truths about mediation analysis. *Journal of consumer research*, 37(2):197–206.

Zhou, B., Zuo, Y.-X., and Jiang, R.-T. (2019). Astrocyte morphology: Diversity, plasticity, and role in neurological diseases. *CNS neuroscience & therapeutics*, 25(6):665–673.

Zibman, S., Daniel, E., Alyagon, U., Etkin, A., and Zangen, A. (2019). Interhemispheric cortico-cortical paired associative stimulation of the prefrontal cortex jointly modulates frontal asymmetry and emotional reactivity. *Brain stimulation*, 12(1):139–147.

Ziegler, G., Hauser, T. U., Moutoussis, M., Bullmore, E. T., Goodyer, I. M., Fonagy, P., Jones, P. B., Lindenberger, U., and Dolan, R. J. (2019). Compulsivity and impulsivity traits linked to attenuated developmental frontostriatal myelination trajectories. *Nature neuroscience*, 22(6):992–999.

Ziemann, U., Rothwell, J. C., and Ridding, M. C. (1996). Interaction between intracortical inhibition and facilitation in human motor cortex. *The Journal of physiology*, 496(3):873–881.